J. Fluid Mech. (1979), *vol.* 92, *part* 3, *pp.* 529–590
Printed in Great Britain

Higher-order theory of the Weissenberg effect

By J. YOO†, D. D. JOSEPH AND G. S. BEAVERS
Department of Aerospace Engineering and Mechanics,
University of Minnesota, Minneapolis

(Received 19 April 1978)

The higher-order theory of the Weissenberg effect is developed as a perturbation of the state of rest. The perturbation is given in powers of the angular frequency Ω of the rod and the solution is carried out to $O(\Omega^4)$. The perturbation induces a slow-motion expansion of the stress into Rivlin–Ericksen tensors in combinations which are completely characterized by five viscoelastic parameters. The effects of each of the material parameters may be computed separately and their overall effect by superposition. The values of the parameters may be determined by measurement of the torque, surface angular velocity and height of climb. Such measurements are reported here for several different sample fluids. Good agreement between the third-order theory and measured values of the velocity is reported. Secondary motions which appear at $O(\Omega^4)$ are computed using biorthogonal series. The analysis predicts the surprising fact that secondary motions run up the climbing bubble against gravity and intuition.

CONTENTS

† Present address: Department of Mechanical Engineering, Seoul National University, Korea.

0022-1120/79/4162-6150 $02.00

1. Introduction

Normal stresses will usually exist in shearing flows of fluids with nonlinear history-dependent relations between stress and deformation. These normal stresses make free surfaces bulge in or out, so that by looking at free surfaces induced by shearing we can find out something about the constitutive equation for the fluid. In the Weissenberg effect, the shearing flow is set up by differential rotation of two concentric cylinders, and the normal stresses will drive the fluid up the inner cylinder, if it is small enough. In the general problem, when the inner cylinder is not small, the free surface responds to normal stresses but the description of the response is not so simple.

A mathematical description of the Weissenberg effect can be obtained as a series of powers of the angular frequency Ω of the inner cylinder. The basic mathematical ideas for this perturbation series were given by Joseph & Fosdick (1973) and Joseph, Beavers & Fosdick (1973). Beavers & Joseph (1975) used the series solution to study the Weissenberg effect observed in experiments on free surfaces induced by the steady rotation of cylinders of small diameter. They showed that the polymeric oils used in their experiments had a second-order range, i.e. a range in which the height of climb was linear in Ω^2. In the second-order theory there is only one viscoelastic parameter, the climbing constant, and it was shown that the values of this parameter, and even its dependence on temperature, could be determined from measurements of the height of climb.

In this paper, we consider the higher-order theory and obtain solutions of the perturbation problems up to and including terms $O(\Omega^4)$. The response of any viscoelastic fluid to steady rotation of the cylinders up to terms $O(\Omega^4)$ depends on the viscosity and on four viscoelastic parameters. All five constants can be determined from measurements of quantities computed in the theory.

The interesting quantities which appear in the analysis arise in the formal ordering of the solution in powers of Ω. We first explain this ordering in physical terms. The head $\Phi = p + \rho g z$, the pressure p, the free surface $z = h(r; \Omega)$ and the secondary motion should not change when the direction of rotation is reversed; therefore the power-series solutions for these quantities contain only even powers of Ω. The circumferential component of velocity v and the associated stress should change sign with Ω. It follows that

$$h(r;\Omega) = h^{[2]}(r)\frac{\Omega^2}{2!} + h^{[4]}(r)\frac{\Omega^4}{4!} + O(\Omega^6), \tag{1.1a}$$

$$\Phi(r,z;\Omega) = p + \rho g z = \Phi^{\langle 2\rangle}\frac{\Omega^2}{2!} + \Phi^{\langle 4\rangle}\frac{\Omega^4}{4!} + O(\Omega^6), \tag{1.1b}$$

$$\mathbf{u}(r,z;\Omega) = \mathbf{e}_\theta\left[v^{\langle 1\rangle}(r)\,\Omega + v^{\langle 3\rangle}(r,z)\frac{\Omega^3}{3!} + O(\Omega^5)\right] + \nabla \wedge \left[\mathbf{e}_\theta\left\{\psi^{\langle 4\rangle}(r,z)\frac{\Omega^4}{4!} + O(\Omega^6)\right\}\right]. \tag{1.1c}$$

The velocity field $\mathbf{u}$ has been split into a circumferential component and a secondary motion, which is given by derivatives of a stream function $\psi(r,z;\Omega)$.

Different characteristic physical effects are associated with different powers of Ω in the series solution. When there is no rotation, the free surface is flat and the pressure is hydrostatic. At first order in Ω, there is a z-independent flow in circles with no change in the pressure or flat free surface. At order two, the pressure must equilibrate the radial forces arising from centripetal accelerations and normal stress. The free surface

acts as the barometer for the interior pressure distribution, rising where the interior pressure is greatest. The free surface can remain flat only if there is no motion. The departure from flatness of the free surface at order two requires that the circumferential velocity at order three should depend on z. This is a consequence of the fact that the circumferential component of the shear stress

$$S_{n\theta} = S_{z\theta} - h' S_{r\theta}, \tag{1.2}$$

which vanishes automatically for z-independent fields when the free surface is flat, can vanish when the free surface is not flat only when $S_{z\theta} = h' S_{r\theta}$ does not vanish. The z dependence of the circumferential field at third order is generated without changing the pressure or shape of the free surface. The z-dependent circumferential field generated at order three is associated at order four with forces that also depend on z; such forces inevitably exert torques in the plane θ = constant, and lead to secondary motions.

The equations which govern the perturbation fields have already been derived by Joseph & Fosdick (1973). However, their equations need to be modified slightly in order to include the effects of surface tension at orders three and four. A second-order theory which includes the effects of surface tension is given in § 12 of Joseph & Fosdick but it applies to the flow induced by a rotating cylinder in an infinite fluid and not to the flow between cylinders. Their solutions at third and fourth order are valid only when the surface tension $T = 0$, and the fourth-order solution is also restricted to the case when the distance between the cylinders is small. It is our purpose to remedy these deficiencies and to complete the solution so that circumferential velocity distributions and secondary motions may be computed in a completely explicit and useful form suitable for the quantitative prediction needed for rheometrical measurements.

Since the solution is constructed by perturbations and each problem in the perturbation sequence is linear, the solution may be constructed by superposition. These superpositions are few in number at second and third order. But in the fourth-order theory there are already a rather large number of possible superpositions among two geometric and four unknown viscoelastic parameters. The viscoelastic parameters are supposed to be unique and they do not change when the cylinder dimensions and speeds are changed. So, in principle (and in fact), we may find these parameters by comparing theory and experiment.

The determination of the values of the viscoelastic parameters up to order four is the main contribution of this paper to rheometry. As far as we know this is the first such determination. However, the procedures required by the fourth-order theory are much more elaborate and less accurate than those used in the second-order theory. It may or may not be possible to simplify these procedures to the extent required for practical rheometers.

This paper also makes a contribution to our understanding of the fluid dynamics of the Weissenberg effect. The analysis shows how the requirement that the free surface be free of shear tractions must lead to a vertical stratification of the circumferential velocity $\mathbf{e}_\theta v(r, z; \Omega)$. We show that when Ω is small the circumferential speed $v(r, h; \Omega)$ on the free surface $z = h(r; \Omega)$ is greater than the speed $\tilde{v}(r; \Omega) = v(r, -\infty; \Omega)$ of a viscometric flow of the same fluid on each circle satisfying the inequality

$$\partial h(r; \Omega)/\partial r < 0;$$

that is, when Ω is small the inequality

$$\frac{v(r,h;\Omega)-\tilde{v}(r;\Omega)}{\partial h(r;\Omega)/\partial r} < 0 \tag{1.3}$$

holds on each circle between the cylinders. The stratification with respect to z of the angular velocity generates secondary motions by inducing torques in azimuthal planes θ = constant. We compute the stratification of the torques and the secondary motions and find, to our surprise, that the fluid is driven up the climbing bubble against gravity. And we show that the same effect occurs in our experiments as in our analysis. The method of analysis of secondary motions, using biorthogonal series, is relatively new and may be of independent interest.

The organization of the paper is as follows. In § 2 we briefly review the theory of steady flow of a viscoelastic fluid perturbing a state of rest; the equations which govern the Weissenberg effect are set down without derivation in § 3; a few of the main results of the theory of domain perturbations which are used in the analysis are reviewed in § 4; and the derivation of the perturbation equations is sketched in § 5. In § 6 we write the solutions in a dimensionless form as a sum over components whose coefficients contain the viscoelastic parameters but which themselves are independent of these parameters. Solutions for some of the component functions and the equations governing the others are also set out in § 6. In § 7 we discuss some properties of the solutions given in §§ 8–11. The solutions are given in the form of series whose coefficients are defined by integrals which must be computed numerically. Graphical representations of the final solutions, suitable for quantitative comparison with experiment, are also given in these sections. In § 12 we explain how to measure the viscoelastic constants and determine the values of these constants for several fluids. In § 13 we invert the mapping and exhibit angular velocity contours and streamlines for the secondary flow in the actual domain occupied by a fluid whose parameters are known from the analysis and the measurements reported in § 12. We show in § 13 that when Ω is small the fluid actually climbs the bubble against gravity and we give an explanation of the observed dynamics of the motion when Ω is outside the fourth-order range. The observed dynamics for larger values of Ω outside the range of our theory consist of large-eddy secondary motions driven by torques associated with the vertical stratification of the angular velocity and a small secondary eddy (or bead) rotating against the big one and joined to it at a cusp-like indentation of the free surface. An appendix is given over to discussion of mathematical properties of the biorthogonal series used to find the secondary motion.

2. Constitutive relations

The total stress in an incompressible simple fluid is given by

$$\mathbf{T} = -p\mathbf{I} + \mathbf{S},$$

where p is a constitutively indeterminate pressure and $\mathbf{S}$ is an extra stress given by

$$\mathbf{S} = \mathscr{F}\left[\overset{\infty}{\underset{s=0}{\mathbf{G}}}(s)\right], \quad \mathbf{G}(s) = \mathbf{C}_t(t-s) - \mathbf{I}, \quad \operatorname{tr}\mathbf{S} = 0, \tag{2.1a}$$

$\mathbf{C}_t$ being the relative right Cauchy–Green strain tensor

$$\mathbf{C}_t = \mathbf{F}_t^{\mathrm{T}}\,\mathbf{F}_t, \quad \mathbf{F}_t = \operatorname{grad}\boldsymbol{\chi}_t, \quad \mathbf{G}(0) = 0. \tag{2.1b}$$

Here $s = t-\tau$, and $\boldsymbol{\chi}_t(\mathbf{x}, t-s)$ denotes the point occupied at time $\tau \leqslant t$ by the particle which at the present time t is at the point $\mathbf{x}$. $\mathbf{G}(s)$ is called the history and $\mathscr{F}$ is a hereditary response functional.

For slow steady flow $\mathscr{F}$ is known except for some material constants whose values are to be obtained by rheometrical measurements (see Beavers & Joseph 1975). We call $\mathbf{u}(\mathbf{x}, \epsilon) = \epsilon\mathbf{v}(\mathbf{x}, \epsilon)$ a smooth slow steady motion if $\mathbf{v}(\mathbf{x}, 0)$ and all of its spatial derivatives are continuous and uniformly bounded in the closure of the domain on which they are defined (Joseph 1974). If it is assumed that $\mathscr{F}$ has Fréchet derivatives of all orders at the point $\mathbf{G}(s) = 0$, then one may formally expand $\mathbf{S}$ in a Taylor series (Coleman & Noll 1960; Giesekus 1961; Langlois & Rivlin 1963) whose partial sum is

$$\mathbf{S}_{(N)} = \sum_{n=1}^{N} \mathbf{S}_n[\mathbf{A}_n, \mathbf{A}_{n-1}, \ldots, \mathbf{A}_1] = \sum_{n=1}^{N} \epsilon^n \mathbf{S}_n[\mathbf{a}_n, \mathbf{a}_{n-1}, \ldots, \mathbf{a}_1],$$

where $\mathbf{A}_n = \epsilon^n \mathbf{a}_n$; the $\mathbf{A}_n$ are Rivlin–Ericksen kinematic tensors defined by

$$\mathbf{A}_1 = \operatorname{grad}\mathbf{u} + (\operatorname{grad}\mathbf{u})^{\mathrm{T}} \tag{2.2a}$$

and

$$\mathbf{A}_{n+1} = (\operatorname{grad}\mathbf{A}_n)\,\mathbf{u} + \mathbf{A}_n \operatorname{grad}\mathbf{u} + (\operatorname{grad}\mathbf{u})^{\mathrm{T}}\,\mathbf{A}_n. \tag{2.2b}$$

The tensor-valued functions $\mathbf{S}_n$ of $\mathbf{A}_n$ can be written out explicitly (see Truesdell & Noll 1965; Truesdell 1974). The first four of the $\mathbf{S}_n$ are

$$\mathbf{S}_1[\mathbf{A}_1] = \mu\mathbf{A}_1, \quad \mathbf{S}_2[\mathbf{A}_1, \mathbf{A}_2] = \alpha_1\mathbf{A}_2 + \alpha_2\mathbf{A}_1^2, \tag{2.3a, b}$$

$$\mathbf{S}_3[\mathbf{A}_1, \mathbf{A}_2, \mathbf{A}_3] = \beta_1\mathbf{A}_3 + \beta_2(\mathbf{A}_2\mathbf{A}_1 + \mathbf{A}_1\mathbf{A}_2) + \beta_3(\operatorname{tr}\mathbf{A}_2)\,\mathbf{A}_1, \tag{2.3c}$$

$$\begin{aligned}\mathbf{S}_4[\mathbf{A}_1, \mathbf{A}_2, \mathbf{A}_3, \mathbf{A}_4] = {} & \gamma_1\mathbf{A}_4 + \gamma_2(\mathbf{A}_3\mathbf{A}_1 + \mathbf{A}_1\mathbf{A}_3) + \gamma_3\mathbf{A}_2^2 \\ & + \gamma_4(\mathbf{A}_2\mathbf{A}_1^2 + \mathbf{A}_1^2\mathbf{A}_2) + \gamma_5(\operatorname{tr}\mathbf{A}_2)\,\mathbf{A}_2 + \gamma_6(\operatorname{tr}\mathbf{A}_2)\,\mathbf{A}_1^2 \\ & + \{\gamma_7 \operatorname{tr}\mathbf{A}_3 + \gamma_8(\operatorname{tr}\mathbf{A}_1\mathbf{A}_2)\}\,\mathbf{A}_1.\end{aligned} \tag{2.3d}$$

The coefficients μ, α_1, α_2, β_1, β_2, β_3, γ_1, γ_2, …, γ_8 are constants, or, more generally, functions of the temperature.

Not all of the rheological constants which appear in (2.3) enter the equations which govern the functions mentioned under (1.1). The rheological constants which do matter in our analysis are

$$\mu, \quad \alpha_1, \quad \alpha_2, \quad \hat{\mu} = \beta_2 + \beta_3, \quad \hat{\gamma} = \gamma_3 + \gamma_4 + \gamma_5 + \tfrac{4}{7}\gamma_6.$$

Joseph & Fosdick (1973, § 2) noted that these constants could be expressed in terms of the constants which arise in the expansion of the three viscometric functions in powers of κ, the shear rate; μ, α_1 and α_2 are determined by the values of two of the viscometric functions and $\hat{\mu}$ and $\hat{\gamma}$ by the slopes of the viscometric functions at zero shear. It is very difficult to find these values, especially the slopes, from measurements with standard rheometers (see Beavers & Joseph 1975, § 3).

Certain important combinations of the viscoelastic parameters appear in the analysis:

$N_2 = 2\alpha_1 + \alpha_2$, second normal-stress coefficient at zero shear,

$\hat{\beta} = 3\alpha_1 + 2\alpha_2$, climbing constant at second order,

$\hat{\alpha} = \alpha_1 + \alpha_2$, torque constant at fourth order.

The second normal-stress coefficient is equal to the climbing constant minus the torque constant. We note that $\alpha_1 < 0$ (see Coleman & Markovitz 1964).

The Rivlin–Ericksen kinematic tensors $\mathbf{A}_n$ and the tensors $\mathbf{S}_n$ are homogeneous functions of degree n in $\mathbf{u}$. It is convenient to define the tensor-valued functionals

$$\begin{aligned}\bar{\mathbf{S}}_n[\mathbf{u},\mathbf{u},\ldots,\mathbf{u}] &\equiv \mathbf{S}_n[\mathbf{A}_n,\mathbf{A}_{n-1},\ldots,\mathbf{A}_1] = \epsilon^n\mathbf{S}_n[\mathbf{a}_n,\mathbf{a}_{n-1},\ldots,\mathbf{a}_1]\\ &\equiv \epsilon^n\bar{\mathbf{S}}_n[\underbrace{\mathbf{v},\mathbf{v},\ldots,\mathbf{v}}_{n\text{ times}}].\end{aligned}$$

3. Governing equations

An incompressible simple fluid is set into an axisymmetric motion by the steady rotation of two concentric cylinders with angular velocities Ω at $r = \hat{a}$ and $\lambda\Omega$ at $r = \hat{b}$, respectively. The free surface on top of the fluid deforms into an axisymmetric shape given by $z = h(r;\Omega)$, which was flat when $\Omega = 0$, i.e. $h(r;0) = 0$. The region occupied by the fluid is designated as

$$\mathscr{V}_\Omega = \{r,\theta,z|\hat{a} \leqslant r \leqslant \hat{b},\quad 0 \leqslant \theta \leqslant 2\pi,\quad -\infty < z \leqslant h(r;\Omega)\},$$

where (r,θ,z) are cylindrical co-ordinates. In $\mathscr{V}_\Omega$ we have

$$\rho(\operatorname{grad}\mathbf{u})\,\mathbf{u} = -\operatorname{grad}\Phi + \operatorname{div}\mathbf{S},\quad \operatorname{div}\mathbf{u} = 0, \tag{3.1a,b}$$

where $(\operatorname{grad}\mathbf{u})\,\mathbf{u} = (\mathbf{u}.\nabla)\,\mathbf{u}$ and $\Phi(r,z) = p(r,z) - p_a + \rho g z$, where p_a is the local atmospheric pressure. The boundary conditions at the cylinder walls are

$$\mathbf{u} = \begin{cases}\mathbf{e}_\theta\,\Omega\hat{a} & \text{at}\quad r = \hat{a},\\ \mathbf{e}_\theta\,\lambda\Omega\hat{b} & \text{at}\quad r = \hat{b},\end{cases} \tag{3.1c}$$

and on the free surface of the fluid domain the shear traction vector and the normal component of the velocity vanish:

$$\mathbf{u}.\mathbf{n} = S_{n\theta} = S_{nt} = 0 \quad \text{at}\quad z = h(r;\Omega), \tag{3.1d,e,f}$$

where $\mathbf{n}$ is the outward unit normal to the free surface and $\mathbf{t}$ is the unit tangent vector in the intersection of the free surface and the plane θ = constant. Moreover, far below the free surface we specify that the axial velocity field and the shear traction field on right cross-sectional planes vanish:

$$\mathbf{u}.\mathbf{e}_z,\ S_{z\theta},\ S_{zr} \to 0 \quad \text{as}\quad z \to -\infty. \tag{3.1g,h,i}$$

We shall refer to (3.1g,h,i) as 'asymptotic conditions' as $z \to -\infty$. The problem may be fully stated if the surface profile $z = h(r;\Omega)$ is known in advance. Assuming the constitutive relations of the classical theory of surface tension, the jump in the normal stress across the free surface is balanced by the surface tension. Thus, at $z = h(r;\Omega)$,

$$\rho g h - \Phi + S_{nn} - T\frac{1}{r}\left(\frac{rh'}{(1+h'^2)^{\frac{1}{2}}}\right)' = 0. \tag{3.1j}$$

Equation (3.1j) is a second-order inhomogeneous ordinary nonlinear differential equation; it is to be solved subject to prescribed conditions for the surface heights and/or the slopes at the end points. We observe that the scalar quantity Φ appears in (3.1j), but from (3.1a) it is determined only up to an arbitrary additive constant.

This constant and the plane on which $z = 0$ are fixed by the condition that the total volume below the free surface is conserved:

$$\int_{\hat{a}}^{\hat{b}} rh(r;\Omega)\,dr = 0. \tag{3.1k}$$

It is useful to decompose the axisymmetric velocity $\mathbf{u}$ into physical components as follows:

$$\mathbf{u} = v(r,z)\,\mathbf{e}_\theta + \mathbf{q} \tag{3.2}$$

and

$$\mathbf{q} = u(r,z)\,\mathbf{e}_r + w(r,z)\,\mathbf{e}_z, \tag{3.3}$$

where $\mathbf{q}$ may be found from a stream function $\psi(r,z)$, namely,

$$\mathbf{q} = \mathbf{e}_\theta \times \frac{1}{r}\nabla\psi = \mathbf{e}_r \frac{1}{r}\frac{\partial\psi}{\partial z} - \mathbf{e}_z \frac{1}{r}\frac{\partial\psi}{\partial r}. \tag{3.4}$$

It is also convenient to decompose $\mathbf{S}$ as follows:

$$\mathbf{S} = \mu\mathbf{A}_1[\mathbf{u}] + \tilde{\mathbf{S}}[\mathbf{u}] \tag{3.5a}$$

and

$$\tilde{\mathbf{S}}[\mathbf{u}] = \bar{\mathbf{S}}_2[\mathbf{u},\mathbf{u}] + \bar{\mathbf{S}}_3[\mathbf{u},\mathbf{u},\mathbf{u}] + \bar{\mathbf{S}}_4[\mathbf{u},\mathbf{u},\mathbf{u},\mathbf{u}] + \ldots, \tag{3.5b}$$

where the $\bar{\mathbf{S}}_n[\mathbf{u},\mathbf{u},\ldots,\mathbf{u}]$ are homogeneous functionals of degree n in $\mathbf{u}$. Then, noting that Φ and the physical components of the extra stress $\mathbf{S}$ are independent of θ, the dynamic equation (3.1*a*) may be replaced by the equivalent set of equations in $\mathscr{V}_\Omega$:

$$\mu\hat{\mathscr{L}}v = \rho\left(\mathbf{q}\cdot\nabla v + \frac{uv}{r}\right) - \frac{1}{r^2}\frac{\partial}{\partial r}(r^2\tilde{S}_{r\theta}) - \frac{\partial\tilde{S}_{z\theta}}{\partial z}, \tag{3.6a}$$

$$\mu\hat{\mathscr{L}}u - \frac{\partial\Phi}{\partial r} = \rho\left(\mathbf{q}\cdot\nabla u - \frac{v^2}{r}\right) - \frac{\partial\tilde{S}_{rr}}{\partial r} - \frac{\partial\tilde{S}_{rz}}{\partial z} - \frac{1}{r}(\tilde{S}_{rr} - \tilde{S}_{\theta\theta}), \tag{3.6b}$$

$$\mu\nabla^2 w - \frac{\partial\Phi}{\partial z} = \rho\mathbf{q}\cdot\nabla w - \frac{\partial\tilde{S}_{rz}}{\partial r} - \frac{\partial\tilde{S}_{zz}}{\partial z} - \frac{1}{r}\tilde{S}_{rz}, \tag{3.6c}$$

where

$$\nabla^2(\ ) = \frac{1}{r}\frac{\partial}{\partial r}\left(r\frac{\partial(\ )}{\partial r}\right) + \frac{\partial^2(\ )}{\partial z^2}, \quad \hat{\mathscr{L}}(\ ) = \nabla^2(\ ) - \frac{(\ )}{r^2}.$$

The boundary conditions are

$$v(\hat{a},z) = \Omega\hat{a}, \quad v(\hat{b},z) = \lambda\Omega\hat{b}, \tag{3.7a}$$

$$u(\hat{a},z) = u(\hat{b},z) = 0, \quad w(\hat{a},z) = w(\hat{b},z) = 0. \tag{3.7b,c}$$

We next express the free-surface conditions in cylindrical co-ordinates, and we find that (3.1*d*, *e*, *f*) become

$$w - (dh/dr)\,u = 0, \tag{3.8a}$$

$$\left(\mu\frac{\partial v}{\partial z} + \tilde{S}_{z\theta}\right) - \frac{dh}{dr}\left(\mu\left(\frac{\partial v}{\partial r} - \frac{v}{r}\right) + \tilde{S}_{r\theta}\right) = 0, \tag{3.8b}$$

$$h'(S_{zz} - S_{rr}) + \mu\left(\frac{\partial w}{\partial r} + \frac{\partial u}{\partial z}\right) + \tilde{S}_{zr} - h'^2 S_{rz} = 0 \tag{3.8c}$$

at $z = h(r;\Omega)$. Likewise, (3.1g, h, i) can be written as

$$w = \mu\frac{\partial v}{\partial z} + \tilde{S}_{z\theta} = \mu\left(\frac{\partial w}{\partial r} + \frac{\partial u}{\partial z}\right) + \tilde{S}_{zr} = 0 \quad \text{as} \quad z \to -\infty. \tag{3.9a, b, c}$$

Finally, we use the condition that $S_{nt} = 0$ on $z = h(r;\Omega)$ to express S_{nn} as

$$S_{nn} = S_{zz} - h'S_{zr};$$

thus (3.1j) becomes

$$\frac{T}{r}\left(\frac{rh'}{(1+h'^2)^{\frac{1}{2}}}\right)' - \rho gh + \Phi + \frac{2\mu}{r}\frac{\partial^2\psi}{\partial r\,\partial z} - \tilde{S}_{zz} + h'S_{zr} = 0 \tag{3.10}$$

at $z = h(r;\Omega)$. The boundary conditions for $h(r;\Omega)$ are selected from the following four possibilities:

$$dh(\hat{a};\Omega)/dr = dh(\hat{b};\Omega)/dr = 0, \tag{3.11a}$$

$$h(\hat{a};\Omega) = h(\hat{b};\Omega) = 0, \tag{3.11b}$$

$$dh(\hat{a};\Omega)/dr = h(\hat{b};\Omega) = 0 \tag{3.11c}$$

and

$$h(\hat{a};\Omega) = dh(\hat{b};\Omega)/dr = 0. \tag{3.11d}$$

Φ is made definite by imposing the condition of constant volume (3.1k).

Equations (3.6)–(3.10) were derived by Joseph & Fosdick (1973) but the solutions developed there are incomplete for reasons already specified in § 1.

Now we shall derive the perturbation equations, skipping all but the most essential details.

4. Domain perturbations

A formal solution of (3.6)–(3.11) can be obtained as a series in powers of Ω whose coefficients are derivatives of the solution evaluated in the rest state. In the rest state all of the components of the stress and velocity, the head and $h(r;0)$ vanish identically. In addition, a simple consideration of symmetry of the problem with respect to a change in the sign of Ω shows that

$$v, S_{z\theta}, S_{r\theta} \text{ are odd functions of } \Omega \tag{4.1}$$

satisfying (3.6a), (3.7a), (3.8b) and (3.9b), whereas

$$u, w, \Phi, h, S_{zz}, S_{rr}, S_{\theta\theta}, S_{rz} \text{ are even functions of } \Omega \tag{4.2}$$

satisfying (3.6b, c), (3.7b, c), (3.8a, c), (3.9a, c), (3.10) and (3.11).

Analytic solutions of (3.6)–(3.11) and (4.1) and (4.2) must therefore be of the form

$$v(r,z;\Omega) = \sum_{n=1}\frac{\Omega^{2n-1}}{(2n-1)!}v^{[2n-1]}(r_0,z_0) \tag{4.3}$$

and

$$\begin{pmatrix}\psi(r,z;\Omega)\\ \Phi(r,z;\Omega)\\ h(r;\Omega)\end{pmatrix} = \sum_{n=1}\frac{\Omega^{2n}}{(2n)!}\begin{pmatrix}\psi^{[2n]}(r_0,z_0)\\ \Phi^{[2n]}(r_0,z_0)\\ h^{[2n]}(r_0)\end{pmatrix}, \tag{4.4}$$

where (r_0, z_0) are the co-ordinates of the rest state defined in

$$\mathscr{V}_0 = \{r_0, \theta_0, z_0 | \hat{a} \leqslant r_0 \leqslant \hat{b}, 0 \leqslant \theta_0 \leqslant 2\pi, -\infty < z_0 \leqslant 0\}.$$

The co-ordinates (r_0, z_0) are related to (r, z) by an invertible *shifting transformation*

$$r = r_0, \quad \theta = \theta_0, \quad z = z_0 + h(r_0; \Omega), \tag{4.5}$$

which maps boundary points $z = h$ in $\mathscr{V}_\Omega$ into boundary points in $\mathscr{V}_0$. The substantial derivatives on the right of (4.3) and (4.4) are taken with respect to Ω at $\Omega = 0$ with r_0 and z_0 fixed.

It is also possible to express the solution in a series of partial derivatives defined in $\mathscr{V}_\Omega$:

$$v(r, z; \Omega) = \sum_{n=1} \frac{\Omega^{2n-1}}{(2n-1)!} v^{\langle 2n-1 \rangle}(r, z) \tag{4.6}$$

and

$$\begin{pmatrix} \psi(r, z; \Omega) \\ \Phi(r, z; \Omega) \\ h(r; \Omega) \end{pmatrix} = \sum_{n=1} \frac{\Omega^{2n}}{(2n)!} \begin{pmatrix} \psi^{\langle 2n \rangle}(r, z) \\ \Phi^{\langle 2n \rangle}(r, z) \\ h^{\langle 2n \rangle}(r) \end{pmatrix}, \tag{4.7}$$

where the derivatives indicated by the angle brackets are taken with respect to Ω at $\Omega = 0$ with r and z fixed. Since $r = r_0$, $h^{\langle 2n \rangle}(r) = h^{[2n]}(r_0)$; but though the series on the right of (4.3) and (4.4) and of (4.6) and (4.7) represent the same functions they are not equal term by term. To be more precise, we note that

$$v^{[n]}(r_0, z_0) = \frac{d^n}{d\Omega^n} v(r(r_0, z_0; \Omega), z(r_0, z_0; \Omega); \Omega)|_{\Omega=0}$$

is a derivative at $\Omega = 0$ with r_0 and z_0 fixed while

$$v^{\langle n \rangle}(r, z) = \frac{\partial^n}{\partial \Omega^n} v(r, z; \Omega)|_{\Omega=0}$$

is a derivative at $\Omega = 0$ with r and z fixed. The two derivative operators $(\ )^{\langle n \rangle}$ and $(\ )^{[n]}$ are related through the chain rule

$$\frac{d^n}{d\Omega^n} v(r, z; \Omega) = \left(\frac{\partial}{\partial \Omega} + \frac{dr}{d\Omega} \frac{\partial}{\partial r} + \frac{dz}{d\Omega} \frac{\partial}{\partial z} \right)^n v = \left(\frac{\partial}{\partial \Omega} + \frac{dh}{d\Omega} \frac{\partial}{\partial z} \right)^n v. \tag{4.8}$$

Since $h^{[1]} = h^{[3]} = 0$ by symmetry and by use of (4.8), we can obtain the explicit formulae relating $(\ )^{\langle n \rangle}$ and $(\ )^{[n]}$ for $n = 1, 2, 3$ and 4:

$$(\ )^{[1]} = (\ )^{\langle 1 \rangle}, \tag{4.9a}$$

$$(\ )^{[2]} = (\ )^{\langle 2 \rangle} + h^{[2]} \left\{ \frac{\partial (\ )}{\partial z} \right\}^{\langle 0 \rangle}, \tag{4.9b}$$

$$(\ )^{[3]} = (\ )^{\langle 3 \rangle} + 3h^{[2]} \left\{ \frac{\partial (\ )}{\partial z} \right\}^{\langle 1 \rangle}, \tag{4.9c}$$

$$(\ )^{[4]} = (\ )^{\langle 4 \rangle} + h^{[4]} \left\{ \frac{\partial (\ )}{\partial z} \right\}^{\langle 0 \rangle} + 6h^{[2]} \left\{ \frac{\partial (\ )}{\partial z} \right\}^{\langle 2 \rangle} + 3(h^{[2]})^2 \left\{ \frac{\partial^2 (\ )}{\partial z^2} \right\}^{\langle 0 \rangle}. \tag{4.9d}$$

In general $v^{\langle n \rangle}(r, z) \neq v^{[n]}(r_0, z_0)$, but

$$\sum_{n=1} \frac{\Omega^{2n-1}}{(2n-1)!} v^{[2n-1]}(r, z - h(r; \Omega)) = \sum_{n=1} \frac{\Omega^{2n-1}}{(2n-1)!} v^{\langle 2n-1 \rangle}(r, z).$$

In the computational algorithm for the series solution (4.3) and (4.4), we solve problems for the functions $v^{\langle 2n-1\rangle}(r_0, z_0)$, $\psi^{\langle 2n\rangle}(r_0, z_0)$, $\Phi^{\langle 2n\rangle}(r_0, z_0)$ and $h^{[2n]}(r_0)$ defined on the convenient reference domain $\mathscr{V}_0$. Then we form the substantial derivatives $v^{[2n-1]}(r_0, z_0)$, $\psi^{[2n]}(r_0, z_0)$, $\Phi^{[2n]}(r_0, z_0)$ and $h^{[2n]}(r_0)$ using the differentiation formulae (4.9). The series solutions (4.3) and (4.4) are then obtained by setting $r_0 = r$ and

$$z_0 = z - h(r; \Omega).$$

5. Perturbation equations

Our main task now is to compute the coefficients appearing in (4.3) and (4.4) up to $O(\Omega^4)$. The equations governing these coefficients are nearly the same as those already derived by Joseph & Fosdick (1973). We shall not repeat all the details of the derivations already developed there. It is necessary, however, to make provision for the effects of surface tension, which were not considered in the equations at orders higher than two, and to list the equations up to order four whose solution is our main goal.

The computation of the series (4.3) and (4.4) is greatly simplified by using the symmetry properties (4.1) and (4.2). At zeroth order there is no motion and the free surface is flat: $v^{[0]} = \psi^{[0]} = \Phi^{[0]} = h^{[0]} = 0$. At order Ω, a circumferential velocity independent of z appears: $\psi^{\langle 1\rangle} = \Phi^{\langle 1\rangle} = h^{\langle 1\rangle} = 0$ and

$$v^{\langle 1\rangle} = \hat{A} r_0 + \frac{\hat{B}}{r_0}, \quad \hat{A} = \frac{\hat{b}^2\lambda - \hat{a}^2}{\hat{b}^2 - \hat{a}^2}, \quad \hat{B} = \frac{\hat{a}^2\hat{b}^2(1-\lambda)}{\hat{b}^2 - \hat{a}^2}. \tag{5.1}$$

The inhomogeneous terms which arise at second order may be balanced by a gradient (see Joseph & Fosdick 1973). We find that $v^{\langle 2\rangle} = \psi^{\langle 2\rangle} = 0$ and a short calculation (see Joseph & Fosdick 1973; or Beavers & Joseph 1975) shows that

$$\tilde{\mathbf{S}}^{\langle 2\rangle} = \bar{\mathbf{S}}_2^{\langle 2\rangle} = \alpha_1 \mathbf{A}_2^{\langle 2\rangle} + 2\alpha_2 \mathbf{A}_1^{\langle 1\rangle 2}, \tag{5.2}$$

where

$$\mathbf{A}_1^{\langle 1\rangle} = -2\hat{B} r_0^{-2} (\mathbf{e}_r \otimes \mathbf{e}_\theta + \mathbf{e}_\theta \otimes \mathbf{e}_r), \tag{5.3}$$

$\otimes$ stands for the dyadic product and

$$\mathbf{A}_2^{\langle 2\rangle} = 16 r_0^{-4} \hat{B}^2 \mathbf{e}_r \otimes \mathbf{e}_r. \tag{5.4}$$

The solution for $\Phi^{\langle 2\rangle}$ is (Joseph & Fosdick 1973)

$$\Phi^{\langle 2\rangle} = \rho \left(\hat{A}^2 r_0^2 + 4\hat{A}\hat{B} \log \frac{r_0}{\hat{a}} - \frac{\hat{B}^2}{r_0^2} \right) + 4(3\alpha_1 + 2\alpha_2) \frac{\hat{B}^2}{r_0^4} + C_2, \tag{5.5}$$

where C_2 can be determined from the condition

$$T \left(r_0 \frac{dh^{[2]}}{dr_0} \right)_{\hat{a}}^{\hat{b}} + \int_{\hat{a}}^{\hat{b}} r_0 \, \Phi^{\langle 2\rangle}(r_0) \, dr_0 = 0,$$

which arises from (3.1 k) and (3.10). Hence

$$\begin{aligned} \Phi^{\langle 2\rangle} = \rho \Bigg\{ & \hat{A}^2 \left(r_0^2 - \frac{\hat{a}^2 + \hat{b}^2}{2} \right) + 4\hat{A}\hat{B} \left(\log \frac{r_0}{\hat{a}} - \frac{\hat{b}^2 \log(\hat{b}/\hat{a})}{\hat{b}^2 - \hat{a}^2} + \tfrac{1}{2} \right) \\ & - \hat{B}^2 \left(\frac{1}{r_0^2} - \frac{2\log(\hat{b}/\hat{a})}{\hat{b}^2 - \hat{a}^2} \right) \Bigg\} + 4(3\alpha_1 + 2\alpha_2) \hat{B}^2 \left(\frac{1}{r_0^4} - \frac{1}{\hat{a}^2\hat{b}^2} \right) \\ & - \frac{2T}{\hat{b}^2 - \hat{a}^2} \left\{ \hat{b} \frac{dh^{[2]}}{dr_0}(\hat{b}) - \hat{a} \frac{dh^{[2]}}{dr_0}(\hat{a}) \right\}. \end{aligned} \tag{5.6}$$

Finally, at second order (3.10) becomes

$$\frac{T}{r_0}\frac{d}{dr_0}\left(r_0\frac{dh^{[2]}}{dr_0}\right)-\rho g h^{[2]}+\Phi^{\langle 2\rangle}=0 \quad \text{at} \quad z=0, \tag{5.7}$$

where $h^{[2]}$ satisfies one of the pairs of end-point conditions (3.11).

We are now ready to calculate the solution at order three. When account is taken of the fact that $v^{\langle 1\rangle}(r_0)$ is independent of z_0 and that $\psi^{\langle 1\rangle}=\Phi^{\langle 1\rangle}=0$, we find from (4.9) that $(\ )^{[3]}=(\ )^{\langle 3\rangle}$. Considering the homogeneity of $\bar{\mathbf{S}}_n$ and using $\mathbf{u}^{\langle 0\rangle}=0$ we obtain

$$\tilde{\mathbf{S}}^{\langle 3\rangle}=\bar{\mathbf{S}}_2^{\langle 3\rangle}+\bar{\mathbf{S}}_3^{\langle 3\rangle}+\bar{\mathbf{S}}_4^{\langle 3\rangle}+\ldots=\bar{\mathbf{S}}_2^{\langle 3\rangle}+\bar{\mathbf{S}}_3^{\langle 3\rangle}, \tag{5.8}$$

where the $\bar{\mathbf{S}}_n=\mathbf{S}_n$ are given by (2.3). To determine $\bar{\mathbf{S}}_2^{\langle 3\rangle}$ and $\bar{\mathbf{S}}_3^{\langle 3\rangle}$ we first note that $\mathbf{u}^{\langle 2\rangle}=0$ leads to $\mathbf{A}_1^{\langle 2\rangle}=0$. Then $\mathbf{A}_1^{\langle 0\rangle}=\mathbf{A}_1^{\langle 2\rangle}=0$ and $\mathbf{u}^{\langle 0\rangle}=\mathbf{u}^{\langle 2\rangle}=0$ yield $\mathbf{A}_2^{\langle 3\rangle}=0$. It follows that $\mathbf{S}_2^{\langle 3\rangle}=0$ and

$$\mathbf{S}_3^{\langle 3\rangle}=\beta_1\mathbf{A}_3^{\langle 3\rangle}+3\{\beta_2(\mathbf{A}_2^{\langle 2\rangle}\mathbf{A}_1^{\langle 1\rangle}+\mathbf{A}_1^{\langle 1\rangle}\mathbf{A}_2^{\langle 2\rangle})+\beta_3(\operatorname{tr}\mathbf{A}_2^{\langle 2\rangle})\mathbf{A}_1^{\langle 1\rangle}\}. \tag{5.9}$$

Similarly, using $\mathbf{u}^{\langle 0\rangle}=\mathbf{u}^{\langle 2\rangle}=0$ and $\mathbf{A}_1^{\langle 0\rangle}=\mathbf{A}_2^{\langle 0\rangle}=\mathbf{A}_2^{\langle 1\rangle}=0$, we derive from (2.2$b$) for $n=2$ that

$$\mathbf{A}_3^{\langle 3\rangle}=3\{(\operatorname{grad}\mathbf{A}_2^{\langle 2\rangle})\,\mathbf{u}^{\langle 1\rangle}+\mathbf{A}_2^{\langle 2\rangle}\operatorname{grad}\mathbf{u}^{\langle 1\rangle}+(\operatorname{grad}\mathbf{u}^{\langle 1\rangle})^{\mathrm{T}}\mathbf{A}_2^{\langle 2\rangle}\}.$$

Substituting $\mathbf{u}^{\langle 1\rangle}=v^{\langle 1\rangle}\mathbf{e}_\theta$, (5.3) and (5.4) in the above equation, we observe that $\mathbf{A}_3^{\langle 3\rangle}=0$ and compute

$$\mathbf{S}_3^{\langle 3\rangle}=-96r_0^{-6}\hat{B}^3(\beta_2+\beta_3)\,(\mathbf{e}_r\otimes\mathbf{e}_\theta+\mathbf{e}_\theta\otimes\mathbf{e}_r), \tag{5.10}$$

where β_2 and β_3 are constants of the fluid of grade three.

To find the problem at third order, we differentiate (3.6a), (3.7a), (3.8b) and (3.9b) three times with respect to Ω and set $\Omega=0$, using $\mathbf{u}^{\langle 2\rangle}=0$ and (5.10). We find that

$$\hat{\mathscr{L}}v^{\langle 3\rangle}=-384\frac{(\beta_2+\beta_3)}{\mu}\frac{\hat{B}^3}{r_0^7} \quad \text{in} \quad \mathscr{V}_0, \tag{5.11}$$

$$v^{\langle 3\rangle}(\hat{a},z_0)=v^{\langle 3\rangle}(\hat{b},z_0)=0, \tag{5.12}$$

$$\frac{\partial v^{\langle 3\rangle}}{\partial z_0}-3\frac{dh^{[2]}}{dr_0}\left(\frac{\partial v^{\langle 1\rangle}}{\partial r_0}-\frac{v^{\langle 1\rangle}}{r_0}\right)=\frac{\partial v^{\langle 3\rangle}}{\partial z_0}+\frac{6\hat{B}}{r_0^2}\frac{dh^{[2]}}{dr_0}=0 \quad \text{at} \quad z_0=0, \tag{5.13}$$

$$\partial v^{\langle 3\rangle}/\partial z_0\to 0 \quad \text{as} \quad z_0\to-\infty. \tag{5.14}$$

The solution to the above problem can be decomposed into two parts:

$$v^{\langle 3\rangle}(r_0,z_0)=v_1^{\langle 3\rangle}(r_0)+v_2^{\langle 3\rangle}(r_0,z_0), \tag{5.15}$$

where

$$\frac{1}{r_0}\frac{d}{dr_0}\left(r_0\frac{dv_1^{\langle 3\rangle}}{dr_0}\right)-\frac{v_1^{\langle 3\rangle}}{r_0^2}=-384\frac{(\beta_2+\beta_3)}{\mu}\frac{\hat{B}^3}{r_0^7}, \tag{5.16a}$$

$$v_1^{\langle 3\rangle}(\hat{a})=v_1^{\langle 3\rangle}(\hat{b})=0, \tag{5.16b}$$

$$\hat{\mathscr{L}}v_2^{\langle 3\rangle}=0, \quad v_2^{\langle 3\rangle}(\hat{a},z_0)=v_2^{\langle 3\rangle}(\hat{b},z_0)=0, \tag{5.17a,b}$$

$$\frac{\partial v_2^{\langle 3\rangle}}{\partial z_0}=-\frac{6\hat{B}}{r_0^2}\frac{dh^{[2]}}{dr_0} \quad \text{at} \quad z_0=0 \tag{5.17c}$$

and

$$\partial v_2^{\langle 3\rangle}/\partial z_0\to 0 \quad \text{as} \quad z_0\to-\infty. \tag{5.17d}$$

The solution of the problem (5.16) can be easily obtained:

$$v_1^{\langle 3\rangle}(r_0) = -\frac{16(\beta_2+\beta_3)}{\mu}\hat{B}^3\left(\frac{1}{r_0^5}+\frac{\hat{a}^2+\hat{b}^2}{\hat{a}^4\hat{b}^4}r_0-\frac{\hat{a}^4+\hat{b}^4+\hat{a}^2\hat{b}^2}{\hat{a}^4\hat{b}^4 r_0}\right). \tag{5.18}$$

The problem (5.17) is an eigenvalue problem for which the solution can be written as

$$v_2^{\langle 3\rangle}(r_0, z_0) = \sum_{n=1}^{\infty}\hat{B}_n \exp(\hat{\lambda}_n z)\,[J_1(\hat{\lambda}_n\hat{a})\,Y_1(\hat{\lambda}_n r_0) - J_1(\hat{\lambda}_n r_0)\,Y_1(\hat{\lambda}_n\hat{a})], \tag{5.19a}$$

where J_1 and Y_1 are Bessel functions of the first and second kinds of order 1, $\hat{\lambda}_n$ is an eigenvalue of

$$J_1(\hat{\lambda}_n\hat{a})\,Y_1(\hat{\lambda}_n\hat{b}) - J_1(\hat{\lambda}_n\hat{b})\,Y_1(\hat{\lambda}_n\hat{a}) = 0, \tag{5.19b}$$

and

$$\hat{B}_n = \frac{\pi^2\hat{\lambda}_n}{2}\frac{[J_1(\hat{\lambda}_n\hat{b})]^2}{[J_1(\hat{\lambda}_n\hat{a})]^2 - [J_1(\hat{\lambda}_n\hat{b})]^2} \times\left\{-6\hat{B}\int_{\hat{a}}^{\hat{b}}\frac{1}{r_0}\frac{dh^{[2]}}{dr_0}(r_0)\,[J_1(\hat{\lambda}_n\hat{a})\,Y_1(\hat{\lambda}_n r_0) - J_1(\hat{\lambda}_n r_0)\,Y_1(\hat{\lambda}_n\hat{a})]\,dr_0\right\}. \tag{5.19c}$$

We note that when $dh^{[2]}(r_0)/dr_0$ has been determined $v_2^{\langle 3\rangle}(r_0, z_0)$ is given explicitly by (5.19).

The secondary motion, which appears first at fourth order, arises from the torque generated by $v_2^{\langle 3\rangle}(r_0, z_0)$. To begin with, we use the results that $\mathbf{u}^{\langle 2\rangle} = 0$ and that $\Phi^{\langle 2\rangle}(r_0)$ is independent of z_0 in $\mathscr{V}_0$ to find from (4.9) that $(\ )^{[4]} = (\ )^{\langle 4\rangle}$. Using the homogeneity of $\mathbf{S}_n$ and the rest-state solution, we establish that

$$\tilde{\mathbf{S}}^{\langle 4\rangle} = \bar{\mathbf{S}}_2^{\langle 4\rangle} + \bar{\mathbf{S}}_3^{\langle 4\rangle} + \bar{\mathbf{S}}_4^{\langle 4\rangle} + \ldots = \bar{\mathbf{S}}_2^{\langle 4\rangle} + \bar{\mathbf{S}}_3^{\langle 4\rangle} + \bar{\mathbf{S}}_4^{\langle 4\rangle}, \tag{5.20}$$

where $\mathbf{S}_n = \mathbf{S}_n$ are given by (2.3). Using $\mathbf{A}_2^{\langle 0\rangle} = \mathbf{A}_2^{\langle 1\rangle} = \mathbf{A}_2^{\langle 3\rangle} = 0$ and $\mathbf{u}^{\langle 0\rangle} = \mathbf{u}^{\langle 2\rangle} = 0$, we have $\mathbf{A}_3^{\langle 4\rangle} = 0$. Then it follows immediately from

$$\mathbf{A}_3^{\langle 0\rangle} = \mathbf{A}_3^{\langle 1\rangle} = \mathbf{A}_3^{\langle 2\rangle} = \mathbf{A}_2^{\langle 3\rangle} = \mathbf{A}_3^{\langle 3\rangle} = 0$$

that $\mathbf{A}_4^{\langle 4\rangle} = 0$.

We differentiate (2.3*b*, *c*, *d*) four times with respect to Ω and set $\Omega = 0$; then, collecting all the results established in the last paragraph, we find

$$\mathbf{S}_2^{\langle 4\rangle} = \alpha_1\mathbf{A}_2^{\langle 4\rangle} + 4\alpha_2(\mathbf{A}_1^{\langle 1\rangle}\mathbf{A}_1^{\langle 3\rangle} + \mathbf{A}_1^{\langle 3\rangle}\mathbf{A}_1^{\langle 1\rangle}), \tag{5.21a}$$

$$\mathbf{S}_3^{\langle 4\rangle} = 0, \tag{5.21b}$$

$$\mathbf{S}_4^{\langle 4\rangle} = 6\gamma_3\mathbf{A}_2^{\langle 2\rangle 2} + 12\gamma_4(\mathbf{A}_2^{\langle 2\rangle}\mathbf{A}_1^{\langle 1\rangle 2} + \mathbf{A}_1^{\langle 1\rangle 2}\mathbf{A}_2^{\langle 2\rangle}) + 6\gamma_5(\operatorname{tr}\mathbf{A}_2^{\langle 2\rangle})\mathbf{A}_2^{\langle 2\rangle} + 12\gamma_6(\operatorname{tr}\mathbf{A}_2^{\langle 2\rangle})\mathbf{A}_1^{\langle 1\rangle 2} + 12\gamma_8(\operatorname{tr}\mathbf{A}_2^{\langle 2\rangle}\mathbf{A}_1^{\langle 1\rangle})\mathbf{A}_1^{\langle 1\rangle}, \tag{5.21c}$$

where

$$\mathbf{A}_1^{\langle 3\rangle} = \operatorname{grad}\mathbf{u}^{\langle 3\rangle} + (\operatorname{grad}\mathbf{u}^{\langle 3\rangle})^{\mathrm{T}} \tag{5.22a}$$

and

$$\mathbf{A}_2^{\langle 4\rangle} = 4\{(\operatorname{grad}\mathbf{A}_1^{\langle 3\rangle})\,\mathbf{u}^{\langle 1\rangle} + (\operatorname{grad}\mathbf{A}_1^{\langle 1\rangle})\,\mathbf{u}^{\langle 3\rangle} + \mathbf{A}_1^{\langle 3\rangle}\operatorname{grad}\mathbf{u}^{\langle 1\rangle} + \mathbf{A}_1^{\langle 1\rangle}\operatorname{grad}\mathbf{u}^{\langle 3\rangle} + (\operatorname{grad}\mathbf{u}^{\langle 3\rangle})^{\mathrm{T}}\mathbf{A}_1^{\langle 1\rangle} + (\operatorname{grad}\mathbf{u}^{\langle 1\rangle})^{\mathrm{T}}\mathbf{A}_1^{\langle 3\rangle}\}. \tag{5.22b}$$

Since $\mathbf{u}^{\langle 3\rangle} = v^{\langle 3\rangle}(r_0, z_0)\,\mathbf{e}_\theta$, we may write

$$\operatorname{grad}\mathbf{u}^{\langle 3\rangle} = \mathbf{e}_\theta \otimes \nabla v^{\langle 3\rangle} - \frac{v^{\langle 3\rangle}}{r}\mathbf{e}_r \otimes \mathbf{e}_\theta \tag{5.23}$$

and thus

$$\mathbf{A}_1^{\langle 3\rangle} = \left(\frac{\partial v^{\langle 3\rangle}}{\partial r} - \frac{v^{\langle 3\rangle}}{r}\right)(\mathbf{e}_\theta \otimes \mathbf{e}_r + \mathbf{e}_r \otimes \mathbf{e}_\theta) + \frac{\partial v^{\langle 3\rangle}}{\partial z}(\mathbf{e}_\theta \otimes \mathbf{e}_z + \mathbf{e}_z \otimes \mathbf{e}_\theta). \tag{5.24}$$

Substituting $\mathbf{u}^{\langle 1\rangle} = v^{\langle 1\rangle}(r_0)\,\mathbf{e}_\theta$, $\mathbf{u}^{\langle 3\rangle} = v^{\langle 3\rangle}(r_0, z_0)\,\mathbf{e}_\theta$, (5.23) and (5.24) into (5.22*b*), we find that

$$\mathbf{A}_2^{\langle 4\rangle} = -\frac{16\hat{B}}{r_0^2}\left(\mathbf{e}_r \otimes \nabla v^{\langle 3\rangle} + \nabla v^{\langle 3\rangle} \otimes \mathbf{e}_r - \frac{2v^{\langle 3\rangle}}{r}\,\mathbf{e}_r \otimes \mathbf{e}_r\right). \tag{5.25}$$

Hence we may compute from (5.3), (5.21*a*), (5.24) and (5.25)

$$\mathbf{S}_2^{\langle 4\rangle} = -\frac{8\hat{B}}{r_0^2}(2\alpha_1 + \alpha_2)\left(\mathbf{e}_r \otimes \nabla v^{\langle 3\rangle} + \nabla v^{\langle 3\rangle} \otimes \mathbf{e}_r - 2\frac{v^{\langle 3\rangle}}{r}\,\mathbf{e}_r \otimes \mathbf{e}_r\right) - \frac{16\hat{B}}{r_0^2}\alpha_2\left(\frac{\partial v^{\langle 3\rangle}}{\partial r} - \frac{v^{\langle 3\rangle}}{r}\right)\mathbf{e}_\theta \otimes \mathbf{e}_\theta. \tag{5.26}$$

Finally, from (5.3) and (5.4), we reduce (5.21*c*) to

$$\mathbf{S}_4^{\langle 4\rangle} = \frac{1536}{r_0^8}\hat{B}^4(\gamma_3 + \gamma_4 + \gamma_5 + \tfrac{1}{2}\gamma_6)\,\mathbf{e}_r \otimes \mathbf{e}_r + \frac{768}{r_0^8}\hat{B}^4\gamma_6\,\mathbf{e}_\theta \otimes \mathbf{e}_\theta \tag{5.27}$$

and thus conclude that

$$\tilde{\mathbf{S}}^{\langle 4\rangle} = \left\{-\frac{16\hat{B}}{r_0^2}(2\alpha_1 + \alpha_2)\left(\frac{\partial v^{\langle 3\rangle}}{\partial r_0} - \frac{v^{\langle 3\rangle}}{r_0}\right) + \frac{1536}{r_0^8}\hat{B}^4(\gamma_3 + \gamma_4 + \gamma_5 + \tfrac{1}{2}\gamma_6)\right\}\mathbf{e}_r \otimes \mathbf{e}_r - \frac{8\hat{B}}{r_0^2}(2\alpha_1 + \alpha_2)\frac{\partial v^{\langle 3\rangle}}{\partial z_0}(\mathbf{e}_r \otimes \mathbf{e}_z + \mathbf{e}_z \otimes \mathbf{e}_r) + \left\{-\frac{16\hat{B}}{r_0^2}\alpha_2\left(\frac{\partial v^{\langle 3\rangle}}{\partial r_0} - \frac{v^{\langle 3\rangle}}{r_0}\right) + \frac{768}{r_0^8}\hat{B}^4\gamma_6\right\}\mathbf{e}_\theta \otimes \mathbf{e}_\theta. \tag{5.28}$$

By symmetry, we have $v^{[4]} = v^{\langle 4\rangle} = 0$. Using the results $\mathbf{u}^{\langle 0\rangle} = \mathbf{q}^{\langle 1\rangle} = \mathbf{u}^{\langle 2\rangle} = \mathbf{q}^{\langle 3\rangle} = 0$, we obtain

$$\mu\hat{\mathscr{L}}\left(\frac{1}{r_0}\frac{\partial \psi^{\langle 4\rangle}}{\partial z_0}\right) - \frac{\partial \Phi^{\langle 4\rangle}}{\partial r_0} = -8\rho\frac{v^{\langle 1\rangle}v^{\langle 3\rangle}}{r_0} - \frac{\partial \tilde{S}_{rr}^{\langle 4\rangle}}{\partial r_0} - \frac{\partial \tilde{S}_{rz}^{\langle 4\rangle}}{\partial z_0} - \frac{1}{r_0}(\tilde{S}_{rr}^{\langle 4\rangle} - \tilde{S}_{\theta\theta}^{\langle 4\rangle}), \tag{5.29a}$$

$$\mu\nabla^2\left(-\frac{1}{r_0}\frac{\partial \psi^{\langle 4\rangle}}{\partial r_0}\right) - \frac{\partial \Phi^{\langle 4\rangle}}{\partial z_0} = -\frac{\partial \tilde{S}_{rz}^{\langle 4\rangle}}{\partial r_0} - \frac{1}{r_0}\tilde{S}_{rz}^{\langle 4\rangle}, \tag{5.29b}$$

$$\psi^{\langle 4\rangle}(\hat{a}, z_0) = \psi^{\langle 4\rangle}(\hat{b}, z_0) = 0, \tag{5.30a}$$

$$\partial\psi^{\langle 4\rangle}(\hat{a}, z_0)/\partial r_0 = \partial\psi^{\langle 4\rangle}(\hat{b}, z_0)/\partial r_0 = 0, \tag{5.30b}$$

$$\partial\psi^{\langle 4\rangle}(r_0, 0)/\partial r_0 = -\partial^2\psi^{\langle 4\rangle}(r_0, 0)/\partial z_0^2 = 0, \tag{5.31a, b}$$

$$\partial\psi^{\langle 4\rangle}/\partial r_0 = -\partial^2\psi^{\langle 4\rangle}/\partial z_0^2 \to 0 \quad \text{as} \quad z_0 \to -\infty, \tag{5.32a, b}$$

where to derive (5.31*b*) and (5.32*b*) we have made use of (5.13) and the conditions $\partial^2\psi^{\langle 4\rangle}(r_0, 0)/\partial r_0^2 = 0$ and $\partial^2\psi^{\langle 4\rangle}/\partial r_0^2 \to 0$ as $z_0 \to -\infty$. Also,

$$\frac{T}{r_0}(r_0 h^{[4]\prime})' - \rho g h^{[4]} + \Phi^{\langle 4\rangle} + \frac{2\mu}{r_0}\frac{\partial^2\psi^{\langle 4\rangle}}{\partial r_0\,\partial z_0} = 0 \quad \text{at} \quad z_0 = 0, \tag{5.33}$$

where $h^{[4]}$ satisfies (3.1k) and one of the conditions (3.11). Using the component expression for $\tilde{\mathbf{S}}^{\langle 4\rangle}$, we may rewrite (5.29$a$, b) as

$$\mu\hat{\mathscr{L}}\left(\frac{1}{r_0}\frac{\partial\psi^{\langle 4\rangle}}{\partial z_0}\right)-\frac{\partial\Phi^{\langle 4\rangle}}{\partial r_0}$$
$$=-8\rho\frac{v^{\langle 1\rangle}v^{\langle 3\rangle}}{r_0}+8\hat{B}(2\alpha_1+\alpha_2)\left\{\frac{1}{r_0^2}\frac{\partial^2 v^{\langle 3\rangle}}{\partial r_0^2}-5\left(\frac{1}{r_0^3}\frac{\partial v^{\langle 3\rangle}}{\partial r_0}-\frac{v^{\langle 3\rangle}}{r_0^4}\right)-384\frac{(\beta_2+\beta_3)}{\mu}\frac{\hat{B}^4}{r_0^9}\right\}$$
$$-16\hat{B}\alpha_2\left(\frac{1}{r_0^3}\frac{\partial v^{\langle 3\rangle}}{\partial r_0}-\frac{v^{\langle 3\rangle}}{r_0^4}\right)+768\gamma_6\frac{\hat{B}^4}{r_0^9}+10\,752(\gamma_3+\gamma_4+\gamma_5+\tfrac{1}{2}\gamma_6)\frac{\hat{B}^4}{r_0^9} \quad (5.34a)$$

and
$$\mu\nabla^2\left(-\frac{1}{r_0}\frac{\partial\psi^{\langle 4\rangle}}{\partial r_0}\right)-\frac{\partial\Phi^{\langle 4\rangle}}{\partial z_0}=8\hat{B}(2\alpha_1+\alpha_2)\left(-\frac{1}{r_0^3}\frac{\partial v^{\langle 3\rangle}}{\partial z_0}+\frac{1}{r_0^2}\frac{\partial^2 v^{\langle 3\rangle}}{\partial r_0\,\partial z_0}\right). \quad (5.34b)$$

Elimination of $\Phi^{\langle 4\rangle}$ from (5.34a, b) leads to

$$\mu\mathscr{L}^2\psi^{\langle 4\rangle}=-8\frac{\partial}{\partial z_0}\left\{\frac{4\hat{B}}{r_0^2}(\alpha_1+\alpha_2)\left(\frac{\partial v^{\langle 3\rangle}}{\partial r_0}-\frac{v^{\langle 3\rangle}}{r_0}\right)+\rho v^{\langle 1\rangle}v^{\langle 3\rangle}\right\}, \quad (5.35)$$

where
$$\mathscr{L}(\,)=r_0\frac{\partial}{\partial r_0}\left(\frac{1}{r_0}\frac{\partial(\,)}{\partial r_0}\right)+\frac{\partial^2(\,)}{\partial z_0^2}.$$

We remark that (5.35) with boundary conditions (5.30), (5.31) and (5.32) forms a well-posed inhomogeneous Stokes-flow problem which is uniquely invertible for $\psi^{\langle 4\rangle}(r_0, z_0)$. It is interesting that $\psi^{\langle 4\rangle}$ *is determined when the material constants for the fluid of second grade are known.*

Given $\psi^{\langle 4\rangle}$, we may compute $\Phi^{\langle 4\rangle}(r_0, z_0)$ up to an additive constant by integrating (5.34). We decompose $\Phi^{\langle 4\rangle}$ into two parts:

$$\Phi^{\langle 4\rangle}(r_0, z_0)=\Phi_1^{\langle 4\rangle}(r_0)+\Phi_2^{\langle 4\rangle}(r_0, z_0).$$

Then from (5.34a) we have

$$\frac{d\Phi_1^{\langle 4\rangle}}{dr_0}=8\rho\frac{v^{\langle 1\rangle}v_1^{\langle 3\rangle}}{r_0}-8\hat{B}(2\alpha_1+\alpha_2)\left\{\frac{1}{r_0^2}\frac{\partial^2 v_1^{\langle 3\rangle}}{\partial r_0^2}-5\left(\frac{1}{r_0^3}\frac{\partial v_1^{\langle 3\rangle}}{\partial r_0}-\frac{v_1^{\langle 3\rangle}}{r_0^4}\right)\right.$$
$$\left.-384\frac{(\beta_2+\beta_3)}{\mu}\frac{\hat{B}^4}{r_0^9}\right\}+16\hat{B}\alpha_2\left(\frac{1}{r_0^3}\frac{\partial v_1^{\langle 3\rangle}}{\partial r_0}-\frac{v_1^{\langle 3\rangle}}{r_0^4}\right)-10\,752(\gamma_3+\gamma_4+\gamma_5+\tfrac{4}{7}\gamma_6)\frac{\hat{B}^4}{r_0^9}, \quad (5.36)$$

$$\frac{\partial\Phi_2^{\langle 4\rangle}}{\partial r_0}=\mu\hat{\mathscr{L}}\left(\frac{1}{r_0}\frac{\partial\psi^{\langle 4\rangle}}{\partial z_0}\right)+8\rho\frac{v^{\langle 1\rangle}v_2^{\langle 3\rangle}}{r_0}-8\hat{B}(2\alpha_1+\alpha_2)$$
$$\times\left\{\frac{1}{r_0^2}\frac{\partial^2 v_2^{\langle 3\rangle}}{\partial r_0^2}-5\left(\frac{1}{r_0^3}\frac{\partial v_2^{\langle 3\rangle}}{\partial r_0}-\frac{v_2^{\langle 3\rangle}}{r_0^4}\right)\right\}+16\hat{B}\alpha_2\left(\frac{1}{r_0^3}\frac{\partial v_2^{\langle 3\rangle}}{\partial r_0}-\frac{v_2^{\langle 3\rangle}}{r_0^4}\right), \quad (5.37a)$$

$$\frac{\partial\Phi_2^{\langle 4\rangle}}{\partial z_0}=\mu\nabla^2\left(-\frac{1}{r_0}\frac{\partial\psi^{\langle 4\rangle}}{\partial r_0}\right)-8\hat{B}(2\alpha_1+\alpha_2)\left(-\frac{1}{r_0^3}\frac{\partial v_2^{\langle 3\rangle}}{\partial z_0}+\frac{1}{r_0^2}\frac{\partial^2 v_2^{\langle 3\rangle}}{\partial r_0\,\partial z_0}\right). \quad (5.37b)$$

If we also decompose $h^{[4]}$ into $h_1^{[4]}+h_2^{[4]}$ so that

$$\frac{T}{r_0}(r_0 h_1^{[4]\prime})'-\rho g h_1^{[4]}+\Phi_1^{\langle 4\rangle}=0 \quad (5.38a)$$

and
$$\frac{T}{r_0}(r_0 h_2^{[4]\prime})'-\rho g h_2^{[4]}+\Phi_2^{\langle 4\rangle}+\frac{2\mu}{r_0}\frac{\partial^2\psi^{\langle 4\rangle}}{\partial r_0\,\partial z_0}=0 \quad \text{at} \quad z_0=0, \quad (5.38b)$$

then the integration constants for $\Phi_1^{\langle 4\rangle}(r_0)$ and $\Phi_2^{\langle 4\rangle}(r_0, z_0)$ can be determined from the conditions

$$T\left(r_0 \frac{dh_1^{[4]}}{dr_0}\right)_{\hat{a}}^{\hat{b}} + \int_{\hat{a}}^{\hat{b}} r_0 \Phi_1^{\langle 4\rangle}(r_0)\, dr_0 = 0 \tag{5.39a}$$

and

$$T\left(r_0 \frac{dh_2^{[4]}}{dr_0}\right)_{\hat{a}}^{\hat{b}} + \int_{\hat{a}}^{\hat{b}} r_0 \Phi_2^{\langle 4\rangle}(r_0, 0)\, dr_0 = 0, \tag{5.39b}$$

which arise from the constant-volume condition and (5.38), and incorporate the fact that

$$\int_{\hat{a}}^{\hat{b}} \frac{\partial^2 \psi^{\langle 4\rangle}}{\partial r_0\, \partial z_0}\, dr_0 = \left(\frac{\partial \psi^{\langle 4\rangle}}{\partial z_0}\right)_{\hat{a}}^{\hat{b}} = 0.$$

We note that $\Phi_2^{\langle 4\rangle}$, like $\psi^{\langle 4\rangle}$, and hence $h_2^{\langle 4\rangle}$, can be determined from the material constants of the second-grade fluid. But in evaluating $\Phi_1^{\langle 4\rangle}$ and $h_1^{\langle 4\rangle}$, we need not only $\beta_2+\beta_3$ but also $\gamma_3+\gamma_4+\gamma_5+\frac{4}{7}\gamma_6$.

In summary, we have found that it is possible to express the series solution (4.3) and (4.4) up to terms $O(\Omega^4)$ as follows:

$$v(r, z; \Omega) = \Omega v^{\langle 1\rangle}(r_0) + \frac{\Omega^3}{3!}\{v_1^{\langle 3\rangle}(r_0) + v_2^{\langle 3\rangle}(r_0, z_0)\} + O(\Omega^5) \tag{5.40}$$

and

$$\begin{pmatrix} \psi(r, z; \Omega) \\ \Phi(r, z; \Omega) \\ h(r; \Omega) \end{pmatrix} = \frac{\Omega^2}{2!}\begin{pmatrix} 0 \\ \Phi^{\langle 2\rangle}(r_0) \\ h^{[2]}(r_0) \end{pmatrix} + \frac{\Omega^4}{4!}\begin{pmatrix} \psi^{\langle 4\rangle}(r_0, z_0) \\ \Phi_1^{\langle 4\rangle}(r_0) + \Phi_2^{\langle 4\rangle}(r_0, z_0) \\ h_1^{[4]}(r_0) + h_2^{[4]}(r_0) \end{pmatrix} + O(\Omega^6), \tag{5.41a, b, c}$$

where $r_0 = r$ and $z_0 = z - h(r; \Omega)$. The coefficient $v^{\langle 1\rangle}(r_0)$ is given by (5.1), $\Phi^{\langle 2\rangle}(r_0)$ by (5.6) and $v_1^{\langle 3\rangle}(r_0)$ by (5.18). It is also easy to solve (5.36) and (5.39*a*) for $\Phi_1^{\langle 4\rangle}(r_0)$. The functions $\Phi^{\langle 2\rangle}(r_0)$, $v_1^{\langle 3\rangle}(r_0)$ and $\Phi_1^{\langle 4\rangle}(r_0)$ may be regarded as arising from the perturbation of the z-independent viscometric flow and as producing the changes in the free surface $h^{[2]}(r_0)$ and $h_1^{[4]}(r_0)$. The functions $v_2^{\langle 3\rangle}(r_0, z_0)$, $\psi^{\langle 4\rangle}(r_0, z_0)$ and $\Phi_2^{\langle 4\rangle}(r_0, z_0)$ may be regarded as arising from the perturbation of the z-independent viscometric flow and as producing $h_2^{[4]}(r_0)$. The solutions of the boundary-value problems for $h^{[2]}$, $v_2^{\langle 3\rangle}$, $\psi^{\langle 4\rangle}$, $h_1^{[4]}$ and $h_2^{[4]}$ are more difficult.

6. Dimensionless representation of solutions

The series solution up to order four may be expressed in dimensionless form. To do this we introduce the following dimensionless quantities:

$$(t, y) = \frac{2}{\hat{b}-\hat{a}}(r_0, z_0), \quad a \leqslant t \leqslant b, \quad y \leqslant 0,$$

$$\eta = \hat{a}/\hat{b}, \quad a = 2\eta/(1-\eta), \quad b = 2/(1-\eta),$$

$$A = -\eta^2/(1-\eta^2), \quad B = 4\eta^2/\{(1-\eta^2)(1-\eta)^2\},$$

$$S = \frac{\rho g \hat{a}^2}{Ta^2} = \frac{\rho g(\hat{b}-\hat{a})^2}{4T},$$

$$R_1 = 1,$$

$$R_2 = 4(3\alpha_1 + 2\alpha_2)/(\rho\hat{a}^2) = 4\hat{\beta}/(\rho\hat{a}^2),$$

$$R_3 = 4(\alpha_1 + \alpha_2)/(\rho\hat{a}^2) = 4\hat{\alpha}/(\rho\hat{a}^2),$$

$$R_4 = R_2 R_3, \quad R_5 = R_2^2.$$

We also introduce three parameters, each with the units s^{-2}:

$$\Omega_0^2 = g/\hat{a} > 0,$$

$$K_1 = \mu/\{16(\beta_2 + \beta_3)\} = \mu/(16\hat{\mu})$$

and

$$K_2 = (3\alpha_1 + 2\alpha_2)/\{336(\gamma_3 + \gamma_4 + \gamma_5 + \tfrac{4}{7}\gamma_6)\} = \hat{\beta}/(336\hat{\gamma}).$$

Then the series solutions (5.40) and (5.41) can be written as

$$\frac{v(r,z;\Omega)}{\hat{a}\Omega} = V_1(t,\eta) + \frac{1}{3!}\frac{\Omega^2}{K_1}\hat{V}_{31}(t,\eta) + \frac{1}{3!}\left(\frac{\Omega}{\Omega_0}\right)^2 \sum_{i=1}^{2} R_i V_{3i}(t,y,\eta,S), \tag{6.1}$$

$$\frac{\Phi(r,z;\Omega)}{\rho\hat{a}^2\Omega^2} = \frac{1}{2!}\sum_{i=1}^{2} R_i \Phi_{2i}(t,\eta) + \frac{1}{4!}\frac{\Omega^2}{K_1}\sum_{i=1}^{3} R_i \hat{\Phi}_{4i}(t,\eta) + \frac{1}{4!}\frac{\Omega^2}{K_2} R_2 \hat{\Phi}_{44}(t,\eta) + \frac{1}{4!}\left(\frac{\Omega}{\Omega_0}\right)^2 \sum_{i=1}^{5} R_i \Phi_{4i}(t,y,\eta,S), \tag{6.2}$$

$$\left(\frac{\Omega_0}{\Omega}\right)^2 \frac{h(r;\Omega)}{\hat{a}} = \frac{1}{2!}\sum_{i=1}^{2} R_i H_{2i}(t,\eta,S) + \frac{1}{4!}\frac{\Omega^2}{K_1}\sum_{i=1}^{3} R_i \hat{H}_{4i}(t,\eta,S) + \frac{1}{4!}\frac{\Omega^2}{K_2} R_2 \hat{H}_{44}(t,\eta,S) + \frac{1}{4!}\left(\frac{\Omega}{\Omega_0}\right)^2 \sum_{i=1}^{5} R_i H_{4i}(t,\eta,S), \tag{6.3}$$

$$\frac{\mu\psi(r,z;\Omega)}{\rho\hat{a}^5\Omega^2} = \frac{1}{4!}\left(\frac{\Omega}{\Omega_0}\right)^2 \sum_{i=1}^{4} R_i \Psi_{4i}(t,y,\eta,S) = \frac{1}{4!}\left(\frac{\Omega}{\Omega_0}\right)^2 \{(\Psi_{41} + R_2\Psi_{42}) + R_3(\Psi_{43} + R_2\Psi_{44})\}. \tag{6.4}$$

We have used the principle of superposition, as far as possible, to reduce the solution to the computation of functions of η and S alone. For fixed values of the group $\rho g/T$, the prescription of η and S is equivalent to prescribing the radii of the inner and outer cylinders. Hence when $\rho g/T$ is fixed, the dimensionless functions defined by (6.1)–(6.4) are independent of material parameters. The dimensionless functions are given in terms of the dimensional functions introduced in § 5:

$$\frac{v^{\langle 1\rangle}(r_0)}{\hat{a}} = V_1(t), \quad \frac{\Omega^2}{\hat{a}} v_1^{\langle 3\rangle}(r_0) = \frac{\Omega^2}{K_1}\hat{V}_{31}(t),$$

$$\frac{\Omega^2}{\hat{a}} v_2^{\langle 3\rangle}(r_0, z_0) = \left(\frac{\Omega}{\Omega_0}\right)^2 \{V_{31}(t,y) + R_2 V_{32}(t,y)\},$$

$$\frac{\Phi^{\langle 2\rangle}(r_0)}{\rho\hat{a}^2} = \Phi_{21}(t) + R_2\Phi_{22}(t),$$

$$\frac{\Omega^2\Phi_1^{\langle 4\rangle}(r_0)}{\rho\hat{a}^2} = \frac{\Omega^2}{K_1}\sum_{i=1}^{3} R_i \hat{\Phi}_{4i}(t) + \frac{\Omega^2}{K_2} R_2 \hat{\Phi}_{44}(t),$$

$$\frac{\Omega^2\Phi_2^{\langle 4\rangle}(r_0,z_0)}{\rho\hat{a}^2}=\frac{\Omega^2}{\Omega_0^2}\sum_{i=1}^{5}R_i\,\Phi_{4i}(t,y),$$

$$\frac{gh^{[2]}(r_0)}{\hat{a}^2}=H_{21}(t)+R_2H_{22}(t),$$

$$\frac{\Omega^2gh_1^{[4]}(r_0)}{\hat{a}^2}=\frac{\Omega^2}{K_1}\sum_{i=1}^{3}R_i\hat{H}_{4i}(t)+\frac{\Omega^2}{K_2}R_2\hat{H}_{44}(t),$$

$$\frac{\Omega^2gh_2^{[4]}(r_0)}{\hat{a}^2}=\frac{\Omega^2}{\Omega_0^2}\sum_{i=1}^{5}R_iH_{4i}(t)$$

and

$$\frac{\Omega^2\mu\psi^{\langle 4\rangle}(r_0,z_0)}{\rho\hat{a}^5}=\frac{\Omega^2}{\Omega_0^2}\sum_{i=1}^{4}R_i\Psi_{4i}(t,y).$$

The following functions, which are independent of y, may be obtained explicitly without resorting to numerical or approximate methods:

$$V_1(t,\eta)=\frac{1}{a}\left(At+\frac{B}{t}\right),\tag{6.5}$$

$$\hat{V}_{31}(t,\eta)=-\frac{B^3}{a}\left(\frac{1}{t^5}+\frac{a^2+b^2}{a^4b^4}t-\frac{a^4+b^4+a^2b^2}{a^4b^4t}\right),\tag{6.6}$$

$$\Phi_{21}(t,\eta)=\frac{A^2}{a^2}\left(t^2-\frac{a^2+b^2}{2}\right)+\frac{4AB}{a^2}\left(\log\frac{t}{a}-\frac{b^2\log(b/a)}{b^2-a^2}+\tfrac{1}{2}\right)$$
$$-\frac{B^2}{a^2}\left(\frac{1}{t^2}-\frac{2\log(b/a)}{b^2-a^2}\right)-\mathscr{H}_{21},\tag{6.7}$$

$$\Phi_{22}(t,\eta)=B^2\left(\frac{1}{t^4}-\frac{1}{a^2b^2}\right)-\mathscr{H}_{22},\tag{6.8}$$

$$\hat{\Phi}_{41}(t,\eta)=\frac{AB^3}{a^2}\left\{2\left(\frac{1}{t^4}-\frac{1}{a^2b^2}\right)-\frac{4(b^2+a^2)}{b^4a^4}\left(t^2-\frac{a^2+b^2}{2}\right)\right.$$
$$\left.+\frac{8(a^4+b^4+a^2b^2)}{a^4b^4}\left(\log\frac{t}{a}-\frac{b^2\log(b/a)}{b^2-a^2}+\tfrac{1}{2}\right)\right\}$$
$$+\frac{B^4}{a^2}\left\{\frac{4}{3}\left(\frac{1}{t^6}-\frac{a^2+b^2}{2a^4b^4}\right)-\frac{8(b^2+a^2)}{b^4a^4}\left(\log\frac{t}{a}-\frac{b^2\log(b/a)}{b^2-a^2}+\tfrac{1}{2}\right)\right.$$
$$\left.-\frac{4(a^4+b^4+a^2b^2)}{a^4b^4}\left(\frac{1}{t^2}-\frac{2\log(b/a)}{b^2-a^2}\right)\right\}-\hat{\mathscr{H}}_{41},\tag{6.9}$$

$$\hat{\Phi}_{42}(t,\eta)=B^4\left\{-\frac{18}{t^8}+\frac{4(a^4+b^4+a^2b^2)}{a^4b^4t^4}+\frac{2(a^4+b^4+a^2b^2)}{a^6b^6}\right\}-\hat{\mathscr{H}}_{42},\tag{6.10}$$

$$\hat{\Phi}_{43}(t,\eta)=B^4\left\{\frac{12}{t^8}-\frac{4(a^4+b^4+a^2b^2)}{a^6b^6}\right\}-\hat{\mathscr{H}}_{43},\tag{6.11}$$

$$\hat{\Phi}_{44}(t,\eta)=B^4\left\{\frac{1}{t^8}-\frac{a^4+b^4+a^2b^2}{3a^6b^6}\right\}-\hat{\mathscr{H}}_{44}=\tfrac{1}{12}\hat{\Phi}_{43}(t,\eta),\tag{6.12}$$

where

$$\mathscr{H}_{mn} = \frac{2}{S(b^2-a^2)}\left[t\frac{dH_{mn}}{dt}(t,\eta,S)\right]_a^b$$

and the functions $\Phi_{2i}(t)+\mathscr{H}_{2i}$ and $\hat{\Phi}_{4i}(t)+\hat{\mathscr{H}}_{4i}$ satisfy (3.1 k).

If the height-rise functions $H_{mn}(t)$ are given numerically, then the Fourier–Bessel coefficients B_{in} given by (6.17) and the biorthogonal series coefficients given by (10.9) can also be computed numerically. The remaining parts of the solution can be expressed analytically.

First, the functions $H_{21}(t,\eta,S)$ and $H_{22}(t,\eta,S)$ satisfy

$$\frac{1}{t}\frac{d}{dt}\left(t\frac{dH_{2i}}{dt}\right) - SH_{2i} + S\Phi_{2i}(t) = 0, \quad i = 1,2, \tag{6.13}$$

and one pair of the four conditions (3.11).

The functions $V_{3i}(t,y,\eta,S)$ satisfy

$$\frac{\partial^2 V_{3i}}{\partial t^2} + \frac{1}{t}\frac{\partial V_{3i}}{\partial t} - \frac{V_{3i}}{t^2} + \frac{\partial^2 V_{3i}}{\partial y^2} = 0, \tag{6.14a}$$

$$V_{3i}(a,y,\eta,S) = V_{3i}(b,y,\eta,S) = 0, \tag{6.14b}$$

$$\frac{\partial V_{3i}}{\partial y} + \frac{6B}{t^2}\frac{dH_{2i}}{dt} = 0 \quad \text{on} \quad y = 0, \tag{6.14c}$$

$$\partial V_{3i}/\partial y \to 0 \quad \text{as} \quad y \to -\infty \quad \text{for} \quad i = 1,2. \tag{6.14d}$$

The solution of (6.14) is

$$V_{3i}(t,y,\eta,S) = \sum_{n=1}^{\infty} B_{in}\exp(\lambda_n y)\mathscr{C}_1(\lambda_n t), \tag{6.15}$$

where
$$\mathscr{C}_1(\lambda_n t) = J_1(\lambda_n a)Y_1(\lambda_n t) - J_1(\lambda_n t)Y_1(\lambda_n a), \quad \mathscr{C}_1(\lambda_n b) = 0 \tag{6.16a, b}$$

and
$$B_{in}\frac{2}{\pi^2\lambda_n}\frac{[J_1(\lambda_n a)]^2 - [J_1(\lambda_n b)]^2}{[J_1(\lambda_n b)]^2} = -6B\int_a^b \frac{1}{t}\mathscr{C}_1(\lambda_n t)\frac{dH_{2i}}{dt}dt. \tag{6.17}$$

The constants $\lambda_n(\eta)$ depend on η alone but the coefficients $B_{in}(\eta,S)$ depend on η and S.

The functions $\Psi_{4i}(t,y,\eta,S)$ $(i = 1,2,3,4)$ satisfy

$$L^2\Psi_{4i} + \frac{\partial F_i}{\partial y}(t,y,\eta,S) = 0, \quad L(\,) = t\frac{\partial}{\partial t}\left(\frac{1}{t}\frac{\partial(\,)}{\partial t}\right) + \frac{\partial^2(\,)}{\partial y^2}, \tag{6.18a}$$

$$F_i(t,y,\eta,S) = \begin{cases} \dfrac{8}{a^4}\left(At + \dfrac{B}{t}\right)V_{3i} & \text{for} \quad i = 1,2, \\ \dfrac{8B}{a^2}\dfrac{1}{t^2}\left(\dfrac{\partial V_{3,i-2}}{\partial t} - \dfrac{V_{3,i-2}}{t}\right) & \text{for} \quad i = 3,4, \end{cases}$$

$$\Psi_{4i} = \partial\Psi_{4i}/\partial t = 0 \quad \text{at} \quad t = a,b, \tag{6.18b}$$

$$\Psi_{4i} = \partial^2\Psi_{4i}/\partial y^2 = 0 \quad \text{on} \quad y = 0, \tag{6.18c}$$

and
$$\Psi_{4i} \to 0 \quad \text{as} \quad y \to -\infty. \tag{6.18d}$$

Assuming that the functions Ψ_{4i} are known, we can obtain the functions $\Phi_{4i}(t, y, \eta, S)$ uniquely to within additive constants of integration from the equations listed below:

$$\frac{\partial\Phi_{41}}{\partial t} = a^3\hat{L}\left(\frac{1}{t}\frac{\partial\Psi_{41}}{\partial y}\right) + \frac{8}{a}\left(A + \frac{B}{t^2}\right)V_{31},$$

$$\frac{\partial\Phi_{42}}{\partial t} = a^3\hat{L}\left(\frac{1}{t}\frac{\partial\Psi_{42}}{\partial y}\right) + \frac{8}{a}\left(A + \frac{B}{t^2}\right)V_{32} + 2Ba\left[-\frac{1}{t^2}\frac{\partial^2 V_{31}}{\partial t^2} + 3\left(\frac{1}{t^3}\frac{\partial V_{31}}{\partial t} - \frac{V_{31}}{t^4}\right)\right],$$

$$\frac{\partial\Phi_{43}}{\partial t} = a^3\hat{L}\left(\frac{1}{t}\frac{\partial\Psi_{43}}{\partial y}\right) + 2Ba\left[\frac{1}{t^2}\frac{\partial^2 V_{31}}{\partial t^2} + \frac{1}{t^3}\frac{\partial V_{31}}{\partial t} - \frac{V_{31}}{t^4}\right],$$

$$\frac{\partial\Phi_{44}}{\partial t} = a^3\hat{L}\left(\frac{1}{t}\frac{\partial\Psi_{44}}{\partial y}\right) + 2Ba\left[\frac{1}{t^2}\frac{\partial^2 V_{32}}{\partial t^2} + \frac{1}{t^3}\frac{\partial V_{32}}{\partial t} - \frac{V_{32}}{t^4}\right],$$

$$\frac{\partial\Phi_{45}}{\partial t} = 2Ba\left[-\frac{1}{t^2}\frac{\partial^2 V_{32}}{\partial t^2} + 3\left(\frac{1}{t^3}\frac{\partial V_{32}}{\partial t} - \frac{V_{32}}{t^4}\right)\right],$$

$$\frac{\partial\Phi_{41}}{\partial y} = a^3\nabla^2\left(-\frac{1}{t}\frac{\partial\Psi_{41}}{\partial t}\right),$$

$$\frac{\partial\Phi_{42}}{\partial y} = a^3\nabla^2\left(-\frac{1}{t}\frac{\partial\Psi_{42}}{\partial t}\right) - 2Ba\left(-\frac{1}{t^3}\frac{\partial V_{31}}{\partial y} + \frac{1}{t^2}\frac{\partial^2 V_{31}}{\partial t\,\partial y}\right),$$

$$\frac{\partial\Phi_{43}}{\partial y} = a^3\nabla^2\left(-\frac{1}{t}\frac{\partial\Psi_{43}}{\partial t}\right) + 2Ba\left(-\frac{1}{t^3}\frac{\partial V_{31}}{\partial y} + \frac{1}{t^2}\frac{\partial^2 V_{31}}{\partial t\,\partial y}\right),$$

$$\frac{\partial\Phi_{44}}{\partial y} = a^3\nabla^2\left(-\frac{1}{t}\frac{\partial\Psi_{44}}{\partial t}\right) + 2Ba\left(-\frac{1}{t^3}\frac{V_{32}}{\partial y} + \frac{1}{t^2}\frac{\partial^2 V_{32}}{\partial t\,\partial y}\right),$$

$$\frac{\partial\Phi_{45}}{\partial y} = -2Ba\left(-\frac{1}{t^3}\frac{\partial V_{32}}{\partial y} + \frac{1}{t^2}\frac{\partial^2 V_{32}}{\partial t\,\partial y}\right),$$

where $$\nabla^2(\,) = \frac{1}{t}\frac{\partial}{\partial t}\left(t\frac{\partial(\,)}{\partial t}\right) + \frac{\partial^2(\,)}{\partial y^2}, \quad \hat{L}(\,) = \nabla^2(\,) - \frac{(\,)}{t^2}.$$

The constants of integration for $\Phi_{4i}(t, y, \eta, S)$ are to be determined so as to satisfy the preservation-of-volume condition (3.1 k):

$$\left(t\frac{dH_{4i}}{dt}(t, \eta, S)\right)_a^b + S\int_a^b t\Phi_{4i}(t, 0, \eta, S)\,dt = 0. \tag{6.19}$$

The functions $\hat{H}_{4i}(t, \eta, S)$ and $H_{4i}(t, \eta, S)$ satisfy

$$\frac{1}{t}\frac{d}{dt}\left(t\frac{d\hat{H}_{4i}}{dt}\right) - S\hat{H}_{4i} + S\hat{\Phi}_{4i}(t, \eta) = 0, \quad i = 1, 2, 3, 4, \tag{6.20}$$

$$\frac{1}{t}\frac{d}{dt}\left(t\frac{dH_{4i}}{dt}\right) - SH_{4i} + S\left\{\Phi_{4i}(t, 0, \eta, S) + \frac{2a^3}{t}\frac{\partial^2\Psi_{4i}}{\partial t\,\partial y}(t, 0, \eta, S)\right\} = 0, \quad i = 1, 2, 3, 4, \tag{6.21a}$$

$$\frac{1}{t}\frac{d}{dt}\left(t\frac{dH_{45}}{dt}\right) - SH_{45} + S\Phi_{45}(t, 0, \eta, S) = 0 \tag{6.21b}$$

and one pair of the four conditions (3.11).

Two remarks on the dimensionless representation of the solutions are appropriate at this point. First, the computation of terms in the perturbation solution proceeds sequentially in the order given in the following flow diagram:

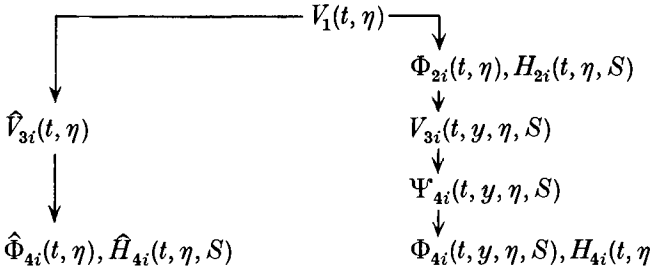

We do not believe that the choice of dimensionless parameters embodied in (6.1)–(6.4) is always the best possible. Our primary aim was to reduce the whole solution to a sum over component functions which, as far as possible, are independent of material parameters and depend on the minimum number of geometric parameters. We found that some of these functions ($V_1(t)$, $\hat{V}_{31}(t)$, $\Phi_{2i}(t)$ and $\hat{\Phi}_{4i}(t)$) depend on η; all the other component functions depend on both η and S. The S dependence can be traced to the height-rise equations at orders two and four.

A second remark concerns the choice for the geometric parameters. A better choice than the one made here uses the shear rate at the inner cylinder rather than Ω as an expansion parameter when η is near one. For any fixed value of Ω, no matter how small, the shear rate at $r_0 = \hat{a}$,

$$-\kappa = \hat{a}\frac{dv^{\langle 1\rangle}(\hat{a})}{dr_0} = \frac{2\Omega}{1-\eta^2} = 2\Omega\frac{B}{a^2} \equiv \hat{\kappa}, \tag{6.22}$$

tends to infinity as $\eta \to 1$. The perturbation solutions are then represented as follows:

$$\Omega V_1(t) = \hat{\kappa} V_{(1)}(t'), \quad \Omega^2\Phi_{2i}(t) = \hat{\kappa}^2\Phi_{(2i)}(t'), \quad \Omega^2 H_{2i}(t) = \hat{\kappa}^2 H_{(2i)}(t'),$$
$$\Omega^3 V_{3i}(t,y) = \hat{\kappa}^3 V_{(3i)}(t',y'), \quad \Omega^4\Psi_{4i}(t,y) = \hat{\kappa}^4\Psi_{(4i)}(t',y'),$$
$$\Omega^4\Phi_{4i}(t,y) = \hat{\kappa}^4\Phi_{(4i)}(t',y'), \quad \Omega^4 H_{4i}(t) = \hat{\kappa}^4 H_{(4i)}(t'), \quad \text{etc.},$$

where $(t',y') = (t/a, y/a)$, $1 \leqslant t' \leqslant 1/\eta$. For example, $\Omega V_1(t) = \frac{1}{2}\hat{\kappa}(-\eta^2 t' + 1/t')$.

7. Some properties of the solutions

It is almost impossible to give a complete account of all of the superpositions possible among the functions of $\eta = \hat{a}/\hat{b}$ and $S = \rho g\hat{b}^2(1-\eta)^2/4T$ which are defined in (6.1)–(6.4). To simplify this problem we have used the value

$$\rho g/T = 28{\cdot}25\,\text{cm}^{-2} \quad (\rho = 0{\cdot}89\,\text{g cm}^{-3}, \quad T = 30{\cdot}9\,\text{dynes cm}^{-1}) \tag{7.1}$$

which Beavers & Joseph (1975) report for a sample of STP at room temperature. This parameter is nearly constant over wide ranges of temperature and has nearly the same value in the different polymeric oils used in our experiments (STP-1, 28·25; STP-2, 27·63; TLA-227, 28·43). With the value of $\rho g/T$ given, all of the component

functions which enter, by superposition, into the final solution may be computed when the radii $\hat{a}$ and $\hat{b}$ of the inner and outer cylinders are specified. To display some of the properties of the solutions we have chosen the following three sets of physical parameters:

$$\text{(i)}\ (\hat{a}, \hat{b}, S) = (0{\cdot}635,\ 6{\cdot}35,\ 231),$$

$$\text{(ii)}\ (\hat{a}, \hat{b}, S) = (4,\ 8{\cdot}5,\ 143),$$

$$\text{(iii)}\ (\hat{a}, \hat{b}, S) = (6,\ 8{\cdot}5,\ 44),$$

where $\hat{a}$ and $\hat{b}$ are in centimetres. In the experiments of Beavers & Joseph (1975) the radius of the outer cylinder was fixed at 15·25 cm and the radius of the inner cylinder was varied, one value being 0·635 cm. We shall show that for a fixed value of $\hat{a}$ the climb near the inner cylinder is independent of $\hat{b}$ for values of $\hat{b}/\hat{a}$ greater than about 5. Thus we can compare the theoretical results from (i) above with the corresponding experiments of Beavers & Joseph (1975).

The four viscoelastic constants which enter our solution up to order four also appear, but only as coefficients in the superposition of the component functions.

A certain amount of numerical work of a routine kind is required in the computation of the component functions. The height rises at orders two and four were computed numerically using Runge–Kutta integration. The integrals defining the coefficients in the series solutions at orders three and four were computed numerically using Simpson's rule. These computations are fully described in the thesis of Yoo (1977). In that thesis the interested reader will find extensive tables of computed values from which we have constructed the graphical representations given here.

8. The rise in height at second order

Equation (6.13) can be solved by the standard Runge–Kutta method for the zero-slope boundary conditions $H'_{2i}(a) = H'_{2i}(b) = 0$ for $i = 1, 2$. In fact, among the four allowed conditions (3.11), only the flat-slope condition gives a solution which is not singular at the contact line [see Sattinger (1976) and the discussion following (9.3)].

The height-rise problems for $H_{21}(t)$ and $H_{22}(t)$ depend on η and S. We first consider the effect of changing S when η is fixed. We may regard S as a surface-tension parameter; when $T = 0$ $(S = \infty)$, $H_{2i}(t) = \Phi_{2i}(t)$ and, when $T = \infty$ $(S = 0)$, $H_{2i}(t) \equiv 0$. Without exploring further the details of the variation of $H_{2i}(t, S)$ with S, we assert that $|H_{2i}(t, S)|$ is an increasing function of S for most $t \in [a, b]$ such that $H_{2i}(t, 0) \equiv 0$ and $H_{2i}(t, \infty) = \Phi_{2i}(t)$.

We next consider the effect of varying η when $S = \rho g(\hat{b} - \hat{a})^2/4T$ is fixed. In experiments this type of variation is obtained by keeping the gap size fixed and varying the radii of the cylinders; $\hat{a} \to 0$ corresponds to a rod rotating in an infinite sea of fluid. When S is fixed the inhomogeneous term $S\Phi_{2i}(t, \eta)$ in (6.13) varies with η and has mean value zero. For small values of η, Φ_{21} and Φ_{22} are approximately given by the terms which are proportional to B^2 in (6.7) and (6.8). For example,

$$\Phi_{21} \sim -\frac{B^2}{a^4}\left[\frac{a^2}{t^2} + \frac{2\eta^2 \log \eta}{1 - \eta^2}\right].$$

The term in the brackets tends to a^2/t^2 when η is small and a^2/t^2 is a decreasing positive function with maximum value one, when $t = a$. In addition, Φ_{2i} differs from zero

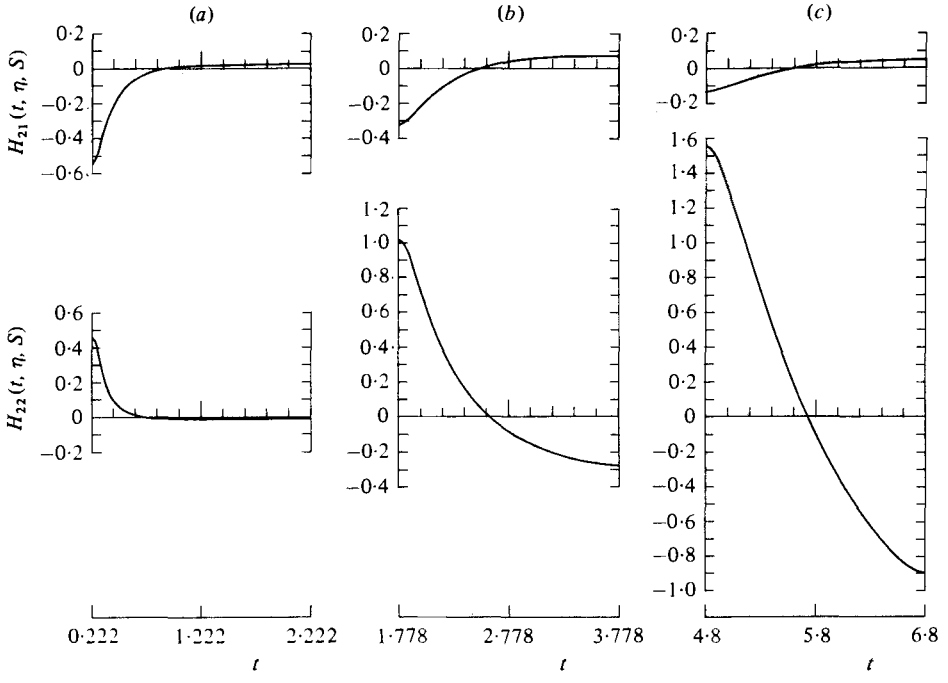

FIGURE 1. Height-rise functions $H_{21}(t, \eta, S)$ and $H_{22}(t, \eta, S)$ at second order satisfying (6.13) with zero-slope boundary conditions, for three pairs of cylinders:

	(a)	(b)	(c)
$\hat{a}$ (cm)	0·635	4·0	6·0
$\hat{b}$ (cm)	6·35	8·5	8·5
$\eta\ (=\hat{a}/\hat{b})$	0·1	0·4706	0·7059
S	231	143	44

The height of climb is given by $h = \frac{1}{2}\Omega^2\hat{a}^2g^{-1}[H_{21}(t) + R_2 H_{22}(t)] + O(\Omega^4)$. The fluid is assumed to be the same as the STP sample used by Beavers & Joseph (1975), with $\rho g/T = 28{\cdot}25\,\mathrm{cm}^{-2}$. When S is large and η is small, $H_{21}(t)$ and $H_{22}(t)$ differ sufficiently from zero only for t close to a, while when S is large and $1-\eta \to 0$, $H_{21}(t)$ and $H_{22}(t)$ are odd functions with respect to the gap centre.

substantially only when t is close to a. For η near to one, $\Phi_{2i}(t)$ is nearly an odd function with respect to the gap centre. Since $H_{2i}(t) \sim \Phi_{2i}(t)$ when S is large and t is outside the capillary boundary layer on the cylinder walls, we may expect that when S is large and η is small $H_{2i}(t)$ differs substantially from zero for t near a, and that when S is large and $1-\eta$ is small $H_{2i}(t)$ is close to an odd function with respect to the gap centre. These features of H_{21} and H_{22} are evident in the graphs shown in figure 1.

Our main observation is that when $\hat{a}$ is small most of the climb occurs near the inner cylinder and that this climb depends very weakly on the radius $\hat{b}$ of the outer cylinder. Our calculations show that the climb near the inner cylinder is independent of the position of the outer one when $\eta < \frac{1}{5}$. In figure 2, we show that when $\hat{a}$ is fixed and $\hat{b}$ is increased the height rise near $\hat{a}$ becomes independent of $\hat{b}$ when $\hat{a}/\hat{b} < \frac{1}{5}$. The height-rise curves for all values of $\hat{b}$ at fixed values of $\hat{a}$ and $\rho g/T$ are barely distinguishable from one another and from the limiting curve for $\hat{b} \to \infty$ shown as figure 13 in the paper of Beavers & Joseph (1975).

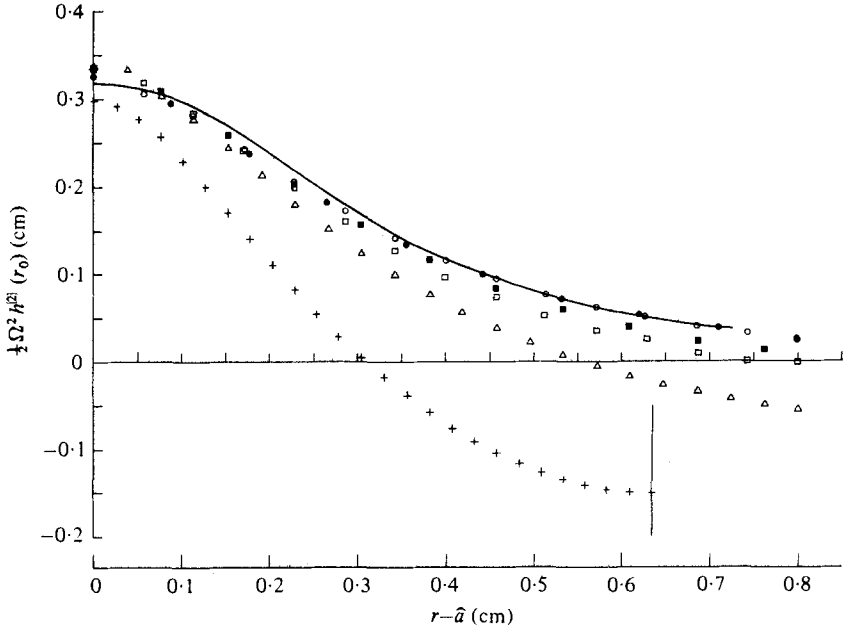

FIGURE 2. Height rise $h = \frac{1}{4}\Omega^2 h^{[2]}(r_0)$ at second order for a fixed inner radius $\hat{a}$ and various outer radii $\hat{b}$. $h^{[2]}(r_0) = \hat{a}^2 g^{-1}\{H_{21}(t, \eta, S) + R_2 H_{22}(t, \eta, S)\}$; $\omega = 2{\cdot}9\,\mathrm{rev\,s^{-1}}$; $\hat{a} = 0{\cdot}635\,\mathrm{cm}$; $\hat{\beta} = 1{\cdot}0\,\mathrm{g\,cm^{-1}}$; ——, experimental curve (Beavers & Joseph 1975).

	●	○	■	□	△	+
$\hat{b}$ (cm)	9·525	6·35	3·175	2·54	1·905	1·27
η	0·0667	0·1	0·2	0·25	0·333	0·5
S	559	231	45·6	25·7	11·4	2·85

Solutions with small values of η (large values of $\hat{b}$ when $\hat{a}$ is fixed) tend to a limiting value for $\eta = 0$ ($\hat{b} \to \infty$) when $\hat{a}/\hat{b} < \frac{1}{8}$ (cf. figure 13*a* of Beavers & Joseph 1975).

Figure 3 shows how $h^{[2]}(r) = \hat{a}^2 g^{-1}[H_{21}(t, \eta, S) + R_2 H_{22}(t, \eta, S)]$ varies when $\hat{b}$ is fixed, $\hat{a}$ varies and S is large. The sensitive variation of the rise curve with $\eta = \hat{a}/\hat{b}$ is fully described in the figure caption. We draw attention to the following remark. When $1-\eta$ is small it is desirable to fix the rate of shear $\hat{\kappa}$ given by (6.22) rather than the angular velocity Ω. The series solution proceeds in powers of $\hat{\kappa}$ and $h(r) = \frac{1}{2}h_2(r)\,\hat{\kappa}^2$, where

$$h_2(r, \eta) = \tfrac{1}{4}h^{[2]}(r, \eta)\,(1-\eta)^2\,(1+\eta)^2$$

tends to zero with $1-\eta$. The nature of the difference in the variation of $h_2(\hat{a}, \eta)$ and $h^{[2]}(\hat{a}, \eta)$ is made dramatically evident by the graph in figure 4, where it is shown that

$$h_2(\hat{a}, 0{\cdot}3) = h_2(\hat{a}, 0{\cdot}6) = h_2(\hat{a}, 1) = 0.$$

In fact, $h_2(r, 1) \equiv 0$ for $\hat{a} \leqslant r \leqslant \hat{b}$.

The analysis of the variation of the climb with η just given may help to explain the seemingly confusing (but actually reasonable) experimental results of Peter & Noetzel (1959), in which they claim to have reduced to zero the height of a climbing fluid in a Couette apparatus by floating the climbing fluid on a bed of mercury. Their figure 3 shows that they did not observe climbing of the pyroxyline solution in butyl

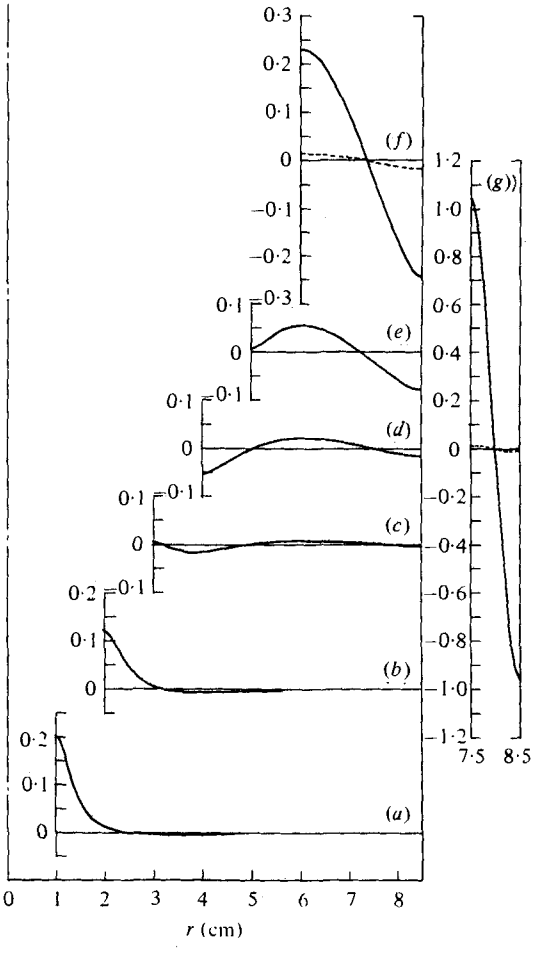

FIGURE 3. Height-rise coefficient $h^{[2]}(r) = \hat{a}^2 g^{-1}[H_{21}(t,\eta,S) + R_2 H_{22}(t,\eta,S)]$ at second order for fixed outer radius $\hat{b}$ and various inner radii $\hat{a}$. $h \sim \frac{1}{2}\Omega^2 h^{[2]}$; $\hat{\rho} = 1{\cdot}0\,\mathrm{g\,cm^{-1}}$.

	(a)	(b)	(c)	(d)	(e)	(f)	(g)
$\hat{a}$ (cm)	1	2	3	4	5	6	7·5
S	398	299	214	143	86·6	44·2	7·07

The maximum rise is not always at the inner cylinder. For intermediate values of η ($= \hat{a}/\hat{b}$) the maximum rise is in the interior. For small values of η, the maximum rise is at the inner-cylinder wall and the rise in the rest of the gap is small. For small values of $1-\eta$ the distribution is anti-symmetric with respect to the gap centre. The magnitude of the rise $h \sim \frac{1}{2}\kappa^2 h_2$ tends to zero with $1-\eta$ (see curves for $h_2(r)$ in (*f*) and (*g*), and $h_2(\hat{a})$ in figure 4). ——, $h^{[2]} \times 10^2\,(\mathrm{cm\,s^2})$; – – –, $h_2 \times 10^2$ $(\mathrm{cm\,s^2})$.

acetate between concentric cylinders ($\hat{a} = 10{\cdot}97$ cm, $\hat{b} = 16$ cm) for various small values of Ω. The inner cylinder was situated in a mercury layer at the bottom of the container to produce a state of pure simple shear in the body of the test solution. They interpreted their observations to mean that the Weissenberg effect is either absent or of smaller order in simple shearing flows. Their observation is correct but their interpretation is not. They did not know that the climb is very sensitive to η and also to

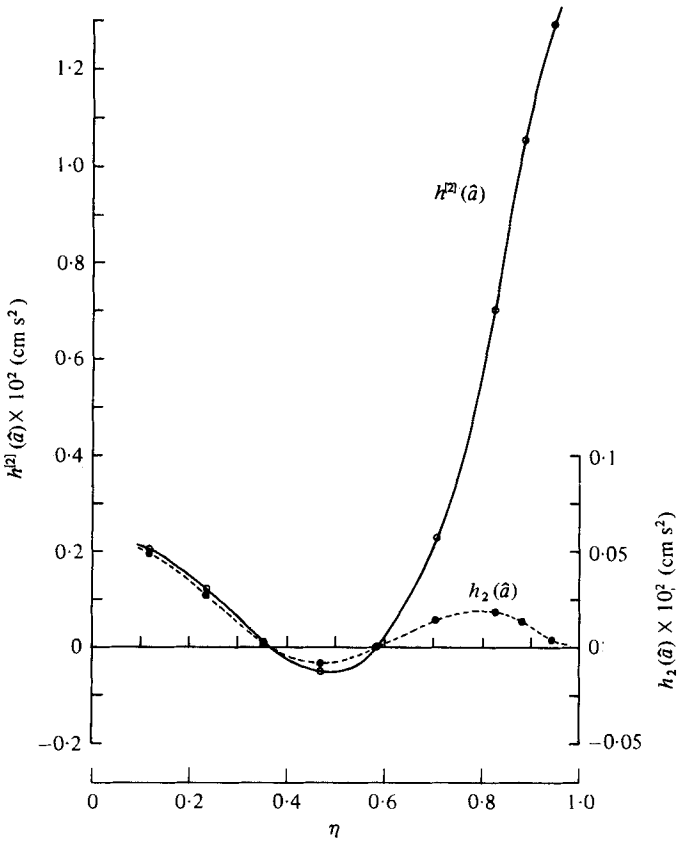

FIGURE 4. Variation of height-rise coefficient at $r = \hat{a}$ as a function of $\eta(\hat{a})$ for fixed values of $\hat{b} = 8{\cdot}5\,\text{cm}$, $\hat{\beta} = 1{\cdot}0\,\text{g cm}^{-1}$ and $\rho g/T = 28{\cdot}25\,\text{cm}^{-2}$.

Rev/min	$h = \dfrac{\Omega^2}{2!} h^{[2]}$ (mm)
2·84	−0·006
4·57	−0·015
7·42	−0·039
11·35	−0·092
18·20	−0·236

TABLE 1. Theoretical height rise of STP motor-oil additive on the wall of the inner cylinder for $\hat{a} = 10{\cdot}97\,\text{cm}$, $\hat{b} = 16\,\text{cm}$ and various small values of Ω.

the size of $\hat{a}$, the inner radius (see figures 3 and 4). In fact, for STP in the apparatus used by Peter & Noetzel, we compute, from (6.3) and (6.13), an almost negligible rise in height (see table 1).

Their observations concerning the climb on non-circular cylinders also has an easy explanation in terms of the induced spatial variations of shear.

9. Circumferential velocity at third order

The circumferential velocity at third order is given by terms proportional to Ω^3 in (5.40). The solution splits into two parts; one part arises from the perturbation of viscometric flow, which is independent of z (or y) and is proportional to $\hat{\mu}$, and the other part is driven from the free surface and depends on z and on $\hat{\beta}$. This z-dependent part of the circumferential velocity is the mainspring of the secondary motion; it is responsible for the vertical stratification of inertia and normal stresses, which gives the torque generating the secondary circulations.

The vanishing of the tangential component of the shear stress on the free surface implies that (1.2) holds:

$$S_{z\theta} - h'(r)\, S_{r\theta} = 0 \quad \text{at} \quad z = h(r;\, \Omega). \tag{9.1}$$

At first order (9.1) is satisfied identically because $h^{[0]}(r)$, $h^{[1]}(r)$ and $S_{z\theta}^{\langle 1\rangle}$ are identically zero. At third order this equation becomes

$$S_{z\theta}^{\langle 3\rangle} - 3h^{[2]\prime}(r_0)\, S_{r\theta}^{\langle 1\rangle} = 0 \quad \text{at} \quad z_0 = 0. \tag{9.2}$$

Since $S_{z\theta}^{\langle 3\rangle} = \mu\, \partial v^{\langle 3\rangle}/\partial z_0$ and $S_{r\theta}^{\langle 1\rangle} = \mu(\partial v^{\langle 1\rangle}/\partial r_0 - v^{\langle 1\rangle}/r_0)$, (9.2) takes the form

$$\partial v^{\langle 3\rangle}/\partial z_0 + h^{[2]\prime}(r_0)\, 6\hat{B}/r_0^2 = 0 \quad \text{at} \quad z_0 = 0, \tag{9.3}$$

which can be identified with (5.13). Now at $r_0 = \hat{a}$, $v^{\langle 3\rangle}(r_0, z_0) = 0$; hence

$$\partial v^{\langle 3\rangle}(\hat{a}, z_0)/\partial z_0 = 0.$$

But (9.3) shows that $\partial v^{\langle 3\rangle}(\hat{a}, z_0)/\partial z_0 \neq 0$ unless $h^{[2]\prime}(\hat{a}) = 0$. If $h^{[2]\prime}(\hat{a}) \neq 0$, we can get a solution which satisfies (9.3), $v^{\langle 3\rangle}(\hat{a}, z_0) = 0$ and all the other conditions but fails at the point $(r_0, z_0) = (\hat{a}, 0)$. This incompatibility of boundary data is true of (9.1) without perturbations when the fluid is Newtonian and it would appear to be related to the unsolved problem of adhesion of the contact line. In any event, we are now considering $h^{[2]\prime}(\hat{a}) = 0$, where there is no incompatibility and the solution, at least in the Newtonian case, is regular even at the corner (Sattinger 1976).

Equation (9.3) shows that $v^{\langle 3\rangle}(r_0, z_0)$ is an increasing function of z_0 for z_0 near zero at each r_0 for which $h^{[2]\prime}(r_0) < 0$. In the typical climbing configuration when η is small, this will imply that $v^{\langle 3\rangle}(r_0, 0)$ is larger than the viscometric value $v_1^{\langle 3\rangle}(r_0)$ to which $v^{\langle 3\rangle}$ tends when z_0 tends to $-\infty$ over the whole of the climbing bubble. We may write (9.3) as

$$\frac{\partial}{\partial z_0}\left\{\Omega v^{\langle 1\rangle}(r_0) + \frac{\Omega^3}{3!}\left(v_1^{\langle 3\rangle}(r_0) + v_2^{\langle 3\rangle}(r_0, z_0)\right)\right\} = -h^{[2]\prime}(r_0)\, \hat{B}\Omega^3/r_0^2 \quad \text{at} \quad z_0 = 0. \tag{9.4}$$

Equation (9.4) implies that the circumferential velocity

$$\tilde{v}(r_0, z_0 = 0, \Omega) = \Omega v^{\langle 1\rangle}(r_0) + \frac{\Omega^3}{3!}\{v_1^{\langle 3\rangle}(r_0) + v_2^{\langle 3\rangle}(r_0, 0)\}$$

is larger than its asymptotic, viscometric value

$$\Omega v^{\langle 1\rangle}(r_0) + \frac{\Omega^3}{3!} v_1^{\langle 3\rangle}(r_0)$$

wherever $h^{[2]\prime}(r_0) < 0$. Since $v_1^{\langle 3\rangle}(\hat{a})$ and $v_2^{\langle 3\rangle}(\hat{a}, z_0)$ both vanish, $v(\hat{a}, z_0; \Omega) = \Omega v^{\langle 1\rangle}(\hat{a})$.

We turn next to a description of the functions giving the third-order approximation

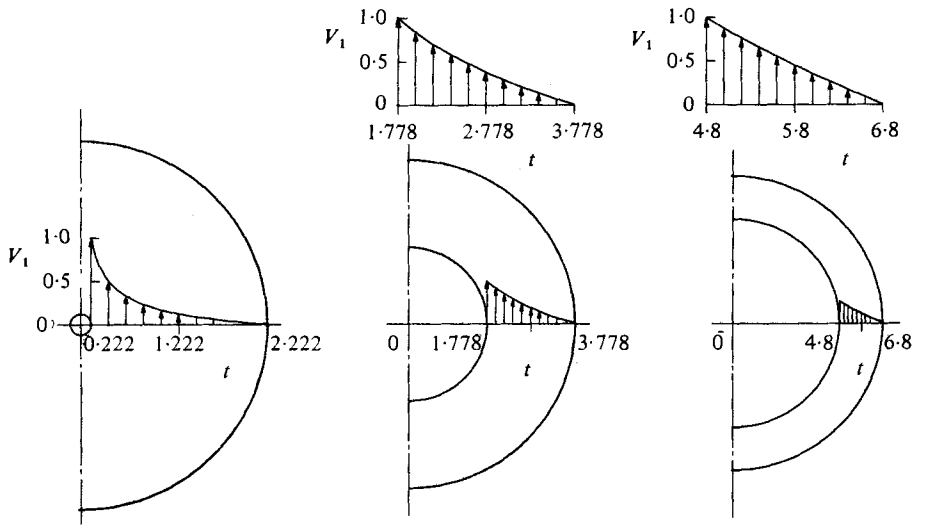

FIGURE 5. Plots of $V_1(t, \eta)$ [$= v^{\langle 1\rangle}(r_0)/\Omega\hat{a}$] for the three cylinder pairs of figure 1; $V_1(t, \eta)$ is given by (6.5). These graphs show that the primary shearing motion reduces to potential flow as $\eta \to 0$ and to linear shearing motion as $\eta \to 1$.

(6.1) to the circumferential component of velocity. The first-order contribution $V_1(t, \eta)$ is given by (6.5), and graphs for three different values of η are shown in figure 5. For the third-order contributions, $\hat{V}_{31}(t, \eta)$ is given by (6.6), $V_{31}(t, y, \eta, S)$ and $V_{32}(t, y, \eta, S)$ are given by (6.15), and the eigenvalues $\lambda_n(\eta)$ are given by (6.16). Graphs of $\hat{V}_{31}$, V_{31} and V_{32} evaluated on the free surface $z_0 = 0$ are shown in figure 6 for the same three values of η as figure 5. The computation and asymptotic properties of λ_n are discussed in appendix E of Yoo (1977). The Fourier–Bessel coefficients B_{in}, which are given by (6.17) and which are needed for the eigenfunction series expansion, depend on S through $dH_{2i}(t, \eta, S)/dt$. The values of dH_{2i}/dt were obtained as a by-product of the numerical method applied to solve (6.13). Thus the integral on the right of (6.17) can be computed numerically using Simpson's rule. The first 40 values of $\lambda_n(\eta)$ and $B_{in}(\eta, S)$ for three different values of (η, S) are given in table 22.2 of Yoo (1977).

The accuracy of this computation can be checked by establishing the convergence of the partial sums on the right of (9.5) to the edge data on the left:

$$-\frac{6B}{t^2}\frac{dH_{2i}}{dt} \sim \sum_{n=1}^{N} B_{in}\lambda_n \mathscr{C}_1(\lambda_n t). \tag{9.5}$$

Yoo (1977) showed that the convergence is faster when $1-\eta$ is small and slower when η is small. In all cases, however, there is convergence with less than 60 terms.

Finally, we consider the total circumferential velocity on the free surface $z_0 = y = 0$:

$$v(r, h; \Omega) \sim \hat{a}\Omega V_1(t) + \frac{\hat{a}}{3!}\frac{\Omega^3}{\Omega_0^2}[V_{31}(t, 0) + R_2 V_{32}(t, 0)]$$
$$\sim \hat{a}v^{\langle 1\rangle}(r_0) + \frac{\Omega^3}{3!}(v_1^{\langle 3\rangle}(r_0) + v_2^{\langle 3\rangle}(r_0, 0)). \tag{9.6}$$

As an example we choose the values $\hat{a} = 0{\cdot}635$ cm, $\eta = 0{\cdot}1$, $S = 231$ and $\hat{\beta} = 1{\cdot}0$ g cm^{-1}. The value of $v(r, h; \Omega)$ depends on K_1 ($= \mu/\{16(\beta_2 + \beta_3)\}$) and Ω. In figure 7 we have

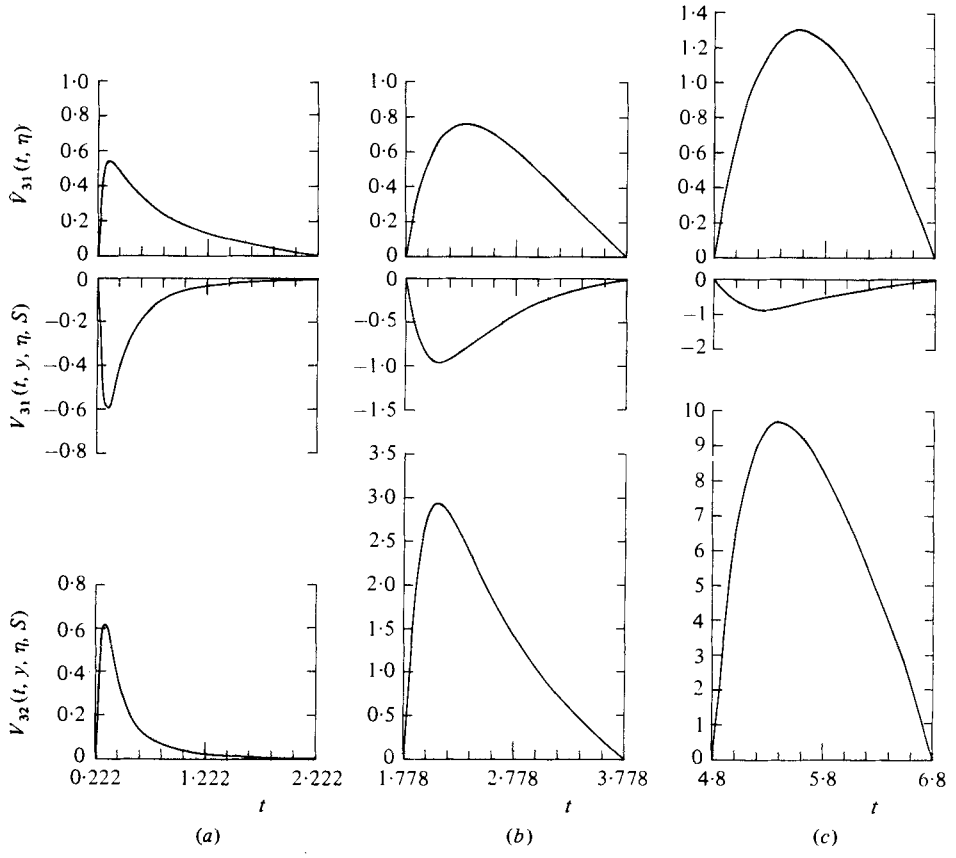

FIGURE 6. Components of the third-order correction to the circumferential velocity evaluated on the free surface $z_0 = 0$ ($y = 0$) for the three cylinder pairs of figure 1. V_{31} is defined by (6.6) while V_{31} and V_{32} are defined by (6.15). In the limit as $\eta \to 1$, all three components are symmetric with respect to the centre-line of the channel.

plotted (9.6) for $\Omega = 4\,\text{rev}\,\text{s}^{-1}$ and different values of $\hat{\mu}$ ($= \beta_2 + \beta_3$). Positive values of $\hat{\mu}$ mean that the fluid is shear thickening when the shear rate $\hat{\kappa}$ is small. Negative values imply a shear-thinning fluid. The circumferential velocity increases all over the climbing bubble ($h^{[2]\prime}(r_0) < 0$) in all fluids except those which are very shear thinning, i.e. in all fluids except those with large negative values of $\hat{\mu}$. Measurements reported by Hoffman & Gottenberg (1973) indicate that this property of the solution may be easily verified in experiments. Their figure 7 shows that the measured values of the angular velocity of polyisobutylene in cetane in a concentric-cylinder apparatus with $\hat{a} = 1{\cdot}267$ cm, $\hat{b} = 3{\cdot}827$ cm and $\Omega = 4\pi\,\text{rad}\,\text{s}^{-1}$ are larger than the Couette-flow values. The distribution curve of the measured values (when rescaled by multiplying by the radial co-ordinate at each point to give the circumferential velocity distribution) is like the one which the present theory would predict for a value of $\hat{\mu}$ which is negative but not large in magnitude. Their figure 3 shows that the polyisobutylene solution is shear thinning and the thinning seems to be moderate at low rates of shear.

Hoffman & Gottenberg also present an argument to show that the circumferential speed at the free surface where $h'(r_0; \Omega) < 0$ is larger than the z-independent value at

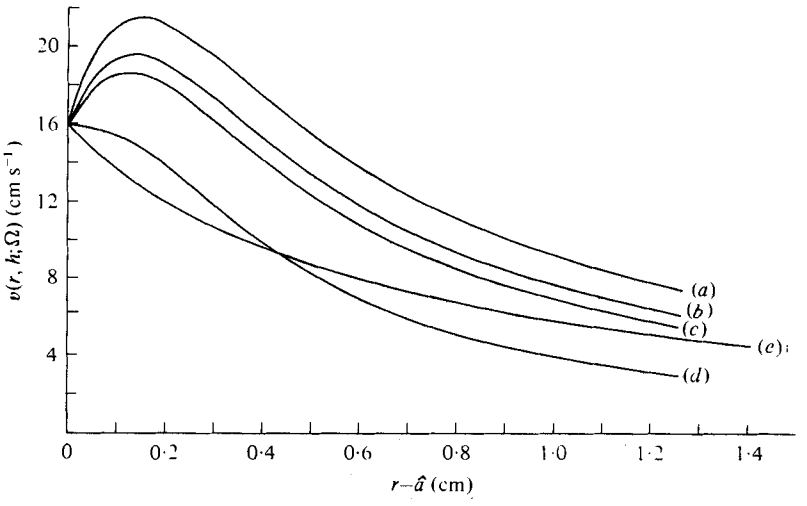

FIGURE 7. Distribution of the total circumferential velocity $v(r, h; \Omega)$ on the free surface up to third order for case (*a*) of figure 1; $v(r, h; \Omega) = \Omega v^{\langle 1\rangle}(r_0) + (\Omega^3/3!)\,[v_1^{\langle 3\rangle}(r_0) + v_2^{\langle 3\rangle}(r_0, 0)]$. $\hat{a} = 0{\cdot}635$ cm; $\eta = 0{\cdot}1$; $S = 231$; $\hat{\beta} = 1{\cdot}0$ g cm^{-1}; $\mu = 150P$; $\Omega = 4$ rev s^{-1}.

	(*a*)	(*b*)	(*c*)	(*d*)
$\hat{\mu}$ (g s cm^{-1})	0·023	0	−0·0117	−0·057

Curve (*e*) shows the primary Couette flow $\Omega v^{\langle 1\rangle}(r_0)$. Only those fluids with large negative values of $\hat{\mu}$ (shear thinning) experience a decrease in speed due to nonlinear effects at third order.

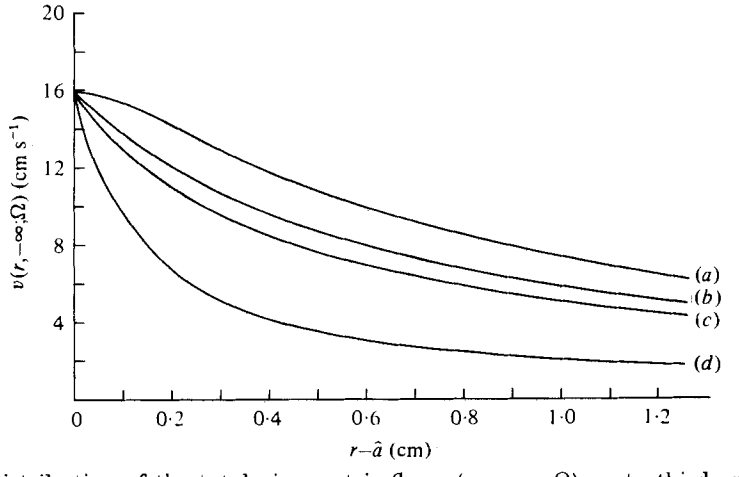

FIGURE 8. Distribution of the total viscometric flow $v(r, -\infty; \Omega)$ up to third order as $z \to -\infty$ for the conditions of figure 7; $v(r, -\infty; \Omega) = \Omega v^{\langle 1\rangle}(r_0) + (\Omega^3/3!)\, v_1^{\langle 3\rangle}(r_0)$. When $\hat{\mu} = 0$,

$$v(r, -\infty; \Omega) = \Omega v^{\langle 1\rangle}(r_0),$$

thus (*b*) represents the primary Couette flow.

the same r which prevails deep in the fluid. They conclude, incorrectly, however, that this z-independent field is given by Couette flow (p. 476) rather than by the z-independent viscometric flow, which differs from Couette flow at order three by the term $v_1^{\langle 3\rangle}(r_0)$. The difference between the two flows is illustrated in figure 8 for the values of $\hat{\mu}$ used in figure 7.

10. Secondary motions

Secondary motions at fourth order are governed by the stream function $\psi(r,z;\Omega)$ defined by (6.4). The component stream functions $\Psi_{4i}(t,y,\eta,S)$ satisfy (6.18). The vertical stratification of inertia and normal stresses, which produces the torques and drives the secondary motions in the planes θ = constant, is embodied in the driving term $\partial F_i/\partial y$ of (6.18a).

We solve (6.18) by the method of biorthogonal eigenfunction expansions discussed in the appendix. It is first necessary to reduce (6.18) to an edge problem in an annular trench. In preparation for this reduction, we write

$$\frac{\partial F_i}{\partial y} = \begin{cases} \dfrac{8}{a^4}\left(At+\dfrac{B}{t}\right)\displaystyle\sum_{n=1} B_{in}\lambda_n \exp(\lambda_n y)\mathscr{C}_1(\lambda_n t), & i=1,2, \quad (10.1a) \\ \dfrac{8B}{a^2t^2}\displaystyle\sum_{n=1} B_{i-2,n}\lambda_n \exp(\lambda_n y)\left(\dfrac{d\mathscr{C}_1(\lambda_n t)}{dt}-\dfrac{\mathscr{C}_1(\lambda_n t)}{t}\right), & i=3,4, \quad (10.1b) \end{cases}$$

and set
$$\Psi_{4i}(t,y,\eta,S) = \hat{\Psi}_{4i}(t,y,\eta,S)+\tilde{\Psi}_{4i}(t,y,\eta,S), \quad (10.2)$$

where
$$L^2\tilde{\Psi}_{4i}+\partial F_i/\partial y = 0, \quad (10.3a)$$
$$\tilde{\Psi}_{4i} = \partial\tilde{\Psi}_{4i}/\partial t = 0 \quad \text{at} \quad t=a,b \quad (10.3b)$$

and
$$L^2\hat{\Psi}_{4i} = 0, \quad (10.4a)$$
$$\hat{\Psi}_{4i} = \partial\hat{\Psi}_{4i}/\partial t = 0 \quad \text{at} \quad t=a,b, \quad (10.4b)$$
$$\hat{\Psi}_{4i}+\tilde{\Psi}_{4i} = \partial^2(\hat{\Psi}_{4i}+\tilde{\Psi}_{4i})/\partial y^2 = 0 \quad \text{on} \quad y=0, \quad (10.4c)$$
$$\hat{\Psi}_{4i}+\tilde{\Psi}_{4i}\to 0 \quad \text{as} \quad y\to-\infty. \quad (10.4d)$$

We find that

$$\tilde{\Psi}_{4i}(t,y) = \begin{cases} \displaystyle\sum_{n=1}^{\infty} B_{in}\exp(\lambda_n y)\zeta_{1n}(t), & i=1,2, \quad (10.5a) \\ \displaystyle\sum_{n=1}^{\infty} B_{i-2,n}\exp(\lambda_n y)\zeta_{2n}(t), & i=3,4, \quad (10.5b) \end{cases}$$

where
$$\zeta_{jn}(t) = \xi_{jn}(t)+\sum_{k=1}^{4} Q_{jk}G_{kn}(t), \quad j=1,2,$$

$$\xi_{1n}(t) = \frac{A}{a^4}\frac{t^3}{\lambda_n}\mathscr{C}_1(\lambda_n t)-\frac{2B}{a^4}\frac{1}{\lambda_n}\left(t\log\frac{t}{a}\mathscr{C}_1(\lambda_n t)+\frac{1}{\lambda_n}\mathscr{C}_0(\lambda_n t)\right),$$

$$\xi_{2n}(t) = \frac{B}{a^2}\mathscr{C}_0(\lambda_n t),$$

with
$$\mathscr{C}_0(\lambda_n t) = J_1(\lambda_n a)\,Y_0(\lambda_n t)-J_0(\lambda_n t)\,Y_1(\lambda_n a)$$

and

$$\begin{pmatrix} G_{1n}(t) \\ G_{2n}(t) \end{pmatrix} = t \begin{pmatrix} J_1(\lambda_n t) \\ Y_1(\lambda_n t) \end{pmatrix}, \quad \begin{pmatrix} G_{3n}(t) \\ G_{4n}(t) \end{pmatrix} = t^2 \begin{pmatrix} J_0(\lambda_n t) \\ Y_0(\lambda_n t) \end{pmatrix}.$$

The constants Q_{jk} $(j = 1, 2)$ are uniquely determined by the boundary conditions (10.3*b*):

$$\zeta_{jn}(a) = \xi_{jn}(a) + \sum_{k=1}^{4} Q_{jk} G_{kn}(a) = 0, \tag{10.6a}$$

$$\zeta_{jn}(b) = \xi_{jn}(b) + \sum_{k=1}^{4} Q_{jk} G_{kn}(b) = 0, \tag{10.6b}$$

$$\zeta'_{jn}(a) = \xi'_{jn}(a) + \sum_{k=1}^{4} Q_{jk} G'_{kn}(a) = 0, \tag{10.6c}$$

$$\zeta'_{jn}(b) = \xi'_{jn}(b) + \sum_{k=1}^{4} Q_{jk} G'_{kn}(b) = 0. \tag{10.6d}$$

The canonical edge problem for $\hat{\Psi}_{4i}$ is defined by (10.4). Using (10.5), we may rewrite the edge conditions (10.4*c*) as

$$\begin{pmatrix} f_i(t) \\ g_i(t) \end{pmatrix} = \begin{pmatrix} \dfrac{\partial^2 \hat{\Psi}_{4i}(t,0)}{\partial y^2} \\ t \dfrac{\partial}{\partial t} \dfrac{1}{t} \dfrac{\partial \hat{\Psi}_{4i}(t,0)}{\partial t} \end{pmatrix} = -\sum_{n=1}^{\infty} B_{in} \begin{pmatrix} \lambda_n^2 \zeta_{1n}(t) \\ t \dfrac{d}{dt} \dfrac{1}{t} \dfrac{d\zeta_{1n}(t)}{dt} \end{pmatrix}, \quad i = 1, 2, \tag{10.7a}$$

$$\begin{pmatrix} f_i(t) \\ g_i(t) \end{pmatrix} = \begin{pmatrix} \dfrac{\partial^2 \hat{\Psi}_{4i}(t,0)}{\partial y^2} \\ t \dfrac{\partial}{\partial t} \dfrac{1}{t} \dfrac{\partial \hat{\Psi}_{4i}(t,0)}{\partial t} \end{pmatrix} = -\sum_{n=1}^{\infty} B_{i-2,n} \begin{pmatrix} \lambda_n^2 \zeta_{2n}(t) \\ t \dfrac{d}{dt} \dfrac{1}{t} \dfrac{d\zeta_{2n}(t)}{dt} \end{pmatrix}, \quad i = 3, 4. \tag{10.7b}$$

The solution of this Stokes-flow edge problem is the same as the one given by Yoo & Joseph (1978) when the data vector, with components $f(t)$ and $g(t)$, is replaced by (10.7). Therefore

$$\hat{\Psi}_{4i} = \sum_{-\infty}^{\infty} C_{im} \frac{\exp(P_m y)}{P_m^2} \phi_1^{(m)}(t),$$

where $\phi_1^{(m)}(t) = A_1^{(m)} t J_1(P_m t) + A_2^{(m)} t\, Y_1(P_m t) + A_3^{(m)} t^2 J_0(P_m t) + A_4^{(m)} t^2 Y_0(P_m t)$

are biorthogonal eigenfunctions with constants $A_k^{(m)}$ and complex eigenvalues P_m chosen (uniquely) such that

$$\phi_1^{(m)}(a) = \phi_1^{(m)}(b) = d\phi_1^{(m)}(a)/dt = d\phi_1^{(m)}(b)/dt = 0.$$

The first 30 values of $P_m(\eta)$ for three different values of η are given in table 23.1 of Yoo (1977). In table 2 we have given the first five values of $P_m(\eta)$ for three values of η.

The constants C_{im} are chosen to represent the edge data at $y = 0$:

$$\begin{pmatrix} f_i(t) \\ g_i(t) \end{pmatrix} = \begin{pmatrix} \dfrac{\partial^2 \hat{\Psi}_{4i}(t,0)}{\partial y^2} \\ t \dfrac{\partial}{\partial t} \dfrac{1}{t} \dfrac{\partial \hat{\Psi}_{4i}(t,0)}{\partial t} \end{pmatrix} = \sum_{-\infty}^{\infty} C_{im} \begin{pmatrix} \phi_1^{(m)}(t) \\ \phi_2^{(m)}(t) \end{pmatrix}. \tag{10.8}$$

m	Re $(P_m(1/10))$	Im $(P_m(1/10))$
	(a)	
1	2·20833076225827	1·04119174170651
2	3·83365774050931	1·31696443616135
3	5·43106064681606	1·49912014659564
4	7·01699724709610	1·63478530623688
5	8·59721592756949	1·74244686387722
	(b)	
m	Re $(P_m(4/8·5))$	Im $(P_m(4/8·5))$
1	2·12450992720923	1·11492116235026
2	3·76107821933820	1·37920072184694
3	5·36548413171664	1·54850353040378
4	6·95735569305069	1·67405570026184
5	8·54282244577007	1·77407454902532
	(c)	
m	Re $(P_m(6/8·5))$	Im $(P_m(6/8·5))$
1	2·11033277215611	1·12312200135300
2	3·75149711564217	1·38332821070635
3	5·35823055726337	1·55098791095229
4	6·95153303253042	1·67571835529977
5	8·53796706049070	1·77526802935806

TABLE 2. The first five values of $P_m(\eta)$ for the three different values of η. (a) $\eta = 1/10$. (b) $\eta = 4/8·5$. (c) $\eta = 6/8·5$.

Application of the biorthogonality conditions (A 13) to (10.8) and integration by parts lead to

$$C_{im} = \frac{1}{K_m}\left\{\int_a^b \frac{P_m^2}{t}[-\hat{\phi}_m(t) - \phi_1^{(m)}(t)]\left[-\sum_{n=1}^{\infty} B_{in}\,\zeta_{1n}(t)\right]dt + \int_a^b \frac{\phi_1^m(t)}{t}\left[-\sum_{n=1}^{\infty} B_{in}\,\lambda_n^2\,\zeta_{1n}(t)\right]dt\right\}, \quad i = 1, 2, \tag{10.9a}$$

$$C_{im} = \frac{1}{K_m}\left\{\int_a^b \frac{P_m^2}{t}[-\hat{\phi}_m(t) - \phi_1^{(m)}(t)]\left[-\sum_{n=1}^{\infty} B_{i-2,n}\,\zeta_{2n}(t)\right]dt + \int_a^b \frac{\phi_1^{(m)}(t)}{t}\left[-\sum_{n=1}^{\infty} B_{i-2,n}\,\lambda_n^2\,\zeta_{2n}(t)\right]dt\right\}, \quad i = 3, 4, \tag{10.9b}$$

where

$$\hat{\phi}_m(t) = \frac{4A_3^{(m)}}{P_m} tJ_1(P_m t) + \frac{4A_4^{(m)}}{P_m} tY_1(P_m t).$$

We note that the edge data (10.8), and thus the integrands in (10.9), are expressed in series forms. We simply truncate these series after N terms or, for small values of η (e.g. $\eta = \frac{1}{10}$), take the Cesaro sum over N partial sums of these series, where N is large enough to ensure that each series is well represented. The integrals in (10.9) are then evaluated numerically using Simpson's rule. The first 30 values of $C_{im}(\eta, S)$ $(i = 1, 2, 3, 4)$ for three different values of (η, S) are given in table 23.2 of Yoo (1977).

Since the edge data $f(t)$ and $g(t)$ are $C^\infty[-1, 1]$ and $f(a) = f(b) = f'(a) = f'(b) = 0$ the

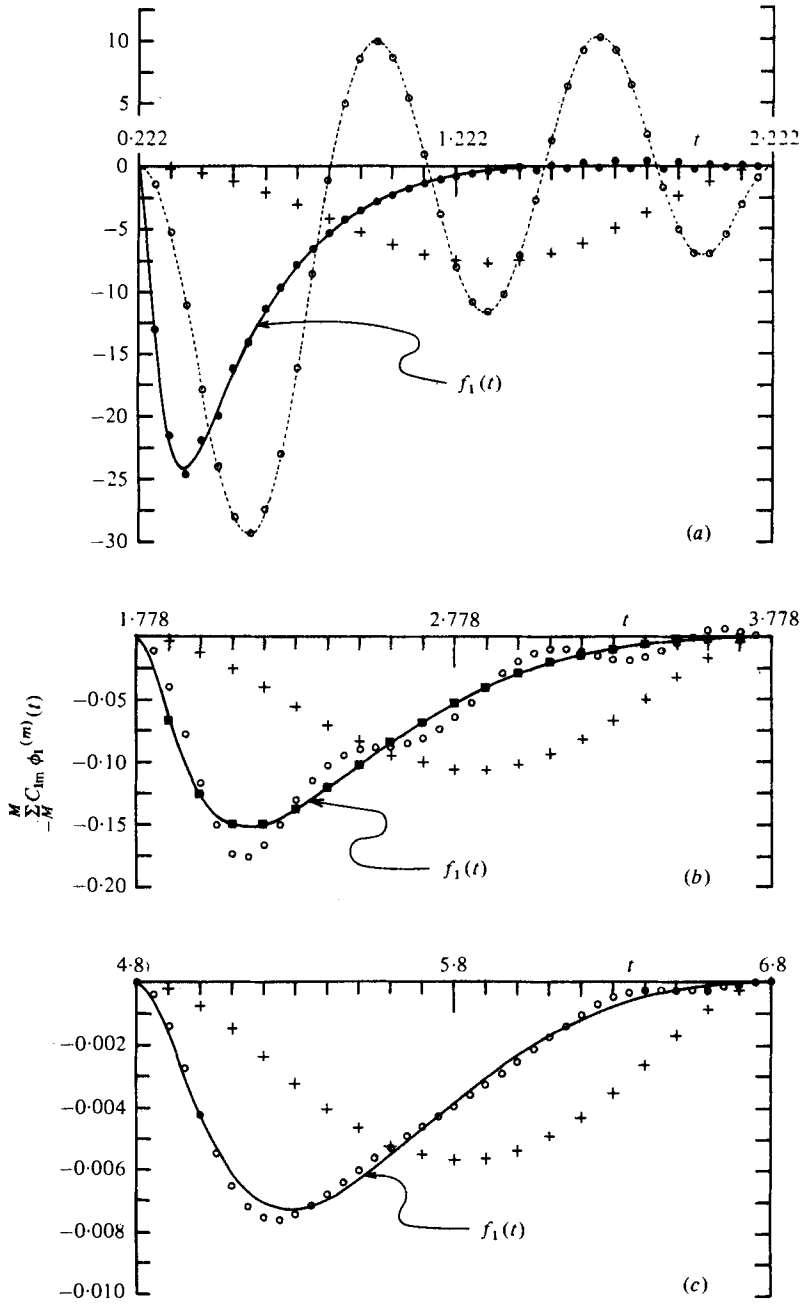

FIGURE 9. Convergence of the biorthogonal series (10.8) to the edge data (solid line) for the three cylinder pairs of figure 1.

	(*a*)	(*b*)	(*c*)
$\eta\left(=\frac{\hat{a}}{\hat{b}}\right)$	$\frac{0{\cdot}635}{6{\cdot}35}$	$\frac{4{\cdot}0}{8{\cdot}5}$	$\frac{6{\cdot}0}{8{\cdot}5}$
S	231	143	44
$f_1(t)$	$\frac{1}{200}\sum_{N=1}^{200}\left(-\sum_{n=1}^{N} B_{1n}\lambda_n^2\zeta_{1n}(t)\right)$	$-\sum_{n=1}^{100} B_{1n}\lambda_n^2\zeta_{1n}(t)$	$-\sum_{n=1}^{60} B_{1n}\lambda_n^2\zeta_{1n}(t)$

Convergence is rapid when the data do not rise too steeply near the wall. M: +, 1; ○, 5; ■, 20; ●, 40.

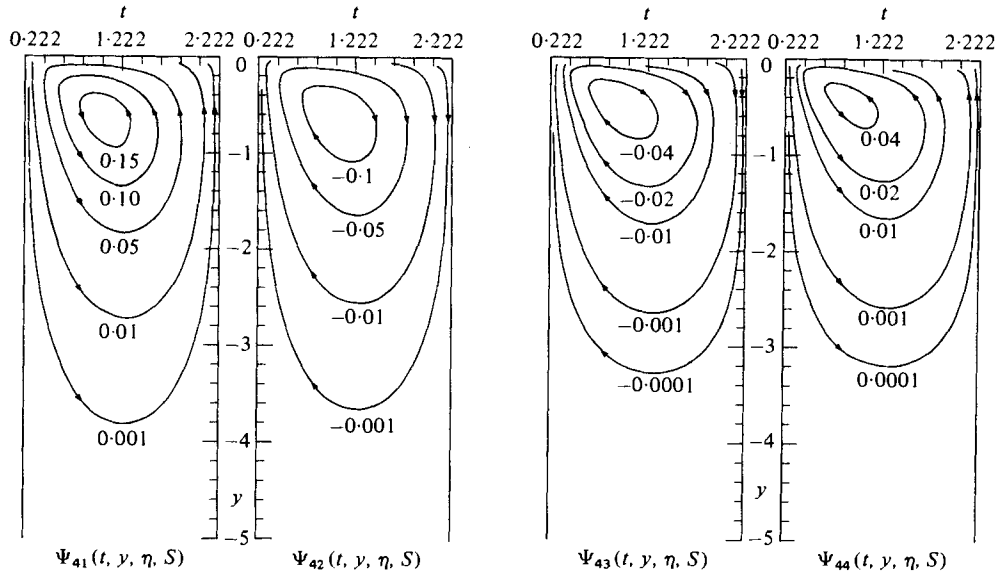

FIGURE 10. Contours in the dimensionless reference domain of the components (10.10) of the total stream function $\Psi_4(t,y) = R_1\Psi_{41} + R_2\Psi_{42} + R_3\Psi_{43} + R_4\Psi_{44}$. The contribution $R_1\Psi_{41} + R_2\Psi_{42}$ is associated with the vertical stratification of inertia represented by the penultimate term in (6.4), while $R_3\Psi_{43} + R_4\Psi_{44}$ is associated with the vertical stratification of the normal stress represented by the last term in (6.4). Since the sign of the corner eddies of Ψ_{42} and Ψ_{43} are opposite to those of Ψ_{41} and Ψ_{44}, superposition of solutions can lead to widely different maps of the contours of the total stream function. $\eta = 0{\cdot}635/6{\cdot}35$; $S = 231$.

convergence theorem of the appendix holds and the series (10.8) eventually converges uniformly and absolutely at a rate better than the numerical series Σn^{-2}. In figure 9 we give some representative examples of how the biorthogonal series (10.8) converge to the prescribed edge data $f_i(t)$ defined in (10.7). In this figure $i = 1$ (the convergence result is the same when $i = 2, 3, 4$), and M is the number of terms in the biorthogonal series which is necessary for acceptable convergence. The number M increases as η decreases. Convergence to the stream function given below is uniform and absolute at a rate faster than the numerical series Σn^{-4}:

$$\Psi_{41}(t,y) = \sum_{-\infty}^{\infty} C_{1m}\frac{\exp(P_m y)}{P_m^2}\phi_1^{(m)}(t) + \sum_{n=1}^{\infty} B_{1n}\exp(\lambda_n y)\zeta_{1n}(t), \qquad (10.10a)$$

$$\Psi_{42}(t,y) = \sum_{-\infty}^{\infty} C_{2m}\frac{\exp(P_m y)}{P_m^2}\phi_1^{(m)}(t) + \sum_{n=1}^{\infty} B_{2n}\exp(\lambda_n y)\zeta_{1n}(t), \qquad (10.10b)$$

$$\Psi_{43}(t,y) = \sum_{-\infty}^{\infty} C_{3m}\frac{\exp(P_m y)}{P_m^2}\phi_1^{(m)}(t) + \sum_{n=1}^{\infty} B_{1n}\exp(\lambda_n y)\zeta_{2n}(t), \qquad (10.10c)$$

$$\Psi_{44}(t,y) = \sum_{-\infty}^{\infty} C_{4m}\frac{\exp(P_m y)}{P_m^2}\phi_1^{(m)}(t) + \sum_{n=1}^{\infty} B_{2n}\exp(\lambda_n y)\zeta_{2n}(t). \qquad (10.10d)$$

We have plotted the contours of the four functions defined in (10.10) for three different values of (η, S) in figures 10, 11 and 12. The total stream functions formed from the component functions of figures 10–12 are shown in figures 13(*a*), (*b*) and (*c*) respectively, where realistic values of α_1 and α_2 have been employed.

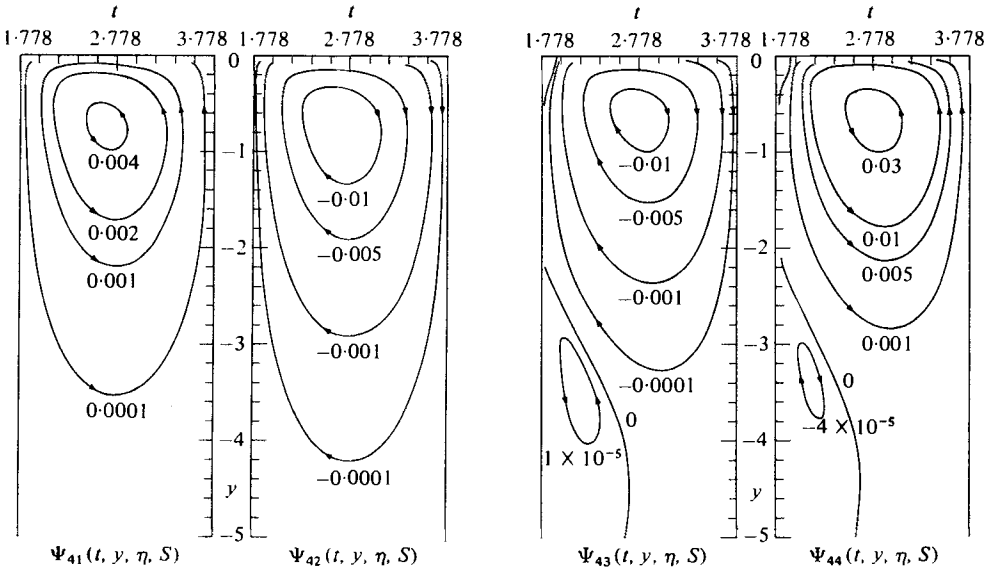

FIGURE 11. As for figure 10 but for $\eta = 4{\cdot}0/8{\cdot}5$; $S = 143$.

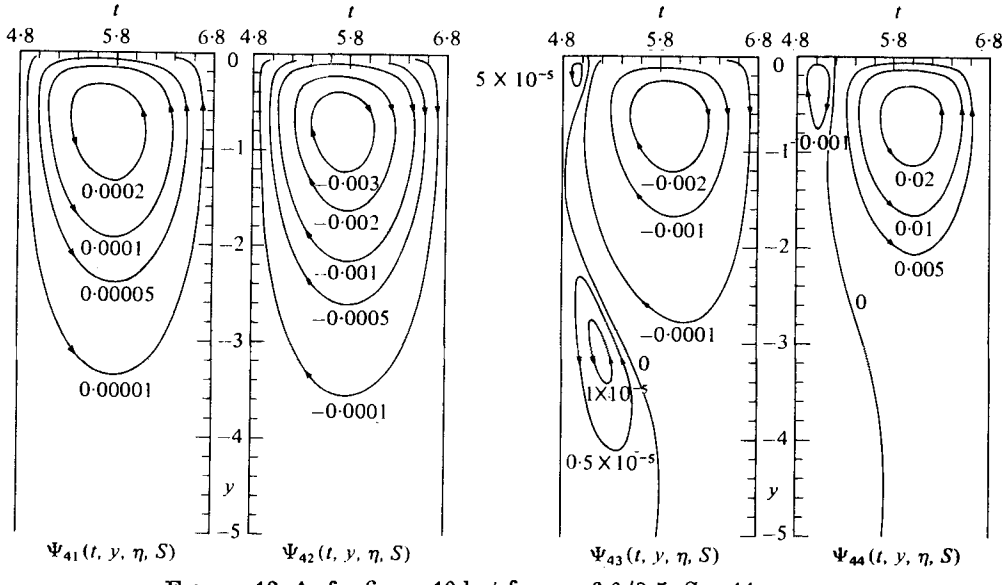

FIGURE 12. As for figure 10 but for $\eta = 6{\cdot}0/8{\cdot}5$; $S = 44$.

To obtain the level lines of the secondary motion in the deformed domain we must invert the mapping of the deformed domain into the reference domain. This inversion is accomplished in two steps; we first reintroduce the physical variables

$$(r_0, z_0) = \tfrac{1}{2}(\hat{b} - \hat{a})(t, y),$$

then we invert the shifting transformation (4.5). The inversion of (4.5) up to order four can be completed after we compute $h^{[4]}$. For now, our main observation is that the secondary motion in the climbing bubble, where the motion is most intense, becomes

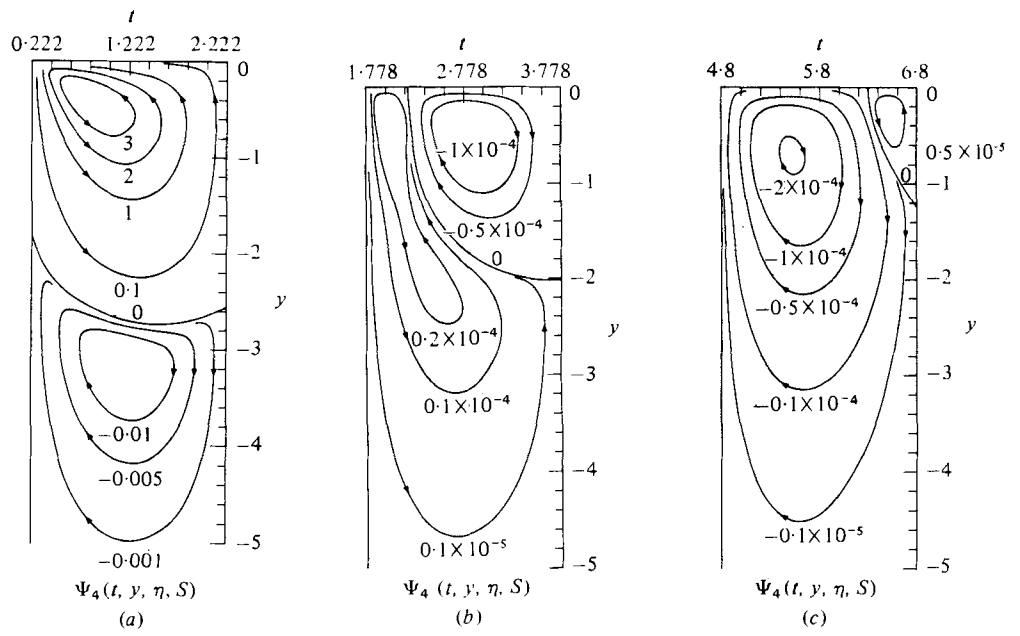

FIGURE 13. Contours of the total stream function $\Psi_4(t,y) = R_1\Psi_{41} + R_2\Psi_{42} + R_3\Psi_{43} + R_4\Psi_{44}$ in the dimensionless reference domain, where $R_1 = 1$, $R_2 = 4(3\alpha_1 + 2\alpha_2)/\rho\hat{a}^2$, $R_3 = 4(\alpha_1 + \alpha_2)/\rho\hat{a}^2$, $R_4 = R_3R_2$. $3\alpha_1 + 2\alpha_2 = 1{\cdot}0\,\mathrm{g\,cm^{-1}}$; $\alpha_1 + \alpha_2 = 1{\cdot}0\,\mathrm{g\,cm^{-1}}$.

	(a)	(b)	(c)
$\eta\left(=\frac{\hat{a}}{\hat{b}}\right)$	$\frac{0{\cdot}635}{6{\cdot}35}$	$\frac{4{\cdot}0}{8{\cdot}5}$	$\frac{6{\cdot}0}{8{\cdot}5}$
S	231	143	44

independent of $\hat{b}$ when $\eta = \hat{a}/\hat{b} < \frac{1}{5}$. The reader may verify this statement by checking the flow in the upper left-hand corners of the two pictures in figures 14(*a*) and (*b*), where $\hat{a} = 0{\cdot}635$ cm, $\hat{b} = 3{\cdot}175$ cm and $\hat{a} = 0{\cdot}635$ cm, $\hat{b} = 6{\cdot}35$ cm respectively.

11. The rise in height at fourth order

To obtain the height rise at fourth order it is necessary to calculate the pressure distribution at fourth order, which has two parts. One part is independent of z (or y) and is induced by z-independent viscometric flow and depends on $\hat{\mu}$ and $\hat{\gamma}$. The other part, which is dependent on r and z, is induced by the combined effect of the z-dependent part of the circumferential velocity and the secondary motion in the azimuthal plane. The component functions of the first part have already been obtained in (6.9)–(6.12). The component functions of the second part may be obtained by integration of the equations preceding (6.19) once the stream functions $\Psi_{4i}(t,y)$ are known. We find that

$$\Phi_{41}(t,y) = a^3\left\{\sum_{-\infty}^{\infty} C_{1m}[\exp(P_m y)\chi_m(t) + D_m] + \sum_{n=1}^{\infty} B_{1n}[\exp(\lambda_n y)q_{1n}(t) + D_{1n}]\right\} - \mathscr{H}_{41}, \quad (11.1)$$

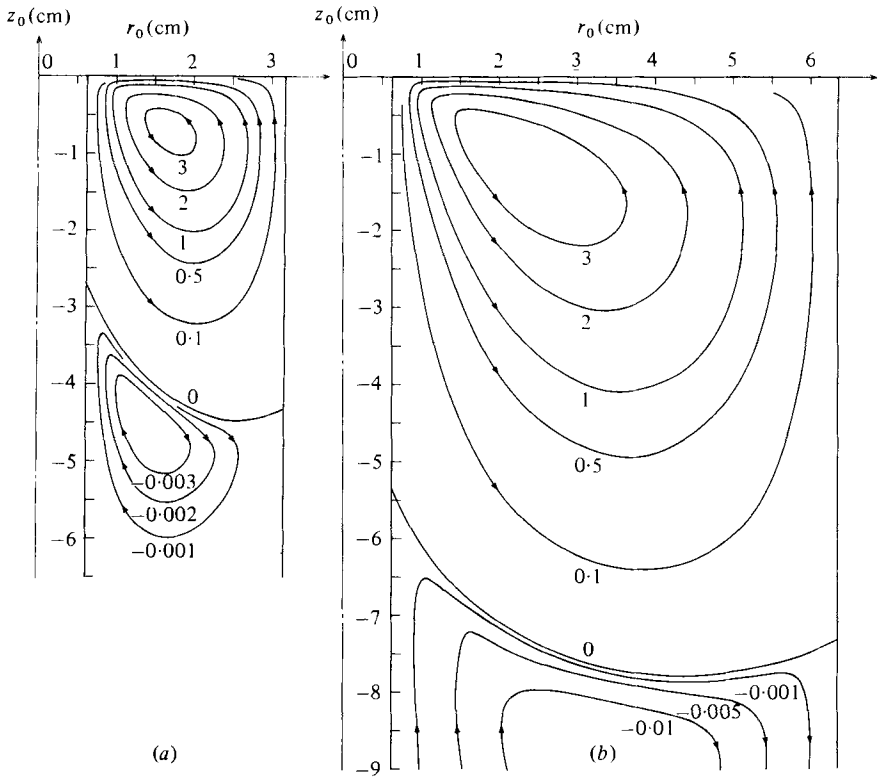

FIGURE 14. Contours of the total stream function in the dimensional reference domain:

$$\frac{\mu g \psi^{\langle 4\rangle}(r_0, z_0)}{\rho \hat{a}^6} \frac{24}{\Omega^4} = \sum_{i=1}^{4} R_i \Psi_{4i}(t, y, \eta, S) = \sum_{i=1}^{4} R_i \psi_{4i}(r_0, z_0).$$

$3\alpha_1 + 2\alpha_2 = 1{\cdot}0\,\mathrm{g\,cm^{-1}}$; $\alpha_1 + \alpha_2 = 1{\cdot}0\,\mathrm{g\,cm^{-1}}$.

	(*a*)	(*b*)
$\hat{a}$ (cm)	0·635	0·635
$\hat{b}$ (cm)	3·175	6·35
η	$\frac{1}{5}$	$\frac{1}{10}$
S	45·6	231

The identification of the contours of the stream function in the upper left-hand corner of the two diagrams indicates that the streamlines in the climbing bubble become independent of $\hat{b}$ when $\hat{a}/\hat{b} < \frac{1}{5}$.

$$\Phi_{42}(t, y) = a^3 \Big\{ \sum_{-\infty}^{\infty} C_{2m}[\exp(P_m y)\chi_m(t) + D_m] + \sum_{n=1}^{\infty} B_{2n}[\exp(\lambda_n y) q_{1n}(t) + D_{1n}] + \sum_{n=1}^{\infty} B_{1n} \exp(\lambda_n y) q_{3n}(t) \Big\} - \mathscr{H}_{42}, \quad (11.2)$$

$$\Phi_{43}(t, y) = a^3 \Big\{ \sum_{-\infty}^{\infty} C_{3m}[\exp(P_m y)\chi_m(t) + D_m] + \sum_{n=1}^{\infty} B_{1n}[\exp(\lambda_n y) q_{2n}(t) + D_{2n}] \Big\} - \mathscr{H}_{43}, \quad (11.3)$$

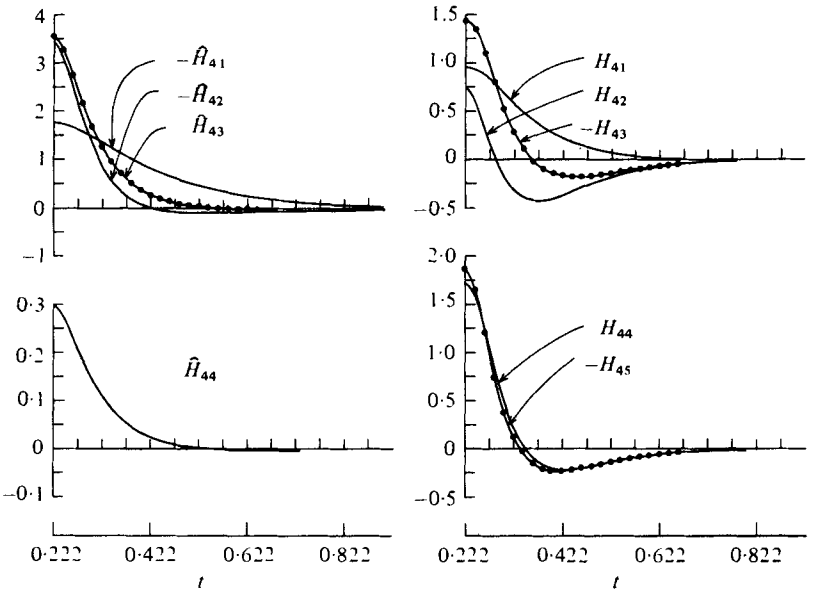

FIGURE 15. Component functions of the height-rise coefficients at fourth order appearing in (6.3): $\hat{H}_{4i}(t,\eta,S)$ $(i=1,2,3,4)$; $H_{4j}(t,\eta,S)$ $(j=1,2,3,4,5)$. $\hat{a}=0{\cdot}635\,\mathrm{cm}$; $\hat{b}=6{\cdot}35\,\mathrm{cm}$; $S=231$.

$$\Phi_{44}(t,y)=a^3\Big\{\sum_{-\infty}^{\infty}C_{4m}[\exp(P_m y)\,\chi_m(t)+D_m]+\sum_{n=1}^{\infty}B_{2n}[\exp(\lambda_n y)\,q_{2n}(t)+D_{2n}]\Big\}-\mathscr{H}_{44}, \quad (11.4)$$

$$\Phi_{45}(t,y)=a^3\sum_{n=1}^{\infty}B_{2n}\exp(\lambda_n y)\,q_{3n}(t)-\mathscr{H}_{45}, \quad (11.5)$$

where

$$\chi_m(t)=2P_m^{-1}\{A_3^{(m)}J_0(P_m t)+A_4^{(m)}Y_0(P_m t)\},$$

$$q_{1n}(t)=\frac{A}{a^4}\Big\{-\frac{8}{\lambda_n}\mathscr{C}_0(\lambda_n t)+4t\mathscr{C}_1(\lambda_n t)\Big\}-\frac{2B}{a^4}\frac{2}{t}\mathscr{C}_1(\lambda_n t)+2\lambda_n\{Q_{13}J_0(\lambda_n t)+Q_{14}Y_0(\lambda_n t)\},$$

$$q_{2n}(t)=2\lambda_n\{Q_{23}J_0(\lambda_n t)+Q_{24}Y_0(\lambda_n t)\},$$

$$q_{3n}(t)=\frac{B}{a^2}\Big\{\frac{4}{t^3}\mathscr{C}_1(\lambda_n t)-\frac{2\lambda_n}{t^2}\mathscr{C}_0(\lambda_n t)\Big\},$$

$$D_m=-\frac{2}{b^2-a^2}\Big(\frac{2}{P_m^2}\Big)[t\{A_3^{(m)}J_1(P_m t)+A_4^{(m)}Y_1(P_m t)\}]_a^b,$$

$$D_{1n}=-\frac{2}{b^2-a^2}\Big[-\frac{A}{a^4}\frac{4t^2}{\lambda_n}\mathscr{C}_0(\lambda_n t)+\frac{2B}{a^4}\frac{2}{\lambda_n}\mathscr{C}_0(\lambda_n t)+2t\{Q_{13}J_1(\lambda_n t)+Q_{14}Y_1(\lambda_n t)\}\Big]_a^b,$$

$$D_{2n}=-\frac{2}{b^2-a^2}[2t\{Q_{23}J_1(\lambda_n t)+Q_{24}Y_1(\lambda_n t)\}]_a^b.$$

Extensive tables of values of the functions $\Phi_{4i}(t,0)$ for three different values of (η,S) and of the functions $\hat{\Phi}_{4i}(t)$ for three different values of η are given in tables 24.1, 24.2 and 24.3 of Yoo (1977).

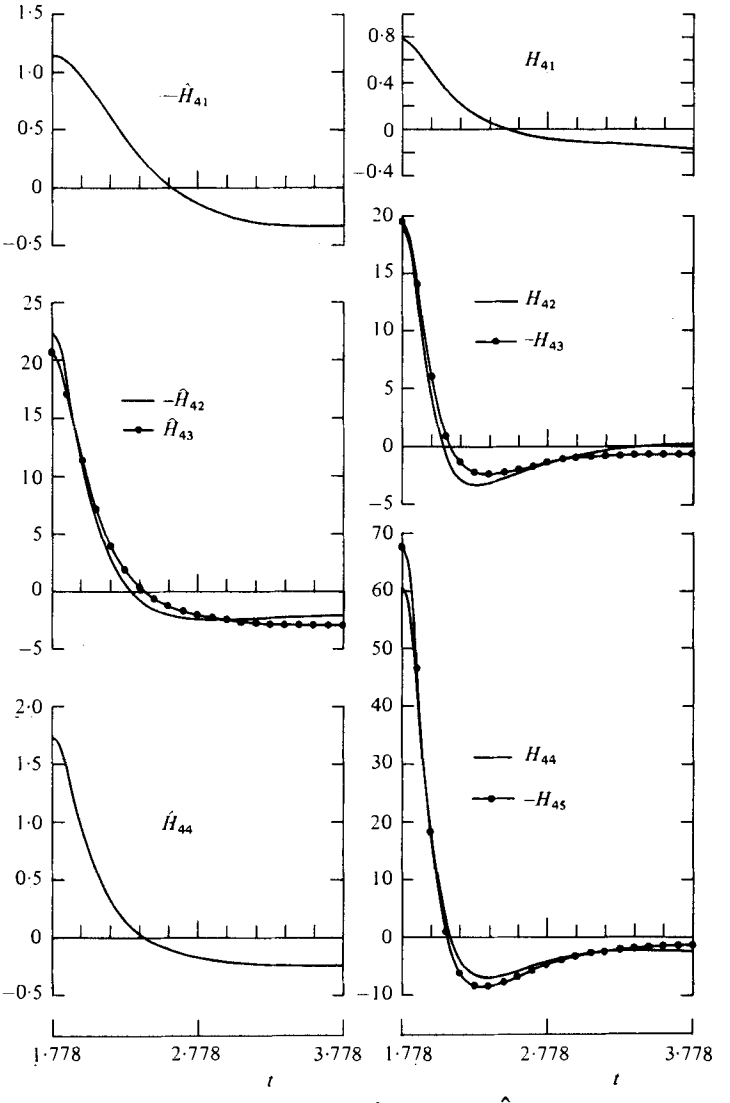

FIGURE 16. As for figure 15 but for $\hat{a} = 4{\cdot}0$ cm; $\hat{b} = 8{\cdot}5$ cm; $S = 143$.

The inhomogeneous terms of the equations (6.21) for the height rise coefficient can w be computed from (10.10) and (11.1)–(11.5):

$$\Phi_{41}(t,0)+\frac{2a^3}{t}\frac{\partial^2\Psi_{41}(t,0)}{\partial t\,\partial y} = a^3\left\{\sum_{-\infty}^{\infty} C_{1m}\hat{\chi}_m(t)+\sum_{n=1}^{\infty} B_{1n}\hat{\zeta}_{1n}(t)\right\}-\mathscr{H}_{41}, \tag{11.6}$$

$$\Phi_{42}(t,0)+\frac{2a^3}{t}\frac{\partial^2\Psi_{42}(t,0)}{\partial t\,\partial y} = a^3\left\{\sum_{-\infty}^{\infty} C_{2m}\hat{\chi}_m(t)+\sum_{n=1}^{\infty} B_{2n}\hat{\zeta}_{1n}(t)+\sum_{n=1}^{\infty} B_{1n}q_{3n}(t)\right\}-\mathscr{H}_{42}, \tag{11.7}$$

$$\Phi_{43}(t,0)+\frac{2a^3}{t}\frac{\partial^2\Psi_{43}(t,0)}{\partial t\,\partial y} = a^3\left\{\sum_{-\infty}^{\infty} C_{3m}\hat{\chi}_m(t)+\sum_{n=1}^{\infty} B_{1n}\hat{q}_{2n}(t)\right\}-\mathscr{H}_{43}, \tag{11.8}$$

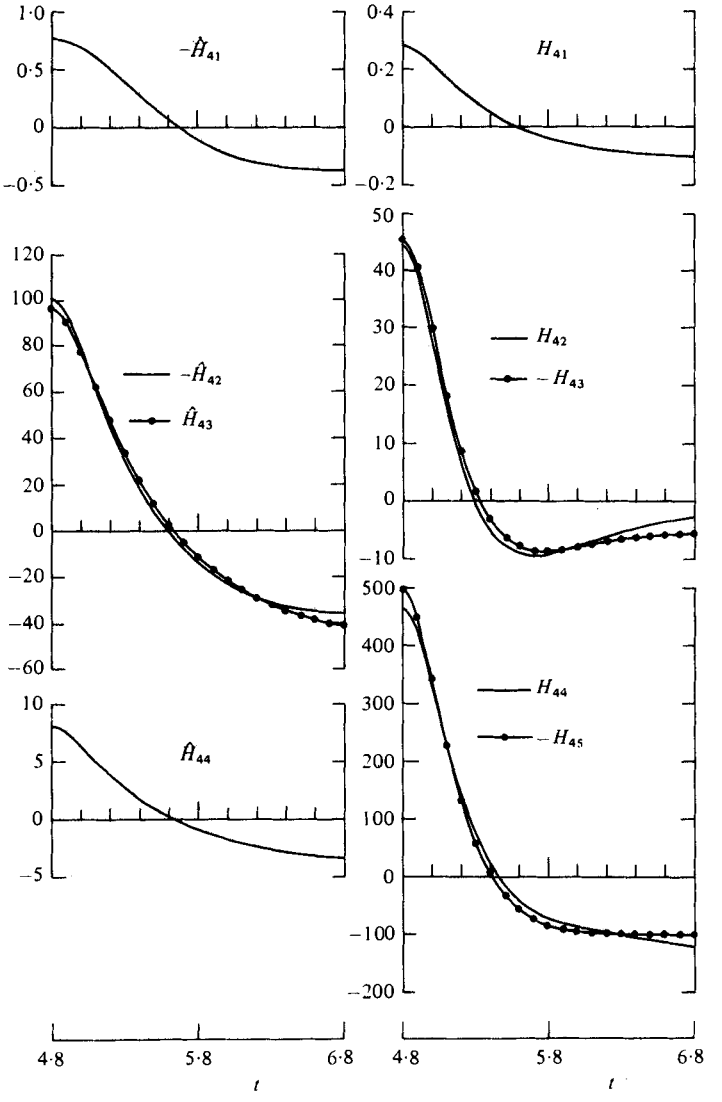

FIGURE 17. As for figure 15 but for $\hat{a} = 6{\cdot}0\,\text{cm}$; $\hat{b} = 8{\cdot}5\,\text{cm}$; $S = 44$.

$$\Phi_{44}(t,0) + \frac{2a^3}{t}\frac{\partial^2 \Psi_{44}(t,0)}{\partial t\,\partial y} = a^3\left\{\sum_{-\infty}^{\infty} C_{4m}\,\hat{\chi}_m(t) + \sum_{n=1}^{\infty} B_{2n}\,\hat{q}_{2n}(t)\right\} - \mathscr{H}_{44}, \tag{11.9}$$

$$\Phi_{45}(t,0) = a^3 \sum_{n=1}^{\infty} B_{2n}\,q_{3n}(t) - \mathscr{H}_{45}, \tag{11.10}$$

where

$$\hat{\chi}_m(t) = 2\{A_1^{(m)} J_0(P_m t) + A_2^{(m)} Y_0(P_m t)\} + \frac{6}{P_m}\{A_3^{(m)} J_0(P_m t) + A_4^{(m)} Y_0(P_m t)\}$$

$$- 2t\{A_3^{(m)} J_1(P_m t) + A_4^{(m)} Y_1(P_m t)\} - \frac{2}{b^2 - a^2}\frac{2}{P_m^2}[t\{A_3^{(m)} J_1(P_m t) + A_4^{(m)} Y_1(P_m t)\}]_a^b,$$

$$\hat{q}_{1n}(t) = \frac{A}{a^4}\left\{-\frac{8}{\lambda_n}\mathscr{C}_0(\lambda_n t) + 8t\mathscr{C}_1(\lambda_n t) + 2\lambda_n t^2\mathscr{C}_0(\lambda_n t)\right\}$$
$$-\frac{2B}{a^4}\left\{\frac{2}{t}\mathscr{C}_1(\lambda_n t) + 2\lambda_n \log\frac{t}{a}\mathscr{C}_0(\lambda_n t)\right\}$$
$$+ 2\lambda_n^2\{Q_{11}J_0(\lambda_n t) + Q_{12}Y_0(\lambda_n t)\} + 6\lambda_n\{Q_{13}J_0(\lambda_n t) + Q_{14}Y_0(\lambda_n t)\}$$
$$- 2\lambda_n^2 t\{Q_{13}J_1(\lambda_n t) + Q_{14}Y_1(\lambda_n t)\}$$
$$-\frac{2}{b^2-a^2}\left[-\frac{A}{a^4}\frac{4t^2}{\lambda_n}\mathscr{C}_0(\lambda_n t) + \frac{2B}{a^4}\frac{2}{\lambda_n}\mathscr{C}_0(\lambda_n t) + 2t\{Q_{13}J_1(\lambda_n t) + Q_{14}Y_1(\lambda_n t)\}\right]_a^b,$$

$$\hat{q}_{2n}(t) = -\frac{2B}{a^2}\frac{\lambda_n^2}{t}\mathscr{C}_1(\lambda_n t) + 2\lambda_n^2\{Q_{21}J_0(\lambda_n t) + Q_{22}Y_0(\lambda_n t)\}$$
$$+ 6\lambda_n\{Q_{23}J_0(\lambda_n t) + Q_{24}Y_0(\lambda_n t)\} - 2\lambda_n^2 t\{Q_{23}J_1(\lambda_n t) + Q_{24}Y_1(\lambda_n t)\}$$
$$-\frac{2}{b^2-a^2}[2t\{Q_{23}J_1(\lambda_n t) + Q_{24}Y_1(\lambda_n t)\}]_a^b.$$

The four component functions satisfying (6.20) and five component functions satisfying (6.21) for the boundary conditions $H'(a) = H'(b) = 0$ are plotted in figures 15–17 for the three different values of (η, S) that have been used in the previous figures.

Various superpositions of these component functions define the shape of the free surface up to order four. These superpositions are discussed next.

12. Determination of the numerical values of the rheological constants up to order four

In principle we can determine the material constants μ, $\hat{\alpha}$, $\hat{\beta}$, $\hat{\mu}$ and $\hat{\gamma}$ by comparing theory and experiment. When these constants are known the distribution of circumferential velocity, secondary motion and height rise up to order four are uniquely determined. We now turn our attention to some methods for converting this point of principle into a practical technique for rheometrical measurements.

The constant μ can be determined by simple torque measurements at the lowest values of the angular velocity. We shall suppose that μ is known. Then the nonlinear response of the fluid up to order four is determined by the values of the four rheological constants $\hat{\beta} = 3\alpha_1 + 2\alpha_2$, $\hat{\alpha} = \alpha_1 + \alpha_2$, $\hat{\mu} = \beta_2 + \beta_3$ and $\hat{\gamma} = \gamma_3 + \gamma_4 + \gamma_5 + \frac{4}{7}\gamma_6$ which appear in the fourth-order theory of the Weissenberg effect. These constants may be determined sequentially. We first find $\hat{\beta}$ from height-rise measurements at the smallest values of the angular velocity Ω. We may then determine $\hat{\mu}$ from the distribution of circumferential velocity at the smallest values of Ω. The two remaining constants $\hat{\alpha}$ and $\hat{\gamma}$ can then be determined by measuring free-surface profiles at slightly larger values of the angular velocity. In this way all five constants which characterize the Weissenberg effect up to order four can be determined from experimental measurements by use of the Weissenberg effect alone.

The rheometrical method just described can be carried out in practice, as we show below, but it is a time-consuming and delicate method.

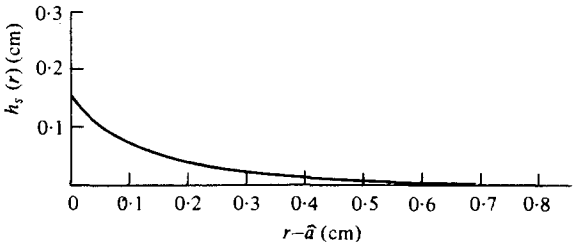

FIGURE 18. The static rise $h_s(r)$ satisfying the nonlinear surface-tension equation (12.3) for the sample of STP used by Beavers & Joseph (1975) to generate the experimental data shown in figure 22. $P_1 = -\tan 55°$; $P_2 = 0$.

12.1. *Determination of $\hat{\alpha}$, $\hat{\gamma}$ and $\hat{\mu}$ by profile fitting*

In our first comparisons of theory and experiment we used data collected by Beavers & Joseph (1975) for STP. Unfortunately, circumferential velocity profiles were not measured by Beavers & Joseph, so that three constants must be determined from the measured height-rise curves. The experiments were performed with circular rods of small radius $\hat{a}$ rotating in a circular container of radius $\hat{b} = 15{\cdot}25$ cm. We confine our attention to the experiments with $\hat{a} = 0{\cdot}635$ cm. In their experiments Beavers & Joseph coated some rods with Scotchgard, while other rods were uncoated. The coated rods are better suited for comparisons with theory because the coating essentially eliminates the static rise and allows the assumption $h'(\hat{a}) = h'(\hat{b}) = 0$ of the theory to be satisfied. Unfortunately, Beavers & Joseph have very little data on climbing onto coated rods in the range of angular velocities of interest in the higher-order theory. For uncoated rods we are therefore forced to use the *ad hoc* procedure of adding to the total rise due to motion a static rise computed from the nonlinear surface-tension equation using experimentally determined contact angles.

The raw experimental data which we shall now use are shown as a solid line in the eight frames of figure 22. The dashed lines are from the second-order theory:

$$h(r;\Omega) = h_s(r_0) + \tfrac{1}{2}h^{[2]}(r_0)\,\Omega^2. \tag{12.1}$$

Beavers & Joseph (1975) found that the second-order theory (12.1) could be made to fit the low angular velocity data ($\omega < 3\,\mathrm{rev\,s^{-1}}$), if

$$\hat{\beta} = 1{\cdot}0\,\mathrm{g\,cm^{-1}} \tag{12.2}$$

(see their figure 9 and table 1). For the uncoated rods, a static climb $h = h_s$ when $\Omega = 0$ has been added in (12.1): $h_s(r)$ satisfies the nonlinear surface-tension equation

$$\frac{T}{r}\left(\frac{rh_s'}{(1+h_s'^2)^{\frac{1}{2}}}\right)' - \rho g h_s = C, \quad h_s'(\hat{a}) = P_1, \quad h_s'(\hat{b}) = P_2, \tag{12.3}$$

where P_1 and P_2 are taken from measured values of the contact angle and C is a constant chosen such that the volume average of h_s is zero:

$$T\left(\frac{\hat{b}P_2}{(1+P_2^2)^{\frac{1}{2}}} - \frac{\hat{a}P_1}{(1+P_1^2)^{\frac{1}{2}}}\right) = C\frac{\hat{b}^2-\hat{a}^2}{2}. \tag{12.4}$$

The static rise for $P_1 = -\tan 55°$ and $P_2 = 0$ (roughly a mean value for the uncoated rods mentioned in figure 22) is shown in figure 18.

We now consider the experimental results in the light of fourth-order theory:

$$h(r;\Omega) = h_s + \frac{1}{2!}h^{[2]}\Omega^2 + \frac{1}{4!}h^{[4]}\Omega^4. \tag{12.5}$$

To compare (12.5) with experiments it is necessary to choose the values of the three remaining rheological constants $\hat{\alpha}$, $\hat{\mu}$ and $\hat{\gamma}$ on which $h^{[4]}(r) = h^{[4]}(r, \hat{\alpha}, \hat{\beta}, \hat{\mu}, \hat{\gamma})$ depends. A method for determining the values of these constants will now be discussed.

The constants to be determined are such that the theoretical and measured rise curves agree over the largest interval of values of Ω. The theoretical expression (12.5) for the height may be written as

$$\begin{aligned} h(r;\Omega) = h_s(r) + \frac{\hat{a}}{2}\left(\frac{\Omega}{\Omega_0}\right)^2 \Big\{ & H_{21}(t,\eta,S) + R_2 H_{22}(t,\eta,S) \\ & + \frac{\Omega^2}{12K_1}[\hat{H}_{41}(t,\eta,S) + R_2\hat{H}_{42}(t,\eta,S) + R_3\hat{H}_{43}(t,\eta,S)] \\ & + \frac{\Omega^2}{12K_2}R_2\hat{H}_{44}(t,\eta,S) + \frac{1}{12}\left(\frac{\Omega}{\Omega_0}\right)^2 [H_{41}(t,\eta,S) + R_2 H_{42}(t,\eta,S) \\ & + R_3 H_{43}(t,\eta,S) + R_4 H_{44}(t,\eta,S) + R_5 H_{45}(t,\eta,S)]\Big\}, \end{aligned} \tag{12.6}$$

where, for the STP motor-oil additive used by Beavers & Joseph, the following quantities are known:

$$g = 980\,\mathrm{cm\,s^{-2}}, \quad \rho = 0{\cdot}89\,\mathrm{g\,cm^{-3}}, \quad T = 30{\cdot}9\,\mathrm{g\,s^{-2}}, \quad \mu = 150\,\mathrm{g\,cm^{-1}\,s^{-1}},$$

$$(\hat{a}, \hat{b}) = (0{\cdot}635\,\mathrm{cm},\ 6{\cdot}35\,\mathrm{cm}),\dagger$$

$$\Omega_0^2 = g/\hat{a} = 1{\cdot}54 \times 10^3\,\mathrm{s^{-2}}, \quad S = \rho g(\hat{b}-\hat{a})^2/(4T) = 231,$$

$$R_2 = 4\hat{\beta}/(\rho\hat{a}^2) = 11{\cdot}15, \quad R_5 = R_2^2 = 124{\cdot}2.$$

The unknown quantities which are to be determined from the experiments are

$$R_3 = 4\hat{\alpha}/(\rho\hat{a}^2), \quad R_4 = R_2 R_3, \quad K_1 = \mu/(16\hat{\mu}), \quad K_2 = \hat{\beta}/(336\hat{\gamma}).$$

In figures 19–21 we have plotted the functions

$$\sum_{i=1}^{5} R_i H_{4i}, \quad \sum_{i=1}^{3} R_i \hat{H}_{4i}, \quad R_2\hat{H}_{44}$$

for various values of $\hat{\alpha}$ for a fixed value of $\hat{\beta} = 1{\cdot}0\,\mathrm{g\,cm^{-1}}$ and $\alpha_1 < 0$ (see Coleman & Markovitz 1964). Thus for each choice of $\hat{\alpha}$ (with $\alpha_1 < 0$) we looked for values of $\hat{\mu}$ and $\hat{\gamma}$ which best fit (12.6) to experimental data. We were able to come near to the data only when $0{\cdot}8 < \hat{\alpha} < 1{\cdot}2\,\mathrm{g\,cm^{-1}}$. For values of $\hat{\alpha}$ outside this range it was not possible to fit the profiles shown in figure 22. We required that the selected values of $\hat{\gamma}$ and $\hat{\mu}$ should not destroy the agreement between theory and experiment when $\omega < 3\,\mathrm{rev\,s^{-1}}$ but should give a proper correction when $\omega = 3$ and $\omega = 4\,\mathrm{rev\,s^{-1}}$. With a certain degree of uncertainty (about which we are unsure) we opted for the values

$$\hat{\alpha} = 1{\cdot}0\,\mathrm{g\,cm^{-1}}, \quad \hat{\mu} = -0{\cdot}0117\,\mathrm{g\,s\,cm^{-1}}, \quad \hat{\gamma} = -0{\cdot}5363 \times 10^{-5}\,\mathrm{g\,s^2\,cm^{-1}}. \tag{12.7}$$

† In the experiments $\hat{b}$ was actually 15·25 cm. But we have already seen that the climb at the inner cylinder is independent of $\hat{b}$ for $\hat{b}/\hat{a} > 5$, so all our calculations have been carried out for $\hat{b} = 10\hat{a}$.

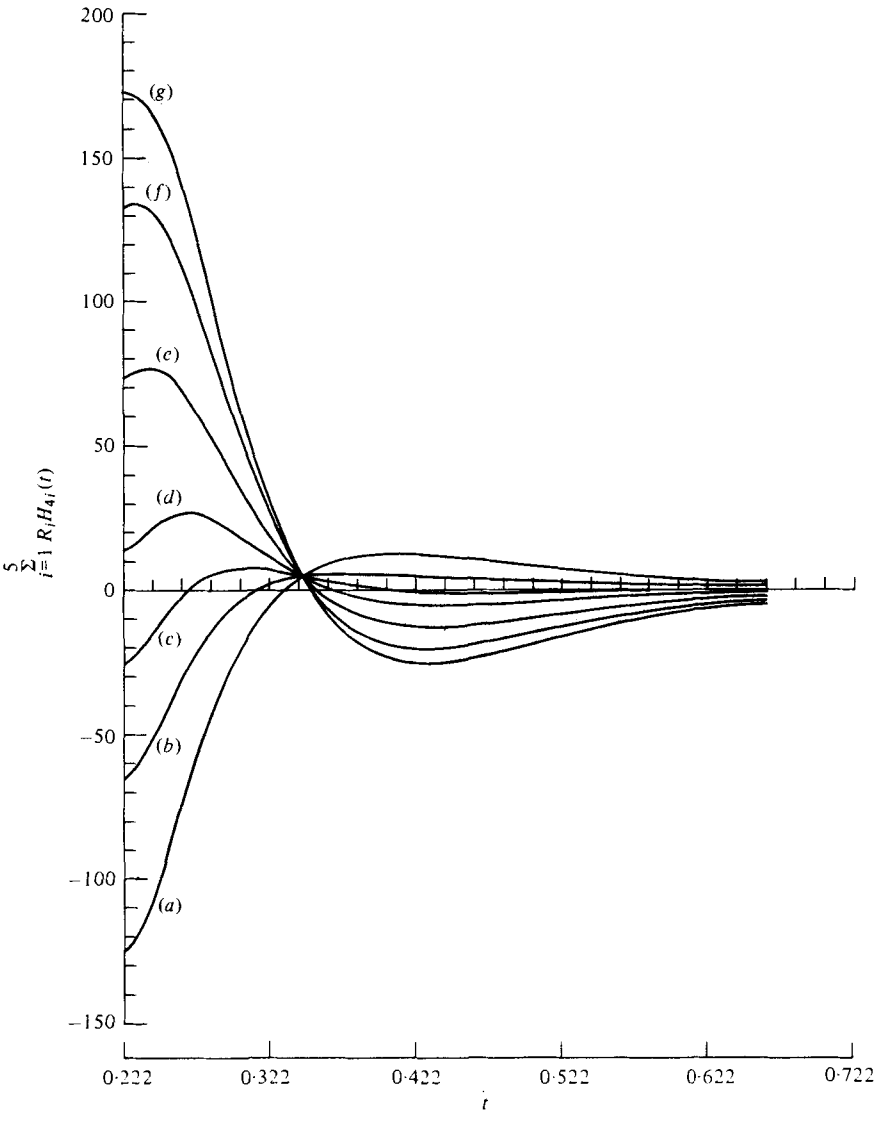

FIGURE 19. $R_1 H_{41} + R_2 H_{42} + R_3 H_{43} + R_4 H_{44} + R_5 H_{45}$ for the STP used by Beavers & Joseph (1975), evaluated for various assumed values of $\hat{\alpha}$ $(= \alpha_1 + \alpha_2)$ and α_1. $\hat{a} = 0{\cdot}635\,\text{cm}$; $\hat{b} = 6{\cdot}35\,\text{cm}$; $\beta (= 3\alpha_1 + 2\alpha_2) = 1{\cdot}0\,\text{g cm}^{-1}$; $R_1 = 1$; $R_2 = 11{\cdot}15$; $R_5 = 124{\cdot}2$; $R_3 = 4\hat{\alpha}/\rho\hat{a}^2$; $R_4 = R_2 R_3$.

	(a)	(b)	(c)	(d)	(e)	(f)	(g)
$\hat{\alpha}$ (g cm^{-1})	0·5	0·8	1·0	1·2	1·5	1·8	2·0
α_1 (g cm^{-1})	0	−0·6	−1·0	−1·4	−2·0	−2·6	−3·0
R_3	5·57	8·92	11·15	13·38	16·72	20·06	22·29

Using these values in (12.6), we plotted the height rise (12.5) as closed dots on figure 22. As a comparison, for cases with higher angular velocity, we have also added the best-fit curves obtained from two other sets of values for $(\hat{\alpha}, \hat{\mu}, \hat{\gamma})$.

There seems to be a region where fourth-order theory works fairly well. Naturally, as we increase Ω (or $\hat{\kappa}$), no matter how carefully we choose the constants, the theory

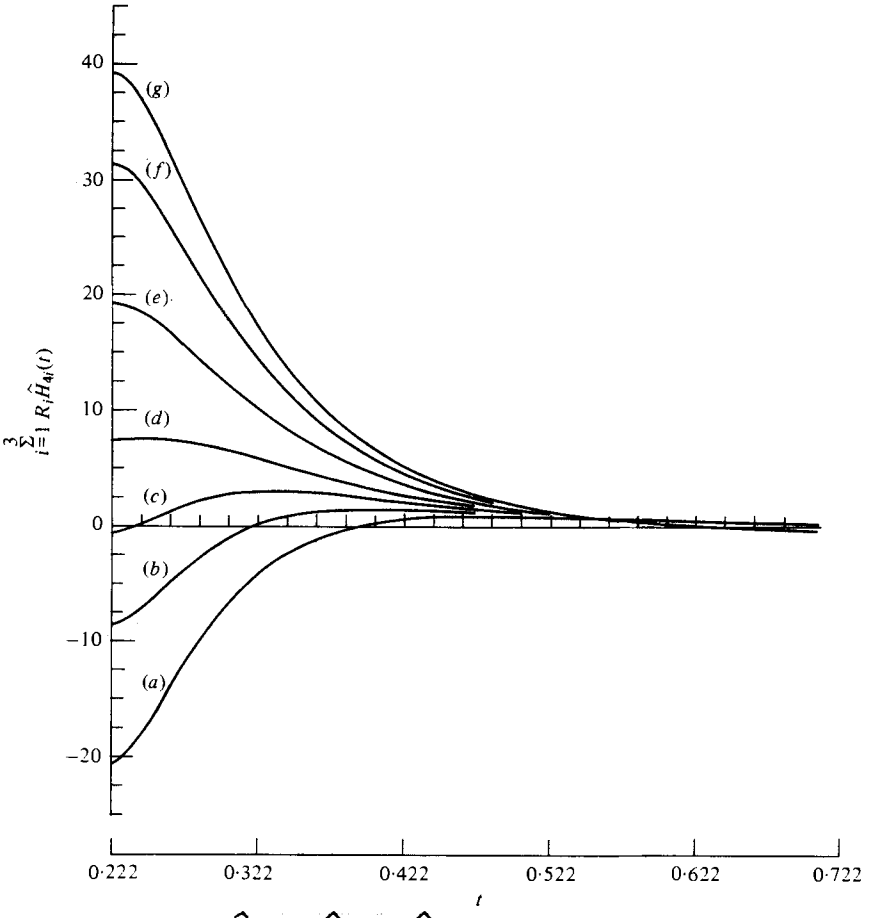

FIGURE 20. $R_1 \hat{H}_{41} + R_2 \hat{H}_{42} + R_3 \hat{H}_{43}$ for the conditions defined in figure 19.

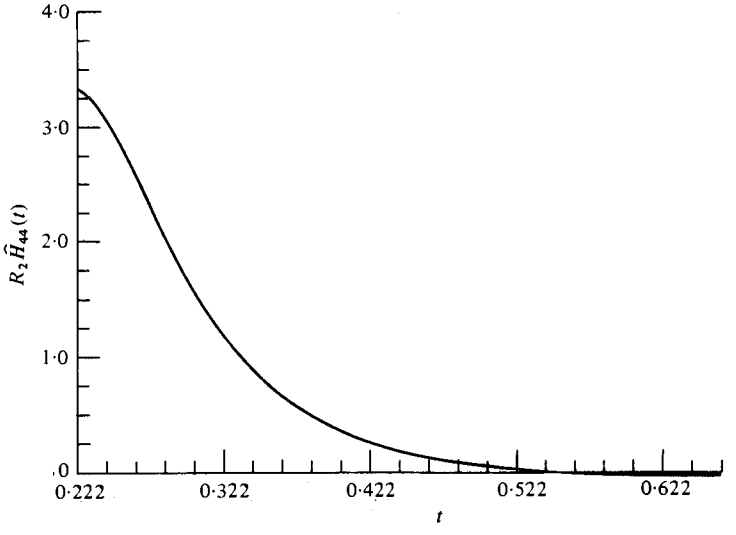

FIGURE 21. $R_2 \hat{H}_{44}$ for the conditions defined in figure 19.

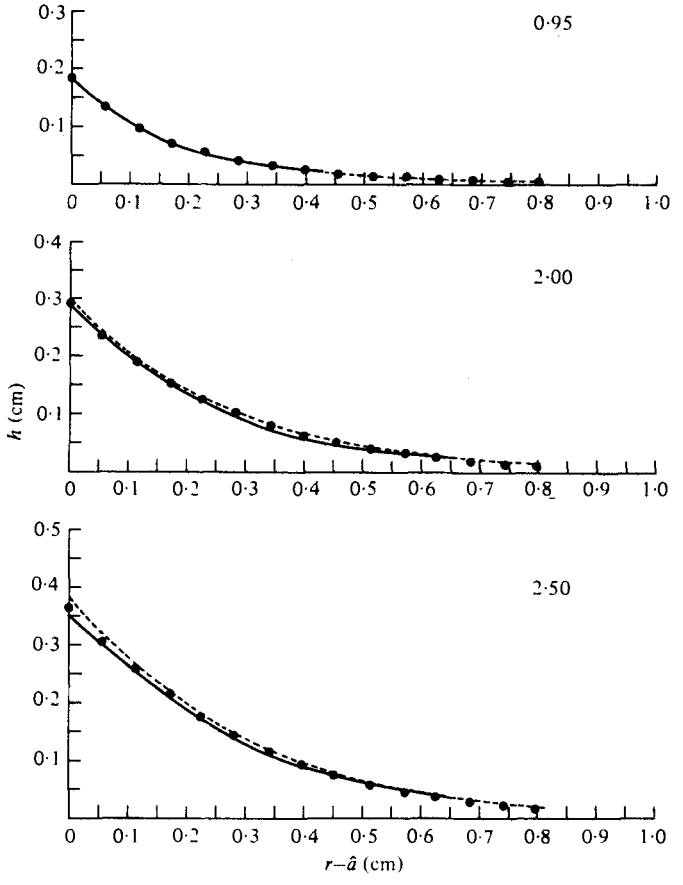

FIGURE 22 (part 1). For legend see p. 577.

fails to agree with the experiment because the effect of terms of order higher than four must be taken into account.

12.2. *Determination of $\hat{\mu}$ by direct measurement of the circumferential velocity*

It is possible to use experimental measurements of the circumferential component of velocity $v(r, h)$ evaluated on the free surface ($z_0 = 0$, $z = h$) to determine the constant $\hat{\mu}$ once $\hat{\beta}$ is given (see figure 7). In fact, as we mentioned at the end of § 9, circumferential velocity measurements have been reported by Hoffman & Gottenberg (1973) for a solution of polyisobutylene in cetane (see their figure 7). Once $\hat{\mu}$ has been determined, we may determine the other two constants, $\hat{\alpha}$ and $\hat{\gamma}$, by fitting theoretical height-rise profiles. To investigate the feasibility of this procedure and to check the validity of the procedures used in § 12.1, we measured circumferential velocity profiles in three fluids by methods described below.

The central part of the apparatus consisted of a large vat of fluid in which a vertical circular rod was made to rotate about its axis. The rod was driven from below by an Electrocraft Motomatic Type E-550 d.c. servomotor with a feedback control system. The upper end of the rod was accurately aligned by means of a spring-loaded cone

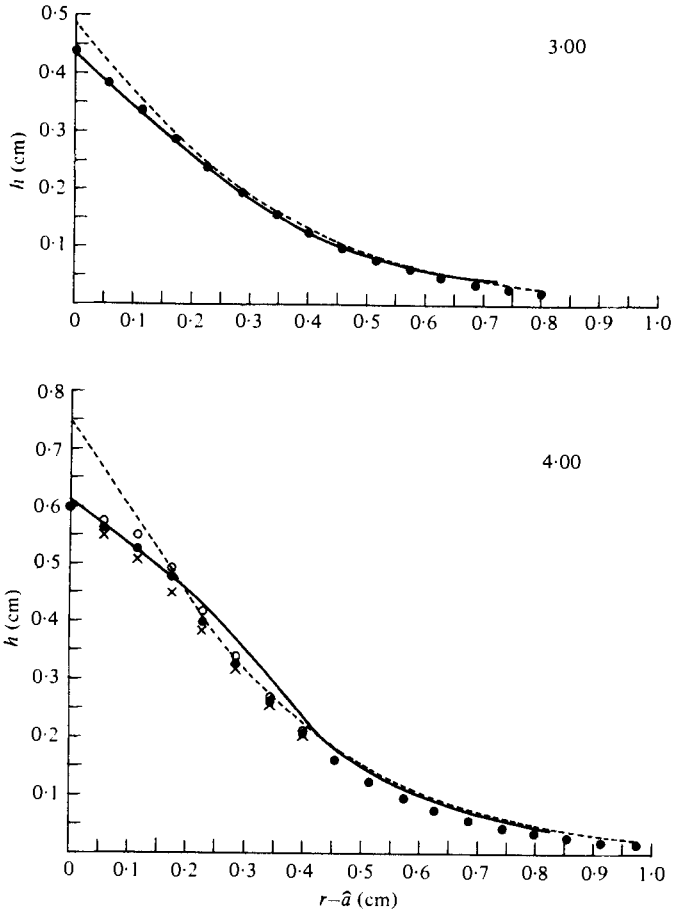

FIGURE 22 (part 2). For legend see p. 577.

bearing set in a transparent Plexiglas plate. Rotational speeds were measured by means of a light source and photomultiplier tube connected to a digital counter, and ten reflecting surfaces on the drive-shaft connecting the motor to the rod. Surface circumferential velocities were measured by a technique similar to that employed by Hoffman & Gottenberg (1973). The fluid surface was illuminated with two General Radio Strobotacs driven in synchronization at a predetermined flashing rate by means of a Wavetec function generator. Small aluminium particles in the size range 0·15–0·30 mm were dropped on the surface and multiple-image photographs were taken with a Nikon-F 35 mm camera incorporating a Nikkor 500 mm catadioptric telephoto lens.

Three different rods were used in the experiments, with radii $\hat{a}$ of 0·4775, 0·6312 and 0·9525 cm. In addition, three fluids were used, consisting of two different samples of STP (polyisobutylene in a petroleum oil) and one sample of TLA-227 (a methacrylate copolymer in petroleum oil, manufactured by the Texaco Oil Company). The density, surface tension, shear viscosity and climbing constant β were determined by the standard procedures described in Beavers & Joseph (1975), and are summarized in table 3.

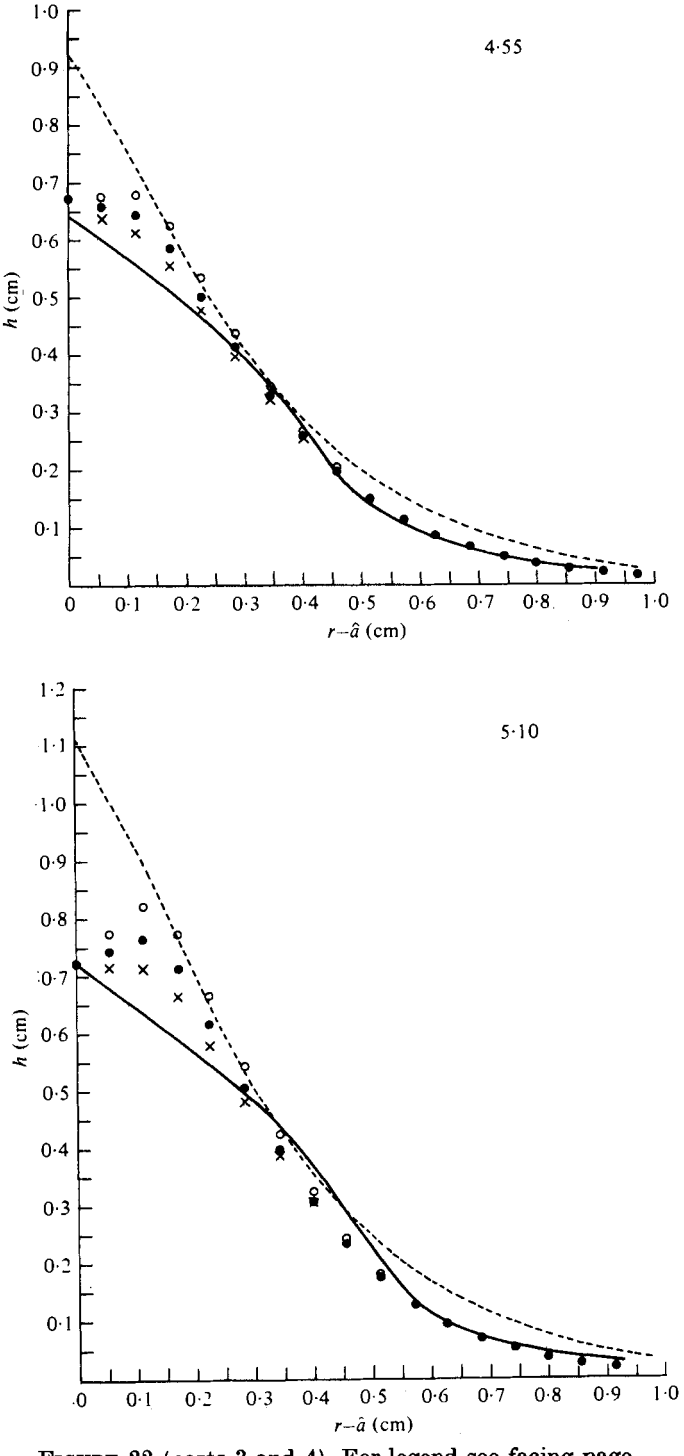

FIGURE 22 (parts 3 and 4). For legend see facing page.

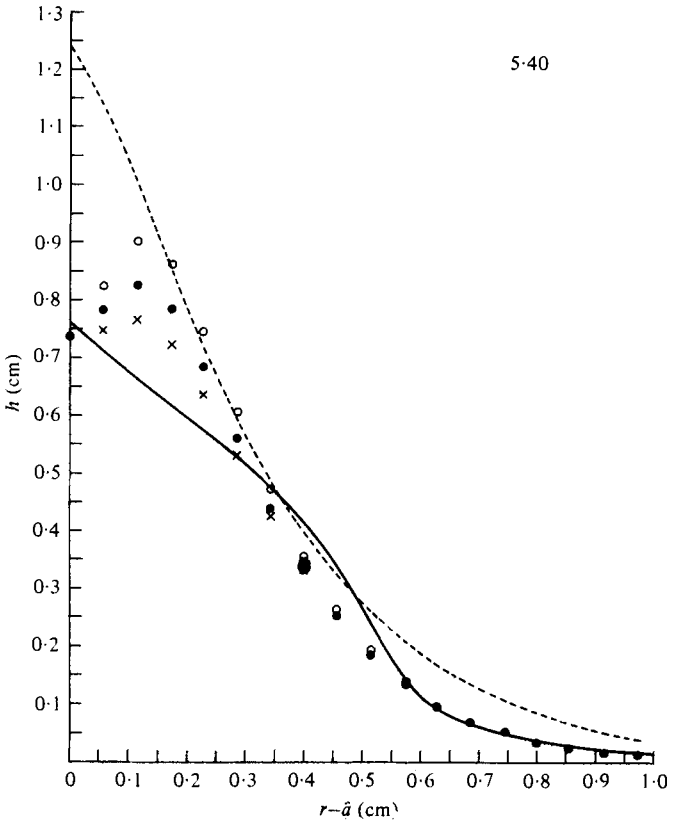

FIGURE 22. Comparisons of experimental profiles with theoretical predictions for a rod of radius 0·635 cm rotating in a large vat of STP. The experimental results are from Beavers & Joseph (1975). ——, experiment; – – –, second-order theory (12.1) with $\hat{\beta} = 1{\cdot}0\,\mathrm{g\,cm^{-1}}$. Three curves from fourth-order theory are also given:

	$\hat{\alpha}$ (g cm^{-1})	$\hat{\mu}$ (g s cm^{-1})	$\hat{\gamma}$ (g s^2 cm^{-1})
●	1·0	−0·0117	$-0{\cdot}5363 \times 10^{-5}$
○	1·2	0·01197	$-0{\cdot}3618 \times 10^{-4}$
×	0·8	−0·03333	$-0{\cdot}8960 \times 10^{-5}$

The comparisons are identified by the rod rotational speed (rev s^{-1}). The fourth-order theory gives the proper correction to the second-order theory for $\omega = 3$ and 4 rev s^{-1}. The best fit of fourth-order theory with experiment occurs for the closed dots. For $\omega > 4$ rev s^{-1} the fourth-order theory no longer agrees with experiment because higher-order terms must be included.

Our first measurements of circumferential velocity were made using the 0·9525 cm rod in the fluid STP-1. The variations of circumferential velocity with radial position for two rod rotational speeds are shown in figure 23. We then used (9.6) to search for a value of $\hat{\mu}$ such that the circumferential velocity distribution predicted by (9.6) gave the best fit with the experimental data for the lower of the two rotational speeds [curve (*a*) in figure 23]. This value of $\hat{\mu}$ was then used in (9.6) to predict the circumferential velocity distribution at the higher rotational speed [curve (*b*)].

For the experiments with STP-2 and TLA-227 all three rods were used in each fluid, and data were recorded at either three or four different rod rotational speeds.

Fluid	STP-1	STP-2	TLA-227
Average temperature during experiments (°C)	23·0	21·9	22·2
Density, ρ (g cm^{-3})	0·890	0·865	0·896
Surface tension, T (dyne cm^{-1})	30·9	30·7	30·9
Shear viscosity, μ (P)	150	90	320
Climbing constant, $\hat{\beta}$ (g cm^{-1})	1·42	0·89	23·5

TABLE 3. The parameters characterizing the fluids used in the circumferential velocity experiments.

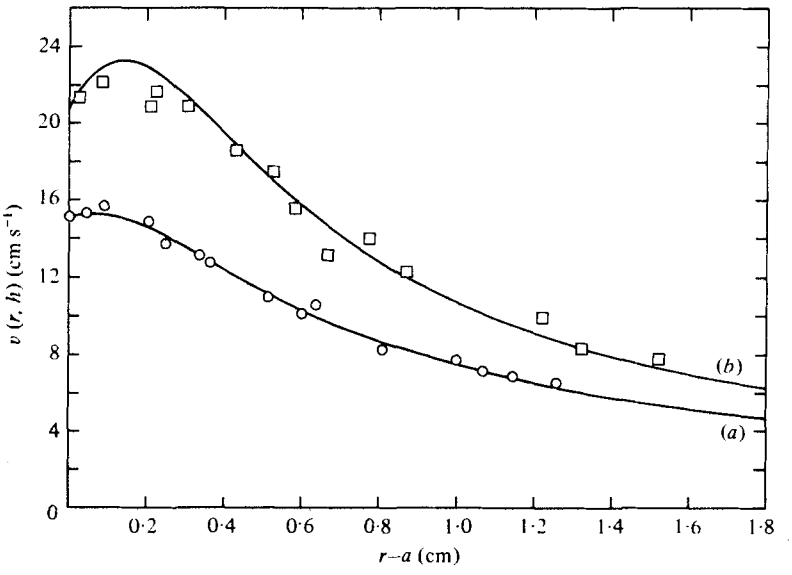

FIGURE 23. Comparison of measured circumferential velocities on the free surface with values predicted using third-order theory (9.6) for STP-1 (see table 3). $\hat{a} = 0{\cdot}9525$ cm; $\hat{\beta} = 1{\cdot}42$ g cm^{-1}; $\hat{\mu} = -0{\cdot}030$ g s cm^{-1}.

	(a)	(b)
ω (rev s^{-1})	2·52	3·48

The circumferential velocities measured in STP-2 and TLA-227 are shown in figures 24 and 25 respectively. Our procedure for the determination of $\hat{\mu}$ was to use (9.6) to locate the value which gave the best fit with the experimental results for the two lowest rotational speeds of the 0·9525 cm rod. We fitted the calculated curves to the experimental data at two rotational speeds because the calculated distributions are more sensitive to changes in $\hat{\mu}$ as the rotational speed is increased. Having found a value for $\hat{\mu}$ for each fluid in this way, we used these values to compute the theoretical circumferential velocity distributions corresponding to all the remaining experimentally measured distributions. The agreement between the measured and predicted velocities is extremely good at all rod rotational speeds except the highest for each

rod. It is clear that at a particular temperature there is a single value of $\hat{\mu}$ for each fluid, and that this is only a property of the fluid and not of the rod size. At the highest rotational speeds the predicted values appear to agree quite well with the measured values away from the rod, but close to the rod (9.6) predicts circumferential velocities which are higher than the measured values. These rotational speeds are outside the region of validity of the third-order perturbation theory.

13. Secondary motions in the deformed domain

We now describe the secondary motions which are generated in the deformed domain. In order to present a quantitative discussion we shall again consider the experimental results used in § 12.1, in which a circular rod ($\hat{a} = 0{\cdot}635\,\mathrm{cm}$) rotates in a large vat of STP for which the rheological constants up to order four have been determined and have the values given by (12.7). The height rise is then given by (5.41 *c*), or equivalently by (6.3). Using (5.41 *c*), we write $h(r;\Omega)$ as an even polynomial (12.5) of fourth degree in Ω consistent with the order of approximation of the analysis.

The distribution of circumferential velocity is given up to terms $O(\Omega^3)$ by (6.1). On the free surface $z = h$, we have $y = az_0/\hat{a} = 0$, so that the circumferential velocity distribution on the free surface is given by

$$v(r,h;\Omega) = \hat{a}\Omega V_1(t,\eta) + \frac{\hat{a}\Omega^3}{3!}\left\{\frac{1}{K_1}\hat{V}_{31}(t,\eta) + \Omega_0^{-2}\left[V_{31}(t,0,\eta,S) + R_2 V_{32}(t,0,\eta,S)\right]\right\}, \tag{13.1}$$

where $t = ar/\hat{a}$. Using the values given by (12.7), we may represent the graph of (13.1) by the curve labelled $\hat{\mu} = -0{\cdot}0117\,\mathrm{g\,s\,cm^{-1}}$ in figure 7. In figure 26 we have plotted this distribution on the actual deformed domain associated with (12.5).

To obtain the velocity and pressure fields in the deformed domain where the real flow takes place, we must invert the shifting transformation (4.5):

$$z_0 = z - \left(h_s + \frac{\Omega^2}{2}h^{[2]}(r_0) + \frac{\Omega^4}{4!}h^{[4]}(r_0)\right).$$

We then have the secondary motion (6.4) in the form

$$\begin{aligned}\frac{\mu g\psi(r,z;\Omega)}{\rho\hat{a}^6}\frac{4!}{\Omega^4} &= \sum_{i=1}^{4} R_i \Psi_{4i}(t,y,\eta,S)\\ &= \sum_{i=1}^{4} R_i \Psi_{4i}\left(\frac{a}{\hat{a}}r, \frac{a}{\hat{a}}[z-h(r;\Omega)],\eta,S\right) \equiv \tilde{\psi}(r,z;\Omega),\end{aligned} \tag{13.2}$$

where $h(r;\Omega)$ is given in terms up to order four in Ω. The contours of $\tilde{\psi}(r,z;\Omega)$ in the deformed domain

$$\mathscr{V}_\Omega = \left[r,z \middle| \hat{a} \leqslant r \leqslant \hat{b},\quad z \leqslant h_s + \frac{\Omega^2}{2!}h^{[2]}(r) + \frac{\Omega^4}{4!}h^{[4]}(r)\right]$$

are shown in figures 27 (*a*) and (*b*), where (*b*) is a magnification of the boxed region shown in (*a*). These representations are not merely sketches; they are uniformly scaled representations of the free surface and secondary motion up to fourth order which are predicted to occur when the parameters have the values assumed by (12.7).

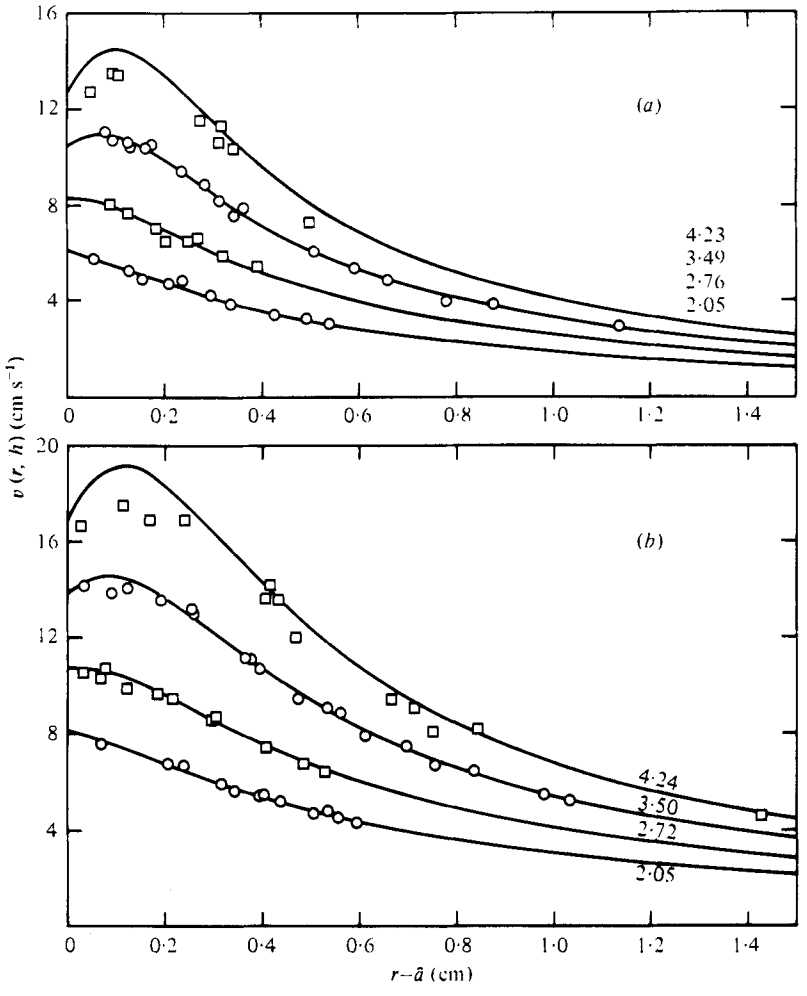

FIGURE 24 (*a*, *b*). For legend see facing page.

Our computation shows that when η is small (say $\frac{1}{10}$) there is a primary eddy at the top of the annulus with a counterclockwise circulation. The circulation is most intense under the climbing bubble and draws the fluid near the free surface in towards the rod while forcing the fluid lower down away from the rod. This direction for the circulation runs against uninformed intuition; intuition suggests that the fluid in the bubble represents an accumulation from a clockwise circulation which drives the fluid up the rod. Intuition fails because the bubble is held up in the first place by static forces associated with the circumferential shearing motion (not the secondary motions) and the secondary motions are driven in an anticlockwise sense by the 'big torque' associated with the vertical stratification of inertia and normal stresses.

In the region where fourth-order theory holds, we may compute the radial and vertical components of velocity from (3.4) and (13.2):

$$u = r^{-1}\,\partial\psi(r,z)/\partial z, \quad w = -r^{-1}\,\partial\psi(r,z)/\partial r. \tag{13.3}$$

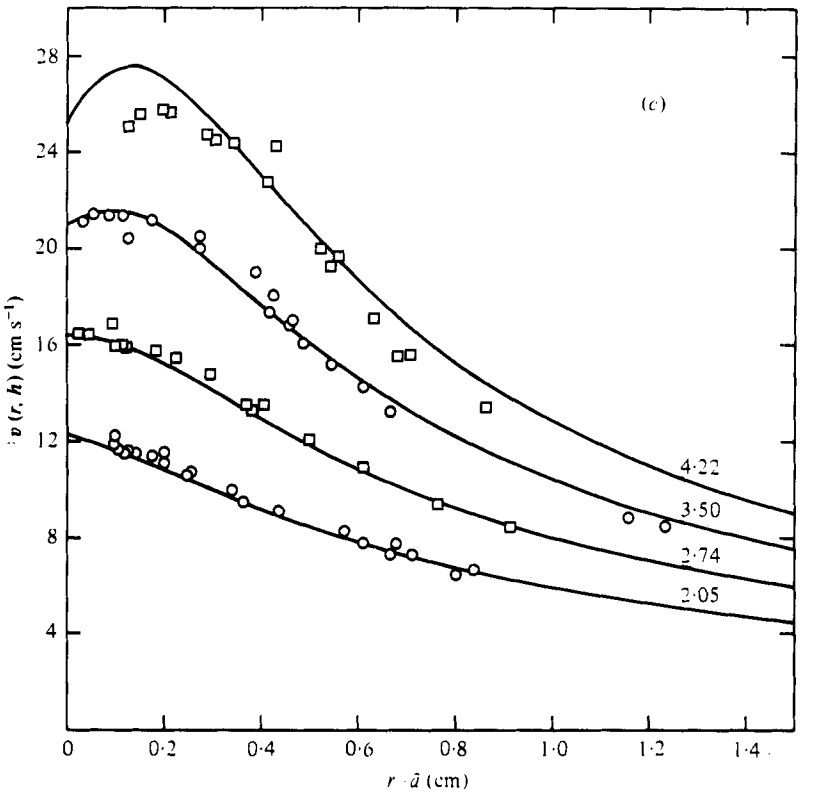

FIGURE 24. Comparison of measured circumferential velocities on the free surface with values predicted using third-order theory (9.6) for STP-2 (see table 3). $\hat{\beta} = 0{\cdot}89\,\mathrm{g\,cm^{-1}}$; $\hat{\mu} = -0{\cdot}010\,\mathrm{g\,s\,cm^{-1}}$. The curves are identified by rod rotational speed (rev $\mathrm{s^{-1}}$).

	(*a*)	(*b*)	(*c*)
$\hat{a}$ (cm)	0·4725	0·6312	0·9525

The value of $\hat{\mu}$ was chosen by finding the best fit between theory and experiment for the two lowest rotational speeds of rod (*c*).

We consider the radial and vertical components of velocity on the free surface $z = h(z_0 = y = 0)$:

$$u(r,h;\Omega) = \frac{\Omega^4}{4!}\frac{\rho\hat{a}^4}{\mu g}\sum_{i=1}^{4} R_i \frac{a^2}{t}\frac{\partial \Psi_{4i}(t,0)}{\partial y}, \tag{13.4a}$$

$$w(r,h;\Omega) = \frac{\Omega^4}{4!}\frac{\rho\hat{a}^4}{\mu g}\sum_{i=1}^{4} R_i \left(-\frac{a^2}{t}\frac{\partial \Psi_{4i}(t,0)}{\partial t}\right). \tag{13.4b}$$

Then we may combine (13.1) and (13.4) to find the distribution of the speed on the free surface. We find that the secondary motion makes the fluid wind up on the free surface of the bubble and sink near the rod. These predicted features of the motion are verified by our experiments in all cases provided that Ω is small enough. For example, figures 28 and 29 (plates 1 and 2) show the motion, viewed from above, of aluminium flakes on the surface of STP and TLA-227. The flakes start well outside the bubble and slowly spiral inwards to the rod, moving up the free surface of the bubble.

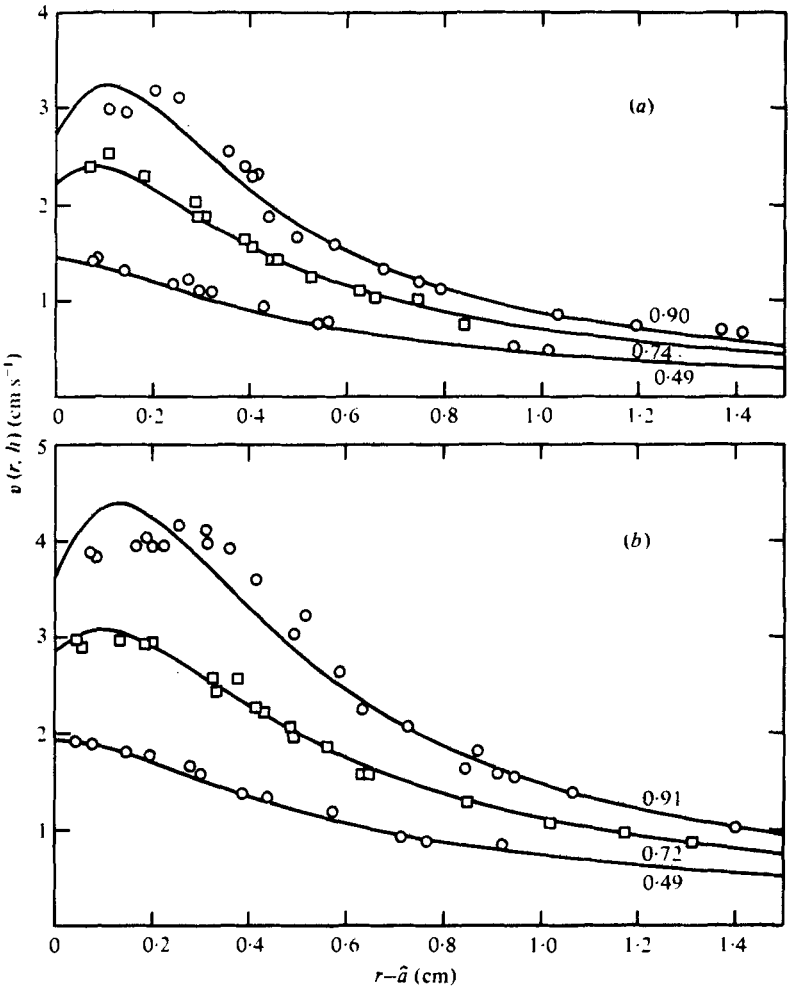

FIGURE 25 (*a*, *b*). For legend see facing page.

At higher angular velocities the experiments by Saville & Thompson (1969), Hoffman & Gottenberg (1973) and ourselves indicate the development of a 'little torque' in the bubble, but not in the body of the fluid, which drives a 'little clockwise eddy' on the top of the 'big counterclockwise eddy' in the body of the fluid. The presence of two eddies probably correlates with the persistent indentation of the free surface which is nearly always observed in climbing experiments when Ω is large. The fluid now moves down the free surface towards the outer edge of the bubble. This motion is shown in the photographs in figures 30 and 31 (plates 3 and 4), which were taken during the same experimental runs as figures 28 and 29 respectively. Aluminium flakes, which were initially deposited on the bubble next to the rod, spiral to the outer edge of the bubble, where they disappear from view below the free surface of the fluid.

The two different situations, one for small values of Ω and the other for larger values of Ω, are sketched in figure 32. The explanation of these two regimes of flow may be as

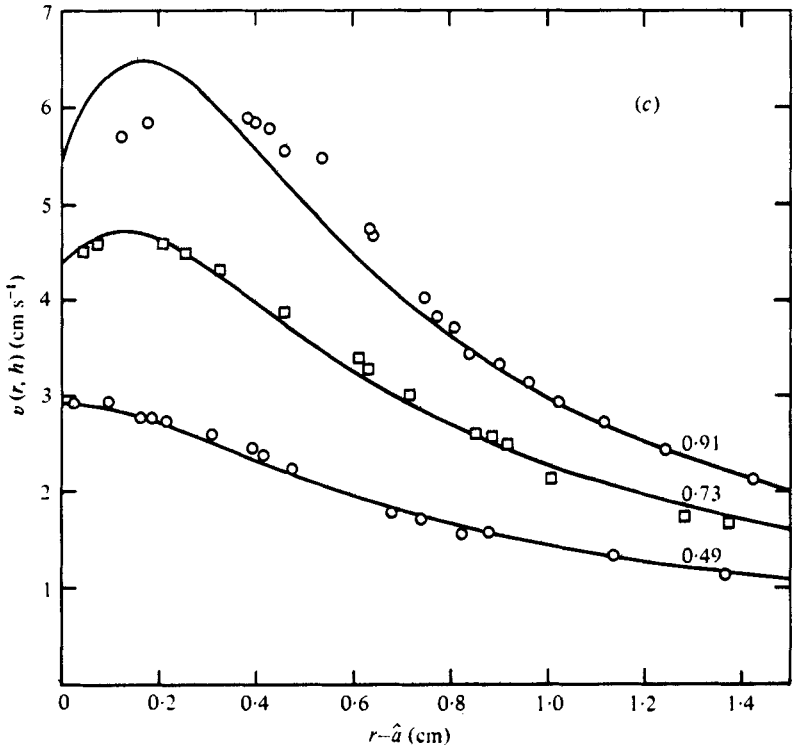

FIGURE 25. Comparison of measured circumferential velocities on the free surface with values predicted using third-order theory (9.6) for TLA 227 (see table 3). $\hat{\beta} = 23{\cdot}5\,\mathrm{g\,cm^{-1}}$; $\hat{\mu} = -1{\cdot}10\,\mathrm{g\,s\,cm^{-1}}$. The curves are identified by rod rotational speed (rev s^{-1}).

	(*a*)	(*b*)	(*c*)
$\hat{a}$ (cm)	0·4725	0·6312	0·9525

The value of $\hat{\mu}$ was chosen by finding the best fit between theory and experiment for the two lowest rotational speeds of rod (*c*).

follows. For small values of Ω, the flow develops in just the way predicted by the perturbation theory up to order four. At larger values of Ω, outside the range of the perturbation theory in general, the bubble height increases to such an extent that the basic distribution of circumferential velocity changes from a kind of vertically stratified viscometric flow to something more akin to a solid-body rotation. The alteration in the circumferential velocity is a consequence of the fact that the free surface, which is now more steeply inclined to the vertical, cannot support shear stresses and, hence, cannot oppose the tendency of the rod to rotate the tall bubble as a solid body. The resistance to such solid-body rotation comes from the velocity field in the body of the fluid below the bubble. Because the shearing in the bubble is diminished in the high bubble, the distribution of shear stresses which generates the 'big eddy' is altered and the 'big torques' in the bubble first diminish and then, in a weak state, change sign. But the 'big eddy' below the bubble is still driven by the same torques arising from vertical stratification of the viscometric flow, and the 'big eddy' then drives the little one. At the point on the free surface where the two eddies are joined there is a suction which indents the free surface. In fact, the indentation

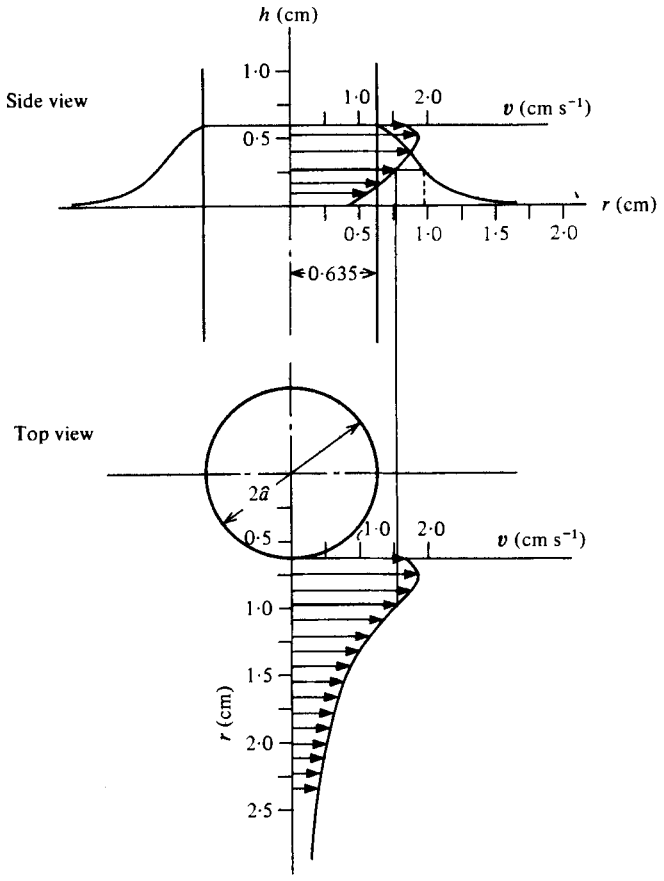

FIGURE 26. The distribution of circumferential velocity superimposed on the actual deformed domain for the fluid (STP) used for the comparisons of § 12.1. $\hat{a} = 0{\cdot}635\,\mathrm{cm}$; $\hat{\beta} = 1{\cdot}0\,\mathrm{g\,cm^{-1}}$; $\hat{\alpha} = 1{\cdot}0\,\mathrm{g\,cm^{-1}}$; $\hat{\mu} = -0{\cdot}0117\,\mathrm{g\,s\,cm^{-1}}$; $\Omega = 4\,\mathrm{rev\,s^{-1}}$.

can become 'cusp like', as shown in the photographs in Beavers & Joseph (1975), Saville & Thompson (1969) and in figure 4 of Hoffman & Gottenberg (1973).

This work was supported by the U.S. Army Research Office and by the National Science Foundation under Grant No. ENG 75-19047-A01.

FIGURE 27. (*a*) Secondary motion in the deformed domain for the situation shown in figure 26. The stream function is given by

$$\frac{\mu g \psi}{\rho \hat{a}^6} \frac{24}{\Omega^4} = \sum_{i=1}^{4} R_i \Psi_{4i}.$$

$\hat{a} = 0{\cdot}635\,\mathrm{cm}$; $\hat{h} = 6{\cdot}35\,\mathrm{cm}$; $\Omega = 4\,\mathrm{rev\,s^{-1}}$; $\hat{\beta} = 1{\cdot}0\,\mathrm{g\,cm^{-1}}$; $\hat{\alpha} = 1{\cdot}0\,\mathrm{g\,cm^{-1}}$. (*b*) Enlargement of the boxed region of (*a*).

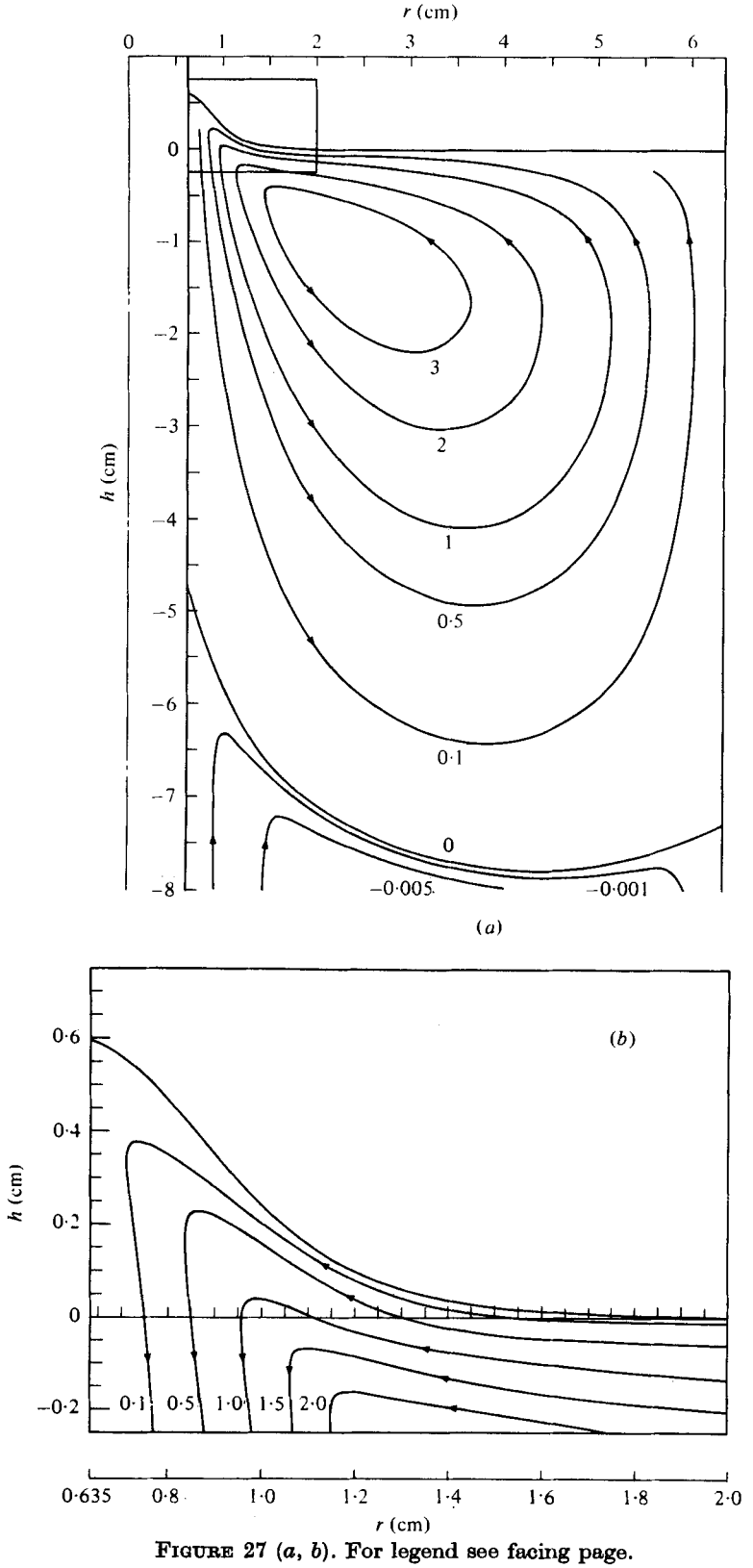

FIGURE 27 (*a*, *b*). For legend see facing page.

Appendix. Stokes flow between concentric cylinders

Yoo & Joseph (1978) have solved the edge problem for Stokes flow between concentric cylinders. The main features of the theory are summarized here. We also justify the formal solution with a convergence theorem, following lines laid out by Joseph (1977) and proved in the thesis of Yoo (1977). We refer the reader to Yoo's thesis for proofs and further details.

Consider the edge problem

$$L^2\Psi(t,y) = \left(\frac{\partial^2}{\partial t^2} - \frac{1}{t}\frac{\partial}{\partial t} + \frac{\partial^2}{\partial y^2}\right)^2 \Psi(t,y) = 0 \tag{A 1a}$$

in $a \leqslant t \leqslant b$, $-\infty < y \leqslant 0$, with boundary conditions

$$\Psi(a,y) = \Psi(b,y) = \partial\Psi(a,y)/\partial t = \partial\Psi(b,y)/\partial t = 0 \tag{A 1b}$$

and with the data

$$\begin{pmatrix} f(t) \\ g(t) \end{pmatrix} = \begin{pmatrix} \dfrac{\partial^2\Psi(t,0)}{\partial y^2} \\ t\dfrac{\partial}{\partial t}\dfrac{1}{t}\dfrac{\partial\Psi(t,0)}{\partial t} \end{pmatrix} \tag{A 1c}$$

real and prescribed on $y = 0$. Here a and b are the radii of the inner and outer cylinders, respectively, made dimensionless with respect to the actual gap size in such a way that the dimensionless gap size $b-a$ always has the value 2, i.e. $a = 2\eta/(1-\eta)$ and $b = 2/(1-\eta)$, where $\eta = a/b$.

The solution of problem (A 1) is obtained in the paper of Yoo & Joseph (1978) and is given by

$$\Psi(t,y) = \lim_{N\to\infty} \sum_{-N}^{N} C_n \exp(P_n y)\, \phi_1^{(n)}(t)/P_n^2, \tag{A 2}$$

where the $\phi_1^{(n)}(t)$ are strip eigenfunctions for Stokes flow between concentric cylinders: $L^2[\exp(\pm P_n y)\,\phi_1^{(n)}(t)] = 0$. The strip eigenfunctions are given by

$$\phi_1^{(n)}(t) = A_1^{(n)} t J_1(P_n t) + A_2^{(n)} t Y_1(P_n t) + A_3^{(n)} t^2 J_0(P_n t) + A_4^{(n)} t^2 Y_0(P_n t), \tag{A 3}$$

where the coefficients $A_i^{(n)}$ and the eigenvalues P_n are defined simultaneously to satisfy the four boundary conditions given in (A 1b), which is now equivalent to

$$\phi_1^{(n)}(a) = \phi_1^{(n)}(b) = d\phi_1^{(n)}(a)/dt = d\phi_1^{(n)}(b)/dt. \tag{A 4}$$

There are a countably infinite number of eigenvalues P_n of (A 4) which are symmetrically located in the complex P plane. We make use of the eigenvalues with positive real parts. The P_n are numbered in a sequence corresponding to the magnitude of their real parts. We define

$$P_{-n} = \bar{P}_n, \tag{A 5}$$

where the overbar designates the complex conjugate. Then $\phi_1^{(-n)}(t) = \bar{\phi}_1^{(n)}(t)$ ($n = 1, 2, 3, 4, \ldots$) is a strip eigenfunction belonging to the eigenvalue P_{-n}. Since the given edge data (A 1c) are real,

$$C_{-n} = \bar{C}_n. \tag{A 6}$$

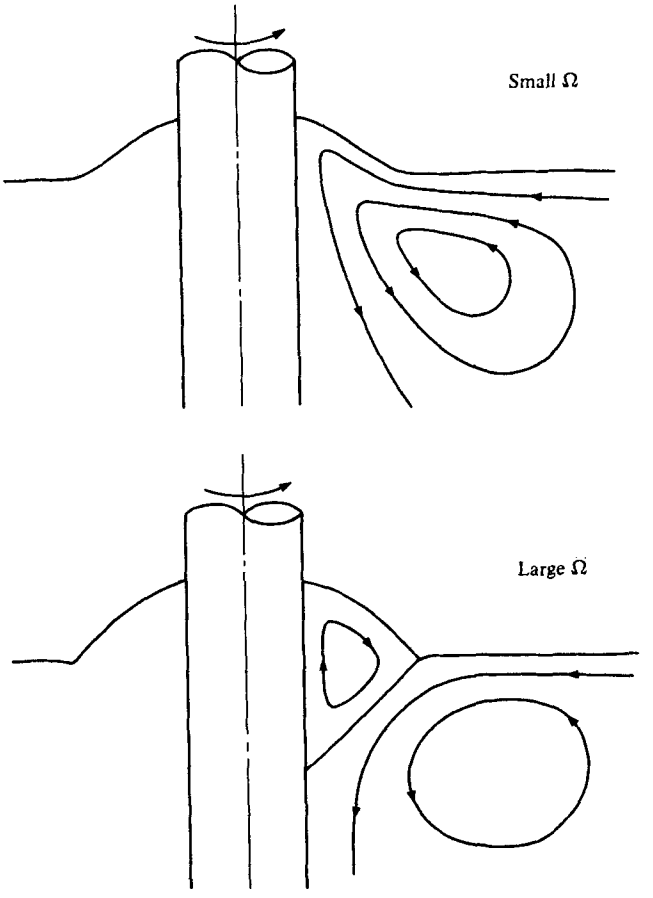

FIGURE 32. Sketch showing the change in the secondary flow pattern from a single large eddy at small rod rotational speeds to a pattern consisting of a large eddy and a small eddy at higher rotational speeds. The secondary motion in the bubble changes direction, and at higher rotational speeds it is driven by the motion in the large eddy.

We define

$$\phi_2^{(n)}(t) = \frac{t}{P_n^2}\frac{d}{dt}\frac{1}{t}\frac{d\phi_1^{(n)}(t)}{dt}$$
$$= -[A_1^{(n)} + (2/P_n)\,A_3^{(n)}]\,tJ_1(P_n t) - [A_2^{(n)} + (2/P_n)\,A_4^{(n)}]\,tY_1(P_n t)$$
$$- A_3^{(n)}\,t^2 J_0(P_n t) - A_4^{(n)}\,t^2 Y_0(P_n t). \quad \text{(A 7)}$$

It is possible to write (A 1*c*) as

$$\begin{pmatrix} f(t) \\ g(t) \end{pmatrix} = \sum_{-\infty}^{\infty} C_n \begin{pmatrix} \phi_1^{(n)}(t) \\ \phi_2^{(n)}(t) \end{pmatrix}. \quad \text{(A 8)}$$

To determine the constants C_n, we introduce the data vector

$$\mathbf{f} = \mathbf{e}_1 f + \mathbf{e}_2 g,$$

the eigenvector

$$\boldsymbol{\varphi}^{(n)} = \mathbf{e}_1 \phi_1^{(n)} + \mathbf{e}_2 \phi_2^{(n)}$$

and the adjoint eigenvector†

$$\boldsymbol{\psi}^{(n)} = \mathbf{e}_1 \psi_1^{(n)} + \mathbf{e}_2 \psi_2^{(n)},$$

where $\mathbf{e}_1$ and $\mathbf{e}_2$ are orthonormal base vectors. We find from (A 1) and (A 7) that the eigenvector $\boldsymbol{\varphi}^{(n)}(t)$ satisfies the differential equation

$$t\frac{d}{dt}\left(\frac{1}{t}\frac{d\phi^{(n)}}{dt}\right) + P_n^2 \mathbf{A}.\boldsymbol{\varphi}^{(n)} = 0 \tag{A 9a}$$

with

$$\boldsymbol{\varphi}^{(n)}.\mathbf{e}_1 = \frac{d\phi^{(n)}}{dt}.\mathbf{e}_1 = 0 \quad \text{at} \quad t = a, b, \tag{A 9b}$$

where $\mathbf{A} = -\mathbf{e}_1\mathbf{e}_2 + \mathbf{e}_2\mathbf{e}_1 + 2\mathbf{e}_2\mathbf{e}_2$, or in matrix notation

$$\mathbf{A} = \begin{pmatrix} 0 & -1 \\ 1 & 2 \end{pmatrix}.$$

The adjoint eigenvector $\boldsymbol{\psi}^{(n)}(t)$ satisfies

$$t\frac{d}{dt}\frac{1}{t}\frac{d\boldsymbol{\psi}^{(n)}}{dt} + P_n^2 \mathbf{A}^{\mathrm{T}}.\boldsymbol{\psi}^{(n)} = 0 \tag{A 10a}$$

with

$$\boldsymbol{\psi}^{(n)}.\mathbf{e}_2 = \frac{d\boldsymbol{\psi}^{(n)}}{dt}.\mathbf{e}_2 = 0 \quad \text{at} \quad t = a, b, \tag{A 10b}$$

where $\mathbf{A}^{\mathrm{T}} = -\mathbf{e}_2\mathbf{e}_1 + \mathbf{e}_1\mathbf{e}_2 + 2\mathbf{e}_2\mathbf{e}_2$. We find that $\psi_2^{(n)}(t)$ and $\phi_1^{(n)}(t)$ both satisfy the reduced biharmonic equation

$$\left(\frac{d^2}{dt^2} - \frac{1}{t}\frac{d}{dt} + P^2\right)^2 F(t) = 0$$

with $F(a) = F(b) = F'(a) = F'(b) = 0$. We therefore put

$$\psi_2^{(n)}(t) = \phi_1^{(n)}(t), \tag{A 11}$$

and $\psi_1^{(n)}(t)$ may be determined directly from the second component of (A 10a), i.e.

$$t\frac{d}{dt}\frac{1}{t}\frac{d\psi_2^{(n)}}{dt} + P_n^2(2\psi_2^{(n)} - \psi_1^{(n)}) = 0.$$

This leads to

$$\psi_1^{(n)}(t) = [A_1^{(n)} - (2/P_n)A_3^{(n)}]tJ_1(P_n t) + [A_2^{(n)} - (2/P_n)A_4^{(n)}]tY_1(P_n t) + A_3^{(n)} t^2 J_0(P_n t) + A_4^{(n)} t^2 Y_0(P_n t). \tag{A 12}$$

The biorthogonality condition follows in a standard way from (A 9a, b) and (A 10a, b):

$$\int_a^b \frac{1}{t}\boldsymbol{\psi}^{(m)\mathrm{T}}.\mathbf{A}.\boldsymbol{\varphi}^{(n)}dt = K_n \delta_{mn}, \tag{A 13}$$

where

$$K_n = (-2b^2/P_n^2)[A_3^{(n)} J_1(P_n b) + A_4^{(n)} Y_1(P_n b)]^2 + (2a^2/P_n^2)[A_3^{(n)} J_1(P_n a) + A_4^{(n)} Y_1(P_n a)]^2. \tag{A 14}$$

† For the derivation of $\boldsymbol{\psi}^{(n)}$ and the following account of the biorthogonality, see Yoo & Joseph (1978).

Expressing the series (A 8) in vector form

$$\mathbf{f}(t) = \sum_{-\infty}^{\infty} C_n \boldsymbol{\varphi}^{(n)}(t), \tag{A 15}$$

we find, using (A 13), that

$$\int_a^b \frac{1}{t} \boldsymbol{\psi}^{(n)\mathrm{T}} . \mathbf{A} . \mathbf{f} dt = C_n K_n. \tag{A 16}$$

Equation (A 16) determines the coefficients

$$C_n = \frac{1}{K_n} \int_a^b \frac{1}{t} \{(2\psi_2^{(n)} - \psi_1^{(n)}) g + \psi_2^{(n)} f\} dt. \tag{A 17}$$

Equations (A 2) and (A 17) define a formal solution of the Stokes-flow edge problem. The formal solution is the solution if the series on the right of (A 15) converges to $\mathbf{f}(t)$.

Suppose that $f(t)$ and $g(t)$ are three-times continuously differentiable and four-times piecewise differentiable with a finite number of bounded jumps when $a \leqslant t \leqslant b$. Suppose further that

$$f(a) = f(b) = f'(a) = f'(b) = 0 \tag{A 18}$$

with no further restrictions on $g(t)$. Then

$$C_n = \frac{-1}{K_n P_n^2} \int_a^b \frac{1}{t} \left[\psi_2^{(n)} t \left(\frac{1}{t} (g+f)' \right)' - \frac{2t}{P_n} (A_3^{(n)} J_1(P_n t) + A_4^{(n)} Y_1(P_n t)) t \left(\frac{1}{t} f' \right)' \right] dt. \tag{A 19}$$

When n is large,

$$C_n = O(n^{-3}) \tag{A 20}$$

and, for all t, $a \leqslant t \leqslant b$, the series (A 15) *may be majorized by a convergent numerical series*

$$C \sum_{n=1} \frac{1}{n^2},$$

where C is a constant independent of n.

The above statement can be regarded as an extension of Joseph's (1977) theorem 1. The proof of this theorem may be found in the thesis of Yoo (1977).

REFERENCES

Beavers, G. S. & Joseph, D. D. 1975 The rotating rod viscometer. *J. Fluid Mech.* **69**, 475–511.

Coleman, B. D. & Markovitz, H. 1964 Normal stress effects in second-order fluids. *J. Appl. Phys.* **35**, 1–9.

Coleman, B. D. & Noll, W. 1960 An approximation theorem for functionals with applications in continuum mechanics. *Arch. Rat. Mech. Anal.* **6**, 355–370.

Giesekus, von H. 1961 Einige Bemerkungen zum Fliessverhalten elasto-viskoser Flüssigkeiten in stationären Schlichtströmungen. *Rheol. Acta* **1**, 404–413.

Hoffman, A. H. & Gottenberg, W. G. 1973 Determination of the material functions for a simple fluid from a study of the climbing effect. *Trans. Soc. Rheol.* **17**, 465–485.

Joseph, D. D. 1974 Slow motion and viscometric motion: stability and bifurcation of the rest state of a simple fluid. *Arch. Rat. Mech. Anal.* **56**, 99–157.

Joseph, D. D. 1977 The convergence of biorthogonal series for biharmonic and Stokes flow edge problems. Part 1. *SIAM J. Appl. Math.* **33**, 337–347.

Joseph, D. D., Beavers, G. S. & Fosdick, R. L. 1973 The free surface on a liquid between cylinders rotating at different speeds. Part 2. *Arch. Rat. Mech. Anal.* **49**, 381–401.

JOSEPH, D. D. & FOSDICK, R. L. 1973 The free surface on a liquid between cylinders rotating at different speeds. Part 1. *Arch. Rat. Mech. Anal.* **49**, 321–380.

LANGLOIS, W. E. & RIVLIN, R. S. 1963 Slow steady-state flow of visco-elastic fluids through non-circular tubes. *Rendiconti di Matematica* **22**, 169–185.

PETER, S. & NOETZEL, W. 1959 Über einige Experimente zur Frage der Existenz des Weissenberg-Effektes. *Ann. Physik. Chem.* **21**, 422–431.

SATTINGER, D. H. 1976 On the free surface of a viscous fluid motion. *Proc. Roy. Soc.* A **349**, 183–204.

SAVILLE, D. A. & THOMPSON, D. W. 1969 Secondary flows associated with the Weissenberg effect. *Nature* **223**, 391–392.

TRUESDELL, C. 1974 The meaning of viscometry in fluid dynamics. *Ann. Rev. Fluid Mech.* **6**, 111–146.

TRUESDELL, C. & NOLL, W. 1965 The non-linear field theories of mechanics. *Handbuch der Physik*, vol. III/3. Springer.

YOO, J. Y. 1977 Fluid motion between two cylinders rotating at different speeds. Ph.D. thesis, University of Minnesota.

YOO, J. Y. & JOSEPH, D. D. 1978 Stokes flow in a trench between concentric cylinders. *SIAM J. Appl. Math.* **34**, 247–285.

DESCRIPTION OF PLATE 1

FIGURE 28. Sequence of photographs showing the motion of aluminium flakes on the surface of STP-2 (see table 3) for a rod of radius 0·9525 cm rotating at a speed $\omega = 2{\cdot}05$ rev s^{-1}. The motion is viewed from above. The aluminium flakes start beyond the bubble radius and spiral radially inwards (i.e. up the surface of the bubble) towards the rod.

	(*a*)	(*b*)	(*c*)	(*d*)	(*e*)	(*f*)	(*g*)	(*h*)
Time (s)	0	28	70	123	163	211	310	392

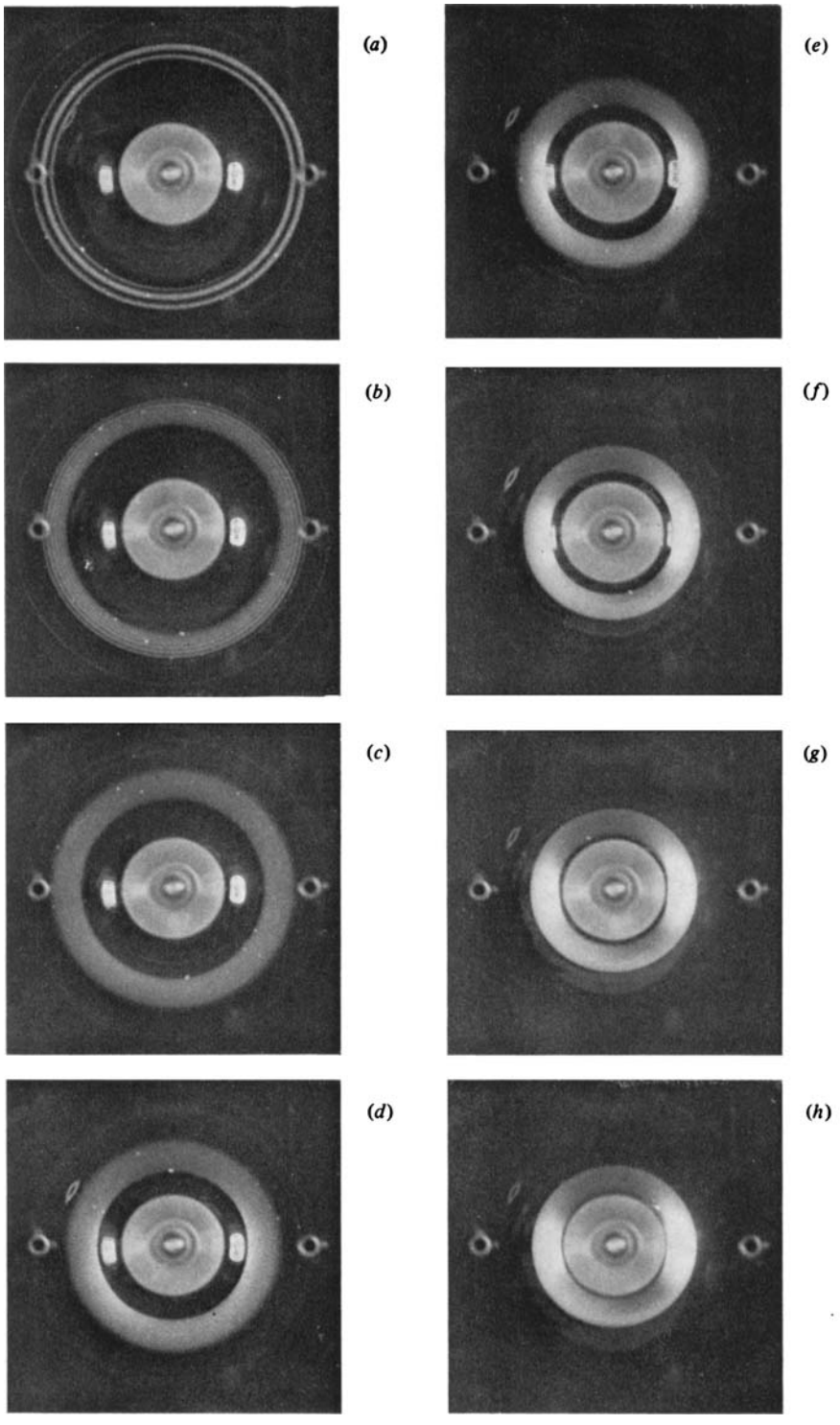

FIGURE 28. For legend see facing page.

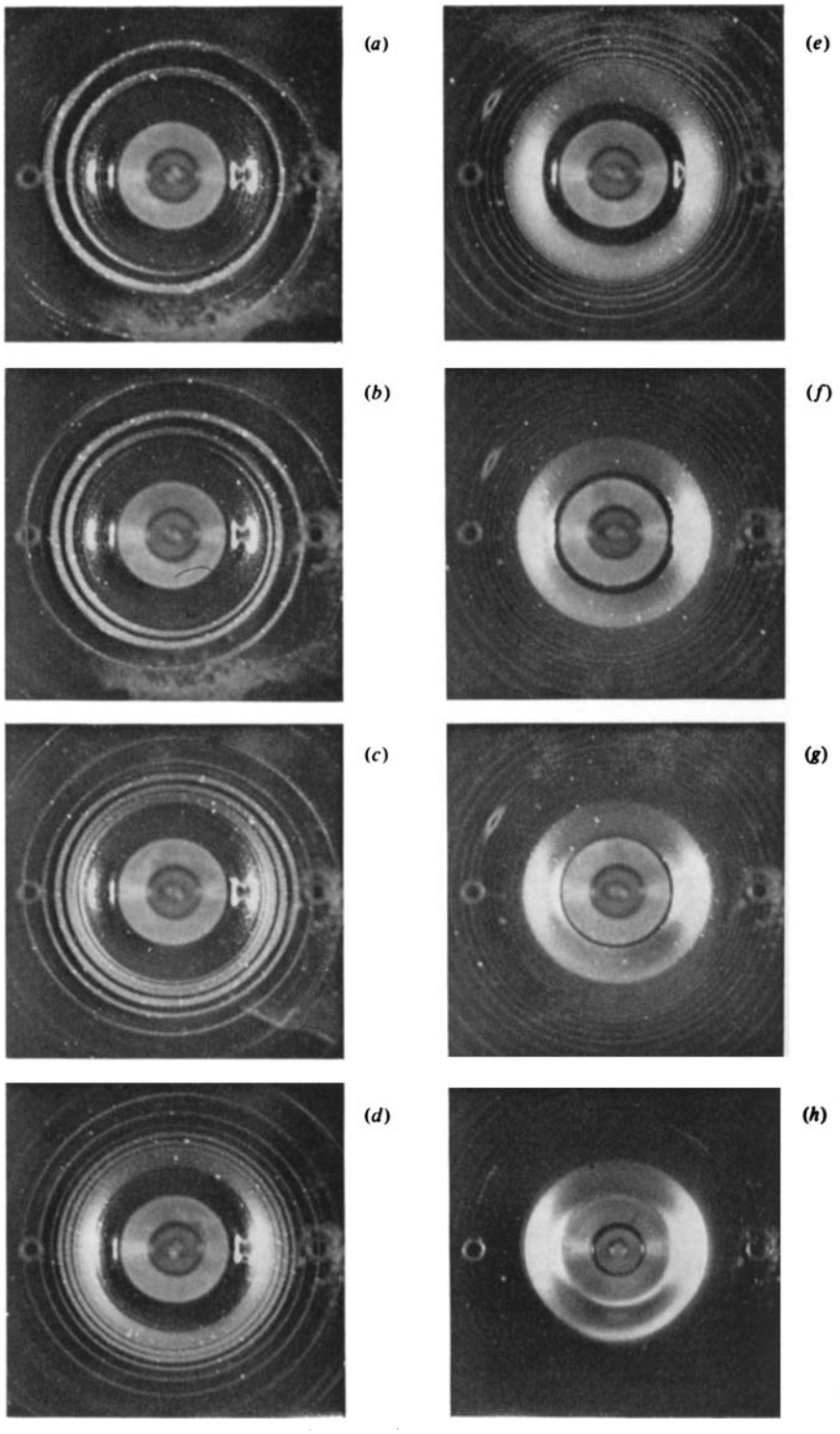

FIGURE 29. For legend see facing page.

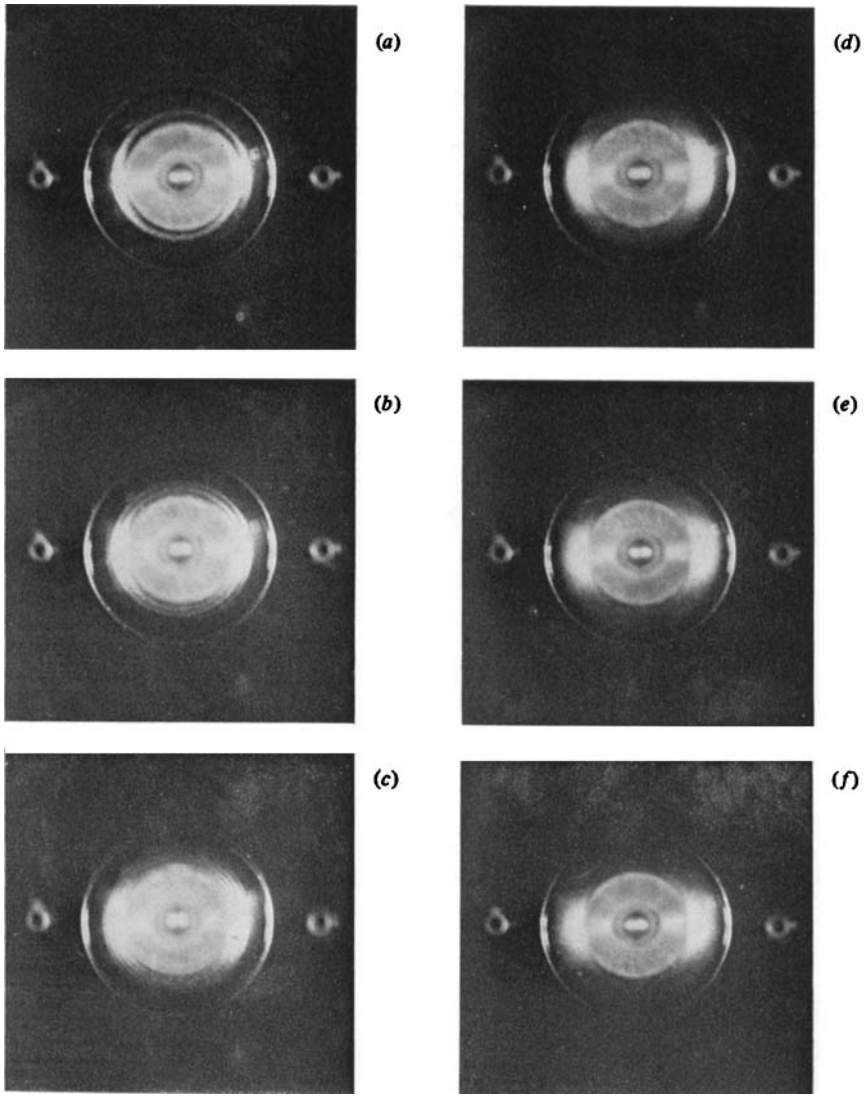

FIGURE 30. Sequence of photographs showing the motion of aluminium flakes on the surface of STP-2 when the rod in figure 28 rotates at $\omega = 4{\cdot}45\,\mathrm{rev\,s^{-1}}$. The aluminium flakes start close to the rod and rapidly spiral down the bubble (radially outwards) to the outer edge of the bubble, where they disappear beneath the surface of the fluid.

	(*a*)	(*b*)	(*c*)	(*d*)	(*e*)	(*f*)
Time (s)	0	2	3	4·5	8·5	14

DESCRIPTION OF PLATE 2

FIGURE 29. Sequence of photographs showing the motion of aluminium flakes on the surface of TLA-227 (see table 3) for a rod of radius 0·9525 cm rotating at a speed $\omega = 0{\cdot}49\,\mathrm{rev\,s^{-1}}$. The motion is viewed from above. The aluminium flakes start beyond the bubble radius and spiral radially inwards (i.e. up the surface of the bubble) towards the rod.

	(*a*)	(*b*)	(*c*)	(*d*)	(*e*)	(*f*)	(*g*)	(*h*)
Time (s)	0	10	30	54	97	177	241	275

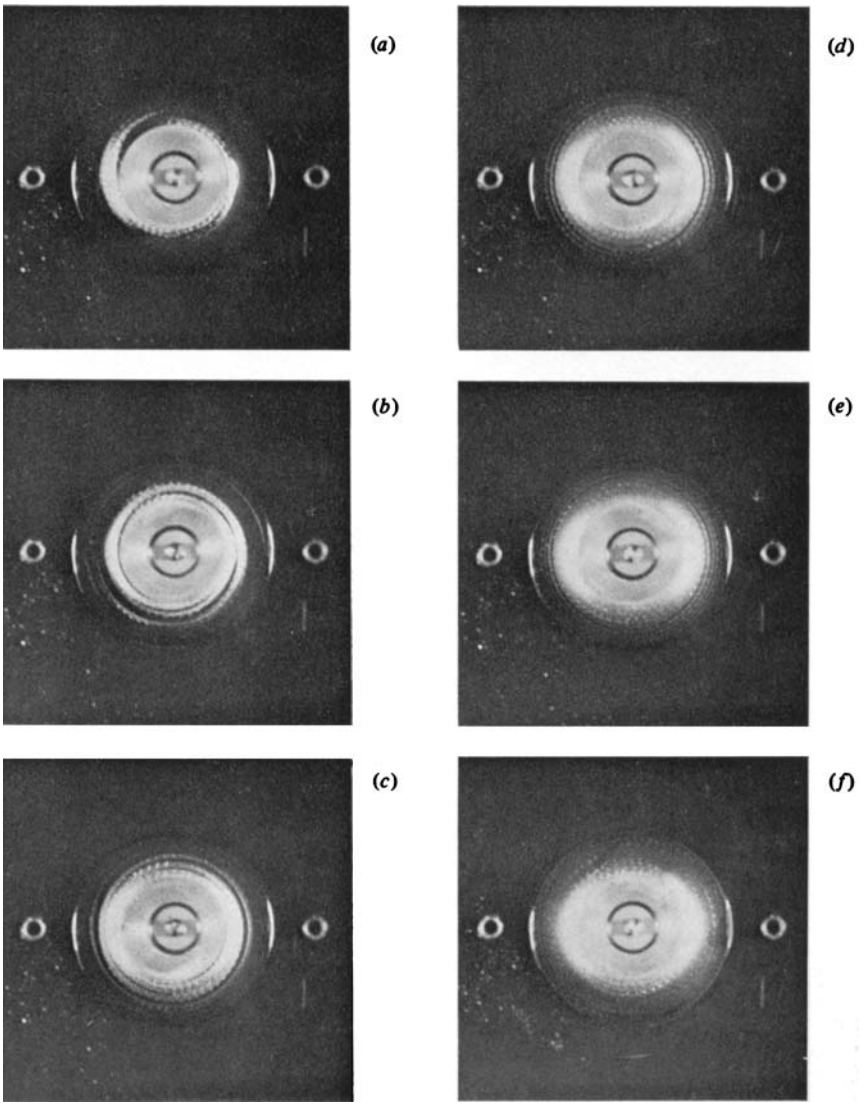

FIGURE 31. Sequence of photographs showing the motion of aluminium flakes on the surface of TLA-227 when the rod in figure 29 rotates at $\omega = 1{\cdot}12\,\mathrm{rev\,s^{-1}}$. The behaviour of the flakes is the same as in figure 30.

	(a)	(b)	(c)	(d)	(e)	(f)
Time (s)	0	4·5	10	17·5	24	44